Institute of Thermoelectricity, Academy of Sciences and Ministry of Education and Science of Ukraine

Journal of THERMOELECTRICITY

International Research

Founded in December, 1993

published 6 times a year

No. 1 *2019*

Editorial Board

International Editorial Board

Founders – National Academy of Sciences, Ukraine
Institute of Thermoelectricity of National Academy of Sciences and Ministry of Education and Science of Ukraine

Certificate of state registration № КВ 15496-4068 ПР

Approved for printing by the Academic Council of Institute of Thermoelectricity of the National Academy of Sciences and Ministry of Education and Science, Ukraine

Address of editorial office:
Ukraine, 58002, Chernivtsi, General Post Office, P.O. Box 86.
Phone: +(380-372) 90 31 65.
Fax: +(380-3722) 4 19 17.
E-mail: jt@inst.cv.ua
http://www.jt.inst.cv.ua

Signed for publication 26.03.2019. Format 70×108/16. Offset paper №1. Offset printing.
Printer's sheet 11.5. Publisher's signature 9.2. Circulation 400 copies. Order 5.

Printed from the layout original made by "Journal of Thermoelectricity" editorial board
in the printing house of "Bukrek" publishers,
10, Radischev Str., Chernivtsi, 58000, Ukraine

CONTENTS

Rifert V.G., *doct. techn. sciences* [1]
Anatychuk L.I., *acad. National Academy of sciences of Ukraine*[2,3]
Barabash P.O., *cand. techn. sciences* [1]**,**
Usenko V.I., *doct. techn. Sciences* [1]
Strikun A.P.[1]
Solomakha A.S., *cand. of techn. sciences* [1]
Petrenko V.G., *cand. of techn. sciences* [1]
Prybyla A.V., *cand. phys. – math. sciences* [2,3]

[1]NTUU KPI, 6 Politekhnicheskaya str, Kyiv, 03056, Ukraine;
[2]Institute of Thermoelectricity, 1 Nauky str.,
Chernivtsi, 58029, Ukraine, *e–mail: anatych@gmail.com*
[3]Yuriy Fedkovych Chernivtsi National University,
2, Kotsiubynsky str., Chernivtsi, 58012, Ukraine

EVOLUTION OF CENTRIFUGAL DISTILLATION SYSTEM WITH A THERMOELECTRIC HEAT PUMP FOR SPACE MISSIONS

Part 1. Review of publications on centrifugal distillation in the period of 1990 – 2017

The article describes the main results of the development and testing of a multistage centrifugal vacuum distillation (MCVD) system with a thermoelectric heat pump (THP). For the most part, these works present information on the integral characteristics of the system, namely: distillate capacity, specific energy consumption per unit mass of the obtained distillate and distillate quality during evaporation (concentration) of an aqueous solution of NaCl, urine and mixtures of urine with condensate and urine with condensate and hygienic water. Bibl. 29, Tabl. 5.
Key words: thermoelectricity, heat pump, distiller

Introduction

Purification of liquid human waste is highly relevant for the success in long flights to the Moon and Mars and the work of astronaut teams, both at these space objects and at the International Space Station (ISS).

Within the span of 2000-2009, a team of engineers and researchers from "Thermodistillation" Co ("TD" Co), Igor Sikorsky Kyiv Polytechnic Institute (KPI) and the Institute of Thermoelectricity of the National Academy of Sciences and the Ministry of Education and Science of Ukraine (ITE) developed a wastewater purification system by the method of multistage centrifugal vacuum distillation (MCVD) using a thermoelectric heat pump (THP) as a heat source. Its use can significantly reduce the energy costs for the operation of the system, which makes it competitive among similar space water purification systems.

The purpose of the work is to analyze the evolution of centrifugal distillation system with a thermoelectric heat pump for space missions.

Characteristics of MCVD with 3 stages and THP

The first prototype of MCVD had three stages of distillation and was developed and manufactured as far back as in the 80s by order of NIIKHIMMASH (Russia, Moscow). Brief data about this device was given in the reports [1] and contained information about some of its parameters at a capacity of up to 3 l/h.

The publications [2 – 6] also provide brief information on the characteristics of a 3-stage distiller. In [2], tables are given indicating the distiller's capacity for purified water (G_D = 0.5 - 3.0 kg / h) and specific power consumption (SPC) with no information on the power consumption for THP (W_{THP}) and the degree of water recovery from the initial liquid.

In [3], the calculated values of the distiller's capacity for purified water $G_D = f(W_{THP})$ are given without explaining the method for calculating the parameters, the degree of water recovery, and the rotation speed of heat-exchange surfaces n (rpm).

In [4], a table is given with the data: G_D = 2.5 - 3.0 kg/h; SPC = 120 W·h/kg (specific power consumption); Rec = 90 % (degree of fluid recovery). Information on W_{THP}, the duration of the distiller operation and the quality of the resulting product is not presented.

In [5], there is a plot of the capacity of a 3-stage distiller versus NTHP and the specific power consumption (155 – 165 W · h / kg), but without specifying the rotor speed and the degree of concentration of the initial liquid.

In [6], a comparison is made of the main characteristics of a three-stage distiller in combination with THP, a vapor compression distiller (VCD), and a TEMES thermoelectric evaporator.

In [7], the operation of the system under extreme conditions was studied, in the event of failure of individual subsystems

Characteristics of MCVD with 5 stages and THP

In [8], the design and operation of a 5-stage distiller in combination with a thermoelectric heat pump was first described, as well as a test bench created on the basis of "TD" Co for testing centrifugal distillers in conjunction with THP under various operating conditions.

In 2001, the first five-stage distiller was developed and manufactured for Honeywell International Inc. [8]. At the suggestion of the customer, it was called the cascade distiller - CD, and the multistage centrifugal vacuum distillation system with a thermoelectric heat pump, manufactured in Ukraine in "TD" Co, was called the cascade distillation system - CDS.

Altogether, in the period from 2000 to 2007, three identical five-stage centrifugal distillers were developed and manufactured by "TD" Co: the first one, as mentioned above, in 2001, the second in 2002, the third in 2006. All three appliances complete with thermoelectric heat pumps ALTEC 7005, developed and manufactured by the Institute of Thermoelectricity of the NAS and MES of Ukraine (ITE) [21 – 29], were transferred to Honeywell International Inc. These devices have been tested in various versions at several test benches in the United States, including the NASA test bench.

Before shipment to the USA, each of the devices was tested at the "TD" Co. test bench.

Table 1 presents the first test results of a 5-stage distiller in the process of urine processing at different speeds and power of the THP.

In total, over 300 tests with the following range of input parameters were carried out at the test bench of "TD" Co in the period of 2000-2007 in the process of working out the design and passing tests of five-stage distillers (3 copies) and heat pumps (2 copies): the rotation speed of the rotor 100 - 1500 rpm, THP power (40 - 520) W, initial (recyclable) liquids: water, aqueous *NaCl* solution (2-4 %), urine. Results obtained: capacity (max.) - 6.7 kg/h; liquid recovery rate (max.) - 0.95, specific power consumption (min.) – 76 W·h/kg.

[8 – 16] describe the stages of CDS development and testing at the test benches of TD Co,

Honeywell International Inc. and the Marshall Center (NASA JSC), which confirms the priority authorship of TD Co and ITE of NASU in the design and manufacture of relevant CDS elements.

In [10–12], CDS submitted by Honeywell International Inc to Johnson Space Center (NASA JSC) for testing were described in detail. The results of tests on concentrating in a centrifugal distiller an aqueous solution of *NaCl* in an amount of 21 l and urine in an amount of 111.8 kg, as well as the evaporation of 25.5 kg of distillate are presented. Data is given on the capacity of the distillers (2.7 - 5.1) kg/h, specific power consumption (88.8 - 116) W · h/kg and the degree of water recovery 0.88 - 0.95.

Table 1

Results of testing 5-stage distiller (urine)

Rotation rate, rpm	Power CD-5, W	Power THP, W	THP Efficiency	Average capacity, l/h	Specific power consumption W h s /l	Degree of water recovery
1100	65	255	2.07	3.70	86.5	0.89
1100	65	382	1.88	4.72	94.7	0.91
1200	84	251	2.30	3.84	87.2	0.88
1200	85	380	2.02	4.90	94.9	0.91
1200	90	400	1.77	5.04	97.2	0.92
1250	96	406	1.90	4.95	101.4	0.95
1300	106	379	2.08	5.08	95.5	0.92
1300	106	411	1.89	5.38	96.1	0.90

In [12, 13] the results of tests on concentration in CD of urine, condensate of atmospheric moisture and sanitary water are presented. The data obtained is close to the results contained in [9, 10] in terms of capacity (~ 5 kg / h), specific power consumption (~ 100 W · h/kg) and the quality of the distillate obtained. There is no data on the power consumed by the heat pump and the rotation speed of the distiller rotor.

[14] outlines the results of CDS testing during purification of wastewater in the amount equivalent to that which can accumulate within 30 days of flight of a crew of 4 people. In total, about 1500 kg of wastewater was recycled as two different solutions. Solution 1 consisted of urine and atmospheric moisture condensate, solution 2 consisted of urine, atmospheric moisture condensate and sanitary water.

The integral test parameters for each of the solutions are as follows:

– solution 1 - capacity 4.1 kg/h with a power of THP 300 W ;.

– solution 2 - capacity 5.2 kg/h with a THP power 400 W;

– the degree of water recovery (recovery) from solution 1 - 93.4 ± 0.7 %, from solution 2 - 90.3 ± 5 %;

– the specific power consumption in both cases was ~ 100 W h/kg ;.

– the quality of the distillate upon evaporation of both solutions corresponded to the requirements for drinking water, except for the *pH* value, which was < 5.

In [15], the characteristics of three centrifugal distillation technologies were compared: a vacuum compression distiller (VCD) developed in the USA from 1962 to 2008 (currently operating in the ISS system), a centrifugal evaporator with a wiped-film rotating disk (WFRD) and cascade distillation systems (CDS).

The initial (evaporated) liquids were the same two solutions as in [11], and in the same quantities (as for the 30-day mission).

The total characteristics of the test results are shown in tables 2 and 3.

The work also presents data on the quality of the product obtained during the experiment. CDS performed better in all test modes when they met the requirements of drinking water standards.

Expert evaluation of the test results: the VCD system will be successful with a probability of 84 % - 90 % and a risk of 3 %; CDS will be successful with a probability of 84 % -87 % and a risk of 5 %; the WFRD system will be successful with a probability of 52 % -61 % and a risk of 7 %.

Table 2

Testing results (1 solution)

	CDS	VCD	WFRD
Capacity (kg/h)	3.7	1,63	16.1
Specific power consumption (W h/kg)	109	188	85
Average power (W)	375	279	1252

Table 3

Testing results (2 solution)

	CDS	VCD	WFRD
Capacity (kg/h)	4.88	1.87	16.8
Specific power consumption (W h/kg)	110	163	86
Average power (W)	485	296	1293

[16] claims that CDS is one of two distillation technologies that are currently being developed to support closed-loop water recovery from mixed waste streams expected for long missions.

The same report presents the results of experiments at the test bench of Honeywell International, Inc., in which the effect of the rotation speed of the distiller rotor on the quality of the resulting product was studied. It was found that the best water quality using CDS can be achieved at a rotor speed of 1300 ... 1400 rpm.

The report concludes as follows. “At the current stage of CDS development testing, the system worked as expected and with acceptable performance when processing reference test solutions (water, aqueous NaCl (2-4%), urine). A preliminary comparison of the reference data with previous tests shows that upgrading the system prior to the current CDS prototype did not show any significant impact on system performance. Similarly, the current testing cycle has shown that CDS is capable of handling analog ISS waste streams and performance values are close to those observed for less complex basic test solutions. This final result is an important step towards demonstrating CDS technology as part of the ISS payload. CDS testing will continue to evaluate updated THP projects, a management system, and new wastewater stabilization methods. In addition, the CDS prototype will also continue to be used as a test bench to inform of currently developed generation 2.0 of CDS system”.

The reports [17, 18] present the main parameters of CDS obtained by processing six solutions (see Table 4 [18]) in order to determine the possibility of using CDS for the recovery of all types of wastewater under the conditions of the international space station. In the experiments, 8 to 9.8 kg of each solution was processed. The quality of the distillate obtained, the temperature level and the mass flow rate satisfy the required requirements (Expected distillate delivery specification) (see Table 5). As a result, it was

concluded that CDS can be used on the ISS and there is a need for additional tests to improve the operation of the heat pump and control system in long space missions (Generation 2.0 of CDS).

Table 4

Parameters of CDS

Solution type	Batch, kg	Recovery, %	Capacity, kg/h	Specific power consumption, W h/kg
Deionized water	9.01 ±1.39	84.6 ±4.7	4.56 ±0.11	74.8 ± 7.9
2% NaCI (1)	9.78 ± 0.02	85.3 ±1.2	4.27 ±0.03	86.5 ±0.9
OxonePTU	9.81 ±0.01	83.1 ±2.7	4.40 ±0.04	97.2 ± 0.3
ISSPTAU	5.79 ±0.03	78.4 ±'1.6	3.89 ±0.00	95.9 ±6.3
JSSAIt-PTAU	9.77 ±0.03	84.4 = 0.8	3.98 ±0.04	105.0 ±2.7
2% NaCI (2)	9.76 ±0.02	83.0 ±0.6	4.32 ±0.09	84.6 ±1.5

Table 5

Quality of CDS distillate obtained

Parameter	Specification	Oxone	ISS Baseline	ISS Alt
Temperature level	61-99 °F	~ 72.0	~ 72.0	~ 72.0
Flow rate	0-5 lb/hr	10.0	8.6	8.8
Conductivity	< 400 μmho/cm	46	100	67
pH	3-8	4.1	3.8	3.9
Ammonium	≤ 3 ppm	< 0.6	< 0.6	< 0.6
Total organic carbon	≤ 150 ppm	8.27	18.7	26.6

Our works, in particular, [20, 21], present the results of studying the influence of primary parameters, namely the distiller rotor rotational speed (n CD) and the thermoelectric heat pump NTHP power on the CDS capacity (GCDS) and the system specific power consumption (SPC). It was found that with decreasing W_{THP} the SPC value decreases. For example, with W_{THP} = 200 W and a rotational speed of 1000 rpm with the same value of SPC = 82 – 87 W h / kg, and with W_{THP} = 400 W, SPC = 100 – 110 W · h / kg.

Conclusions

The works from 1990 to 2017 have been reviewed which describe the results of the development, manufacture and testing at the test benches of TD Co, Honeywell Co and NASA of centrifugal distillers CD with 3 and 5 stages and a thermoelectric heat pump THP. During the tests, by means of CD an aqueous *NaCl* solution, a mixture of urine and sweat condensate, and a mixture of urine, atmospheric moisture condensate, and sanitary water were concentrated (evaporated). The stability of the distillers with the high quality of the resulting product – water was shown. In the JSC Center alone, 1575 kg of wastewater were processed in 352 hours, which corresponded to an average system capacity of about 5 l / h. The degree of

water recovery in these tests reached 93 %. In 2015, NASA plans (roadmap) recorded that the CDS system was chosen for promising space flights. For unknown reasons, the works on CDS are currently stopped.

It should be noted that in the majority of publications devoted to the study of the functioning of various centrifugal distillers, their integral, average for the full cycle of operation, characteristics (capacity, SPC, product quality) are given, and practically no information is available on the effect produced on the operation of the distiller by such important indicators as heat pump power NTHP and the distiller rotor rotational speed.

References

1. Rifert V., Barabash P., Goliad N. (1990). Methods and processes of thermal distillation of water solutions for closed water supply systems . *SAE Paper 901249, 20th Intersociety Conference on Environmental Systems* (Williamsburg, July 1990).
2. Samsonov N., Bobe L., Novikov V., Rifert V., et al. (1994). Systems for water reclamation from humidity condensate and urine for space station. *SAE Paper 941536, 24th International society Conference on Environmental Systems* (June, 1994).
3. Samsonov N.M., Bobe L.S, Novikov V., Rifert V.G., Barabash P.A, et al. (1995). Development of urine processor distillation hardware for space stations. *SAE Paper 951605, 25th International Conference on Environmental Systems* (San Diego, July 1995).
4. Samsonov N.M., Bobe L.S, Novikov V., Rifert V.G., et al (1997). Updated systems for water recovery from humidity condensate and urine for the International space station. *SAE Paper 972559, 27th International Conference on Environmental Systems* (Nevada, July 1997).
5. Samsonov N.M., Bobe L.S, Novikov V., Rifert V.G., et al. (1999). Development and testing of a vacuum distillation subsystem for water reclamation from urine. *SAE Paper 1999-01-1993, 29th International Conference on Environmental Systems, 1999.*
6. Rifert, V., Usenko V., Zolotukhin I., MacKnight A., Lubman A. (1999). Comparison of secondary water processors using distillation for space applications. (1999). *SAE Paper 99-70466, 29th International Conference on Environmental Systems* (Denver, July 1999).
7. Rifert V, Stricun, A., Usenko, V. (2000). Study of dynamic and extreme performances of multistage centrifugal distiller with the thermoelectric heat pump. *SAE Technical Papers 2000, 30th International Conference on Environmental Systems (*Toulouse; France, 10-13 July 2000).
8. Rifert, V., Usenko V., Zolotukhin I., MacKnight A. and Lubman A. (2001). Design optimisation of cascade rotary distiller with the heat pump for water reclamation from urine. *SAE Paper 2001-01-2248, 31st International Conference on Environmental Systems (Orlando, July 2001).*
9. Rifert, V. G., Usenko V.I., Zolotukhin I.V., MacKnight A. and Lubman A. (2003). Cascaded distillation technology for water processing in space. SAE Paper 2003-01-2625. *34st International Conference on Environmental Systems* (Orlando, July 2003).
10. Lubman A, MacKnight A, Rifert V, Zolotukhin I and Pickering K. (2006). Wastewater processing cascade distillation subsystem. design and evaluation (2006). *SAE International, 2006-01-2273, July* 2006.
11. Lubman A., MacKnight A., Rifert V., and Barabash P.,(2007). Cascade distillation subsystem hardware development for verification testing. *SAE International, 2007-01-3177, July 2007.*
12. Callahan M., Lubman A., MacKnight A., Thomas H.and Pickering K.. Cascade distillation subsystem development testing (2008). *SAE International, 2008-01-2195, July 2008.*
13. Callahan M., Lubman A., and Pickering K. (2009). Cascade distillation subsystem development: progress toward a distillation comparison test. *SAE International, 2009-01 -2401, July 2009.*
14. Callahan M., Patel V. and Pickering K. (2010). Cascade distillation subsystem development: early

results from the exploration life support distillation technology comparison test. *American Institute of Aeronautics and Astronautics, 2010-6149, July 2010.*

15. McQuillan Jeff, Pickering Karen D., Anderson Moly, Carter Layne, Flynn Michael, Callahan Michael, Vega Leticia, Allada Rama and Yeh Jannivine Distillation technology down-selection for the exploration life support (ELS) water recovery systems element (2010). *40th International Conference on Environmental Systems, AIAA 2010-6125.*
16. Patel V., Au H., Shull S., Sargusingh M., Callahan M.. (2014). Cascade distillation system – a water recovery system for deep space missions. *ICES-2014-12, 44 International Conference on Environmental Systems* (Tucson, Arizona, July 2014).
17. Loeftelholz David, Baginski Ben, Patel Vipul, MacKnight Allen, Schull Sarah, Sargusingh Miriam, Callahan Michael (2014). Unit operation performance testing of cascade distillation subsystem. *ICES-2014-0014*, *44th International Conference on Environmental Systems*, (Tucson, Arizona, 13-17 July 2014).
18. Callahan Michael R., Sargusingh Mirian J. Honeywell cascade distiller system performance testing interim results. *American Institute of Aeronautics and Astronautics.*
19. Sargusingh Miriam, Callahan Michael (2015). Development of an exploration-class cascade distillation subsystem: performance testing of the generation 1.0 prototype. ICES-2015-150, *45th International Conference on Environmental Systems, 13-17 July 2015.*
20. Rifert Vladimir G, Barabash Petr A., Usenko Vladimir, Solomakha Andrii S., Anatychuk Lukyan I., Prybyla A.V. (2017). *Improvement the cascade distillation system for long-term space flights. 68th International Astronautical Congress (IAC)* (Adelaide, Australia, 25-29 September 2017 IAC-17-A1.IP.25).
21. Rifert V.G., Anatychuk L.I., Barabash P.A, Usenko V.I., Strikun A.P., Prybyla A.V. (2017). Improvement of the distillation methods by using centrifugal forces for water recovery in space flight applications. *J.Thermoelectricity*, 1, 71-83.
22. Rifert V.G., Usenko V.I., Anatychuk L.I., Rozver Yu.Yu. (2011). Development and test of water regeneration from liquid waste on board of manned space crafts with the use of thermoelectric heat pumps. *J.Thermoelectricity*, 2, 14-25.
23. Anatychuk L.I., Brabash P.A., Rifert V.G., Rozver Yu.Yu., Usenko V.I., Cherkez R.G. (2013). Thermoelectric heat pump as a means of improving efficiency of water purification systems for biological needs for space missions. *J.Thermoelectricity*, 6, 78-83.
24. Aanatychuk L.I.., Prybyla A.V. (2015). Optimization of thermal connections in thermoelectric liquid-liquid heat pumps for water purification systems of space application. *J.Thermoelectricity*, 4, 45 – 51.
25. Anatychuk L.I. Prybyla A.V. (2015). Optimization of power supply system of thermoelectric liquid-liquid heat pump. *J.Thermoelectricity*, 6, 53 – 58.
26. Anatychuk L.I., Rozver Yu.Yu., Prybyla A.V. (2017). Experimental study of thermoelectric liquid-liquid heat pump. *J.Thermoelectricity*, 3, C. 33 – 39.
27. Anatychuk L.I., Prybyla A.V. (2017). Limiting possibilities of thermoelectric liquid-liquid heat pump. *J.Thermoelectricity*, 4, 33 – 39.
28. Anatychuk L.I., Prybyla A.V. (2017). The influence of quality of heat exchangers on the properties of thermoelectric liquid-liquid heat pumps. *J.Thermoelectricity*, 5, 33 – 39.
29. Anatychuk L.I., Prybyla A.V. (2017). On the coefficient of performance of thermoelectric liquid-liquid heat pumps with regard to energy loss for heat carrier transfer. *J.Thermoelectricity*, 6, 33 – 39.

Submitted 19.02.2019

Риферт В.Г., *док. техн. наук* [1]
Анатичук Л.І., *акад. НАН України*[2,3]
Барабаш П.О., *канд. техн. наук*[1]
Усенко В.І., *док. техн. наук*[1]
Соломаха А.С., *канд. техн. наук*[1,2]
Петренко В.Г., *канд. техн. наук*[1]
Прибула А.В., *канд. фіз.-мат. наук* [2,3]
Стрикун А.П.[1]

[1]НТУ «КПИ», вул. Політехнічна, 6, Київ, 03056, Україна;
[2]Інститут термоелектрики, вул. Науки, 1,
Чернівці, 58029, Україна, *e–mail: anatych@gmail.com*;
[2]Чернівецький національний університет імені Юрія Федьковича,
вул. Коцюбинського 2, Чернівці, 58012, Україна

ЕВОЛЮЦІЯ СИСТЕМИ ВІДЦЕНТРОВОЇ ДИСТИЛЯЦІЇ З ТЕРМОЕЛЕКТРИЧНИМ ТЕПЛОВИМ НАСОСОМ ДЛЯ КОСМІЧНИХ МІСІЙ

Частина 1. Огляд публікацій по відцентровій дистиляції в період 1990 – 2017 рр.

У статті описані основні результати розробок і випробувань системи багатоступінчастої відцентрової вакуумної дистиляції (СМЕД) з термоелектричним тепловим насосом (ТНР). У цих роботах дані в основному відомості по інтегральних характеристиках роботи системи, а саме: продуктивності по дистиляту, питомій витраті енергії на одиницю маси одержуваного дистиляту і якості дистиляту при випарюванні (концентруванні) водяного розчину NaCl, урини й сумішей – урини з конденсатом, урини з конденсатом і гігієнічною водою. Бібл. 29, Табл. 5.
Ключові слова:

Риферт В.Г., *док. техн. наук* [1]
Анатычук Л.И., *акад. НАН Украины*[2,3]
Барабаш П.О. *канд. техн. наук*[1]
Усенко В.И. *док. техн. наук*[1]
Соломаха А. С., *канд. техн. наук*[1]
Петренко В. Г., *канд. техн. наук*[1]
Прибила А. В. *канд. физ.-мат. наук* [2,3]
Стрикун А.П.[1]

[1]НТУ «КПИ», вул. Политехническая, 6, Киев, 03056, Украина;
[2]Институт термоэлектричества НАН и МОН Украины, ул. Науки, 1,
Черновцы, 58029, Украина, *e–mail: anatych@gmail.com*;
[3]Чернивецький национальный университет им. Юрия Федьковича,
ул. Коцюбинского 2, Черновцы, 58000, Украина

ЭВОЛЮЦИЯ СИСТЕМЫ ЦЕНТРОБЕЖНОЙ ДИСТИЛЛЯЦИИ С ТЕРМОЭЛЕКТРИЧЕСКИМ ТЕПЛОВЫМ НАСОСОМ ДЛЯ КОСМИЧЕСКИХ МИССИЙ

Часть 1. Обзор публикаций по центробежной дистилляции в период 1990 – 2017 гг.

В статье описаны основные результаты разработок и испытаний системы многоступенчатой центробежной вакуумной дистилляции (СМЕД) с термоэлектрическим тепловым насосом (ТНР). В этих работах даны в основном сведения по интегральным характеристикам работы системы, а именно: производительности по дистилляту, удельному расходу энергии на единицу массы получаемого дистиллята и качеству дистиллята при выпаривании (концентрировании) водного раствора NaCl, урины и смесей – урины с конденсатом, урины с конденсатом и гигиенической водой. Библ. 29, Табл. 5.

Ключевые слова: термоэлектричество, тепловой насос, дистиллятор.

References

1. Rifert V., Barabash P., Goliad N. (1990). Methods and processes of thermal distillation of water solutions for closed water supply systems . *SAE Paper 901249, 20th Intersociety Conference on Environmental Systems* (Williamsburg, July 1990).
2. Samsonov N., Bobe L., Novikov V., Rifert V., et al. (1994). Systems for water reclamation from humidity condensate and urine for space station. *SAE Paper 941536, 24th International society Conference on Environmental Systems* (June, 1994).
3. Samsonov N.M., Bobe L.S, Novikov V., Rifert V.G., Barabash P.A, et al. (1995). Development of urine processor distillation hardware for space stations. *SAE Paper 951605, 25th International Conference on Environmental Systems* (San Diego, July 1995).
4. Samsonov N.M., Bobe L.S, Novikov V., Rifert V.G., et al (1997). Updated systems for water recovery from humidity condensate and urine for the International space station. *SAE Paper 972559, 27th International Conference on Environmental Systems* (Nevada, July 1997).
5. Samsonov N.M., Bobe L.S, Novikov V., Rifert V.G., et al. (1999). Development and testing of a vacuum distillation subsystem for water reclamation from urine. *SAE Paper 1999-01-1993, 29th International Conference on Environmental Systems, 1999.*
6. Rifert, V., Usenko V., Zolotukhin I., MacKnight A., Lubman A. (1999). Comparison of secondary water processors using distillation for space applications. (1999). *SAE Paper 99-70466, 29th International Conference on Environmental Systems* (Denver, July 1999).
7. Rifert V, Stricun, A., Usenko, V. (2000). Study of dynamic and extreme performances of multistage centrifugal distiller with the thermoelectric heat pump. *SAE Technical Papers 2000, 30th International Conference on Environmental Systems (*Toulouse; France, 10-13 July 2000).
8. Rifert, V., Usenko V., Zolotukhin I., MacKnight A. and Lubman A. (2001). Design optimisation of cascade rotary distiller with the heat pump for water reclamation from urine. *SAE Paper 2001-01-2248, 31st International Conference on Environmental Systems (Orlando, July 2001).*
9. Rifert, V. G., Usenko V.I., Zolotukhin I.V., MacKnight A. and Lubman A. (2003). Cascaded distillation technology for water processing in space. SAE Paper 2003-01-2625. *34st International Conference on Environmental Systems* (Orlando, July 2003).
10. Lubman A, MacKnight A, Rifert V, Zolotukhin I and Pickering K. (2006). Wastewater processing cascade distillation subsystem. design and evaluation (2006). *SAE International, 2006-01-2273, July*

2006.

11. Lubman A., MacKnight A., Rifert V., and Barabash P.,(2007). Cascade distillation subsystem hardware development for verification testing. *SAE International, 2007-01-3177, July 2007.*
12. Callahan M., Lubman A., MacKnight A., Thomas H.and Pickering K.. Cascade distillation subsystem development testing (2008). *SAE International, 2008-01-2195, July 2008.*
13. Callahan M., Lubman A., and Pickering K. (2009). Cascade distillation subsystem development: progress toward a distillation comparison test. *SAE International, 2009-01 -2401, July 2009.*
14. Callahan M., Patel V. and Pickering K. (2010). Cascade distillation subsystem development: early results from the exploration life support distillation technology comparison test. *American Institute of Aeronautics and Astronautics, 2010-6149, July 2010.*
15. McQuillan Jeff, Pickering Karen D., Anderson Moly, Carter Layne, Flynn Michael, Callahan Michael, Vega Leticia, Allada Rama and Yeh Jannivine Distillation technology down-selection for the exploration life support (ELS) water recovery systems element (2010). *40th International Conference on Environmental Systems, AIAA 2010-6125.*
16. Patel V., Au H., Shull S., Sargusingh M., Callahan M.. (2014). Cascade distillation system – a water recovery system for deep space missions. *ICES-2014-12, 44 International Conference on Environmental Systems* (Tucson, Arizona, July 2014).
17. Loeftelholz David, Baginski Ben, Patel Vipul, MacKnight Allen, Schull Sarah, Sargusingh Miriam, Callahan Michael (2014). Unit operation performance testing of cascade distillation subsystem. *ICES-2014-0014*, *44th International Conference on Environmental Systems*, (Tucson, Arizona, 13-17 July 2014).
18. Callahan Michael R., Sargusingh Mirian J. Honeywell cascade distiller system performance testing interim results. *American Institute of Aeronautics and Astronautics.*
19. Sargusingh Miriam, Callahan Michael (2015). Development of an exploration-class cascade distillation subsystem: performance testing of the generation 1.0 prototype. ICES-2015-150, *45th International Conference on Environmental Systems, 13-17 July 2015.*
20. Rifert Vladimir G, Barabash Petr A., Usenko Vladimir, Solomakha Andrii S., Anatychuk Lukyan I., Prybyla A.V. (2017). *Improvement the cascade distillation system for long-term space flights. 68th International Astronautical Congress (IAC)* (Adelaide, Australia, 25-29 September 2017 IAC-17-A1.IP.25).
21. Rifert V.G., Anatychuk L.I., Barabash P.A, Usenko V.I., Strikun A.P., Prybyla A.V. (2017). Improvement of the distillation methods by using centrifugal forces for water recovery in space flight applications. *J.Thermoelectricity*, 1, 71-83.
22. Rifert V.G., Usenko V.I., Anatychuk L.I., Rozver Yu.Yu. (2011). Development and test of water regeneration from liquid waste on board of manned space crafts with the use of thermoelectric heat pumps. *J.Thermoelectricity*, 2, 14-25.
23. Anatychuk L.I., Brabash P.A., Rifert V.G., Rozver Yu.Yu., Usenko V.I., Cherkez R.G. (2013). Thermoelectric heat pump as a means of improving efficiency of water purification systems for biological needs for space missions. *J.Thermoelectricity*, 6, 78-83.
24. Aanatychuk L.I.., Prybyla A.V. (2015). Optimization of thermal connections in thermoelectric liquid-liquid heat pumps for water purification systems of space application. *J.Thermoelectricity*, 4, 45 – 51.
25. Anatychuk L.I. Prybyla A.V. (2015). Optimization of power supply system of thermoelectric liquid-liquid heat pump. *J.Thermoelectricity*, 6, 53 – 58.
26. Anatychuk L.I., Rozver Yu.Yu., Prybyla A.V. (2017). Experimental study of thermoelectric liquid-liquid heat pump. *J.Thermoelectricity*, 3, C. 33 – 39.
27. Anatychuk L.I., Prybyla A.V. (2017). Limiting possibilities of thermoelectric liquid-liquid heat pump. *J.Thermoelectricity*, 4, 33 – 39.

28. Anatychuk L.I., Prybyla A.V. (2017). The influence of quality of heat exchangers on the properties of thermoelectric liquid-liquid heat pumps. *J.Thermoelectricity*, 5, 33 – 39.
29. Anatychuk L.I., Prybyla A.V. (2017). On the coefficient of performance of thermoelectric liquid-liquid heat pumps with regard to energy loss for heat carrier transfer. *J.Thermoelectricity*, 6, 33 – 39.

Submitted 19.02.2019

V.V. Lysko, *cand. phys.– math. sciences*

Lysko V.V.

[1]Institute of Thermoelectricity of the NAS and MES of Ukraine,
1, Nauky str, Chernivtsi, 58029, Ukraine,
e-mail: anatych@gmail.com;
[2]Yuriy Fedkovych Chernivtsi National University,
2, Kotsiubynsky str., Chernivtsi, 58012, Ukraine

VISCOUS FLUID APPROXIMATION WHEN SIMULATING Bi_2Te_3 BASED THERMOELECTRIC MATERIAL EXTRUSION PROCESS

In the process of extrusion, billets of material are deformed under virtually perfect plastic conditions. Such a process can be simulated using the hydrodynamic theory, where a material is regarded as a fluid of very high viscosity which is a function of velocity and temperature. The internal friction of the moving layers of the material serves as a heat source, so it is also necessary to use the heat transfer equation in conjunction with the hydrodynamic aspect of the problem. This approach is especially effective for simulating the extrusion process of thermoelectric materials when large deformations are present. This paper presents the results of an object-oriented computer simulation of the process of hot extrusion of Bi_2Te_3 based thermoelectric material. Cases of producing cylindrical samples of circular cross section for various matrix configurations for single-stage and multi-stage extrusion are considered. The distributions of temperature and flow velocity of material in the matrix are obtained, as well as stress distribution in the matrix due to external pressure and thermal loads, which formed the basis for optimization of equipment for producing extruded thermoelectric material. Bibl. 5, Fig. 8, Tabl. 1.

Key words: extrusion, thermoelectric material, modeling.

Introduction

The hot extrusion process is widely used in the production of thermoelectric materials [1 – 3]. The essence of it is punching a thermoelectric material through a hole in a heated mold. The main advantage of this method is associated with an improvement in the strength characteristics of material. Moreover, their thermoelectric properties can remain at the level of the properties of materials obtained by crystallization from the melt.

Since hot extrusion is usually carried out at sufficiently high temperatures, the structure of the extruded material is formed in the process of plastic deformation, resulting in a deformation texture. The extrusion conditions, namely the shape of the die, the temperature and strain rate, the strain value, the structure of the initial billet, affect the final structure and properties of the extruded material. One of the effective ways to study the influence of these conditions on the formation of the structure and texture of the extruded material is mathematical simulation of the extrusion process in combination with the experimental results of structural studies [4].

The purpose of this work is to create a computer model of the hot extrusion process of Bi_2Te_3 based thermoelectric material to study the distributions of temperature and material flow velocity in the matrix, as

well as the stress distribution in the matrix due to external pressure and thermal loads, which can be the basis for optimization of equipment for producing extruded thermoelectric material.

Physical, mathematical and computer extrusion models

To build a computer model of the hot extrusion process, the application package of object-oriented simulation Comsol Multiphysics was used [5]. In extrusion processes, the initial billets of material are deformed in a hot solid state under practically ideal plastic conditions. Such processes can be simulated using the hydrodynamic theory, where a material is regarded as a fluid of high viscosity which is a function of velocity and temperature. The internal friction of the moving layers of material serves as a heat source; therefore, heat transfer equations are also used in conjunction with the hydrodynamic aspect of the problem. This approach is especially effective for simulating the extrusion of thermoelectric materials in the presence of large strains. In addition, the developed computer model allows one to determine stress distribution in the matrix due to external pressure and thermal loads.

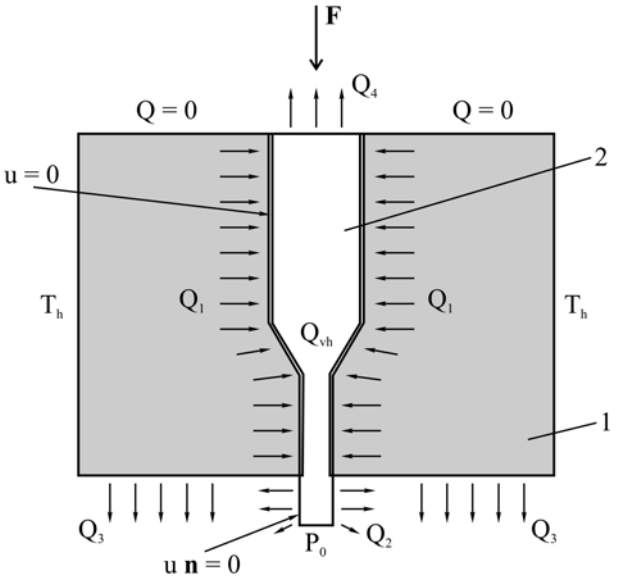

Fig. 1. Physical model of extrusion process

The physical model of the extrusion process is shown in Fig. 1. The model considers the stationary case of flow through matrix 1 of the cylindrical billet of material 2 obtained by cold pressing.

To find the distributions of velocities and temperatures, one should solve the following system of equations [5]

$$\rho(u\cdot\nabla u)=\nabla\left[-pI+\eta(\nabla u+(\nabla u)^T)-\frac{2}{3}\eta(\nabla\cdot u)I\right]+F;$$
$$\nabla\cdot(\rho u)=0; \qquad (1)$$
$$\rho C_p u\cdot\nabla T=\nabla\cdot(\kappa\nabla T)+Q_{vh};$$
$$Q_{vh}=\eta(\nabla u+(\nabla u)^T-\frac{2}{3}(\nabla\cdot u)I):\nabla u.$$

with the corresponding boundary conditions:

- thermostated lateral surface of matrix: $T = T_h$,
- convective heat exchange of the lateral surface of sample after leaving the matrix

$$-n\cdot(-\kappa\nabla T)=h_2(T-T_0),$$

- heat removal along structural members, not shown in Fig.1, from lower matrix part and upper part of thermoelectric material billet:

$$-n\cdot(-\kappa\nabla T)=h_3(T-T_0),\ -n\cdot(-\kappa\nabla T)=h_4(T-T_0),$$

- thermal insulation of upper matrix part:

$$-n\cdot(-\kappa\nabla T)=0,$$

- input pressure on the billet: $p = p_1$,
- atmospheric pressure at sample exit from the matrix: $p = p_0 = 1$ atm,
- equality to zero of fluid velocity at the boundary of contact with the matrix: $u = 0$,
- equality to zero of liquid velocity component perpendicular to the lateral side of the sample after leaving the matrix $u\ n = 0$,

where: u is velocity field, ρ is density, p is pressure, η is dynamic viscosity factor, κ is thermal conductivity, F is vector field of mass forces, Qvh is volumetric heat source due to internal friction, I is unit matrix, h_2 - h_4 are heat exchange coefficients, T_0 is ambient temperature.

Heating due to internal friction and contact thermal resistance at the boundary of contact between material and matrix are taken into account. The properties of thermoelectric material and matrix material used in simulation are given in Table 1.

Table 1

Material properties

1.	Thermoelectric material	Thermal conductivity, W/(m*K)	4
		Density, kg/ m ^{3}	7600
		Heat capacity, J/(kg*K)	150
2.	Steel (matrix)	Thermal conductivity, W/(m*K)	24.3
		Density, kg/ m ^{3}	7850
		Heat capacity, J/(kg*K)	500

The properties of thermoelectric material, which in simulation is considered to be a high-viscosity fluid, were determined experimentally, and their correlation was verified with the published data. For this model, it was necessary to determine the equivalent viscosity of the test fluid. The equivalent von Mises stresses can be found from the general deviator stress tensor [5] as

$$\sigma_{eqv}=\sqrt{\frac{3}{2}\tau:\tau}$$

or, using $\tau=2\eta\dot{\varepsilon}$, where $\dot{\varepsilon}$ is strain rate, η is velocity, as

$$\sigma_{eqv}=\sqrt{6\eta^2\varepsilon:\varepsilon}\ . \qquad (3.2)$$

Representing the equivalent strain rate as

$$\phi_{eqv}=\sqrt{\frac{3}{2}\varepsilon:\varepsilon}$$

the expression (3.2) can be re-written as

$$\sigma_{eqv}=3\eta\phi_{eqv}\ .$$

Strain rate tensor is determined as follows

$$\dot{\varepsilon} = \frac{\nabla u + (\nabla u)^T}{2} = \frac{1}{2}\dot{\gamma}.$$

Shear velocity:

$$\dot{\gamma} = |\dot{\gamma}| = \sqrt{\frac{1}{2}\dot{\gamma} : \dot{\gamma}}.$$

Accordingly,

$$\phi_{eqv} = \frac{1}{\sqrt{3}}\dot{\gamma}.$$

Flow rule

$$\sigma_{eqv} = \kappa_f$$

The flow rule specifies that plastic flow occurs when the equivalent stress σ_{eqv} reaches the flow stress, κf. Viscosity is defined as

$$\eta = \frac{\kappa_f}{3\phi_{eqv}}$$

The magnitude of the total flow stress is given by the expression for the generalized Zener-Hollomon function

$$\eta = \frac{asinh\left(\left(\frac{Z}{A}\right)^{1/n}\right)}{\sqrt{3}\alpha\dot{\gamma}}$$

where: A = 2.39*10^8 1/s, n = 2.976, α = 0.052 1/MPa, $Z = \frac{1}{\sqrt{3}}\dot{\gamma}e^{\left(\frac{Q}{RT}\right)}$, Q=153kJ/mole, R=8.314 J/K*mole [5].

Fig. 2 shows a mesh of finite element method which is used in Comsol Multiphysics.

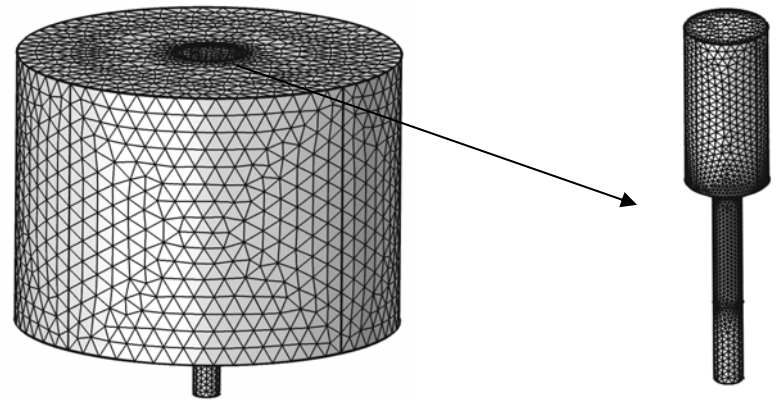

Fig. 2. Finite-element method mesh.

Computer simulation results

Velocity fields and temperature distributions in the matrix and thermoelectric material obtained by computer simulation for different matrix configurations (angles γ) are shown in Fig. 3-6. The velocity in mm/min and temperature in degrees Celsius are marked in colour.

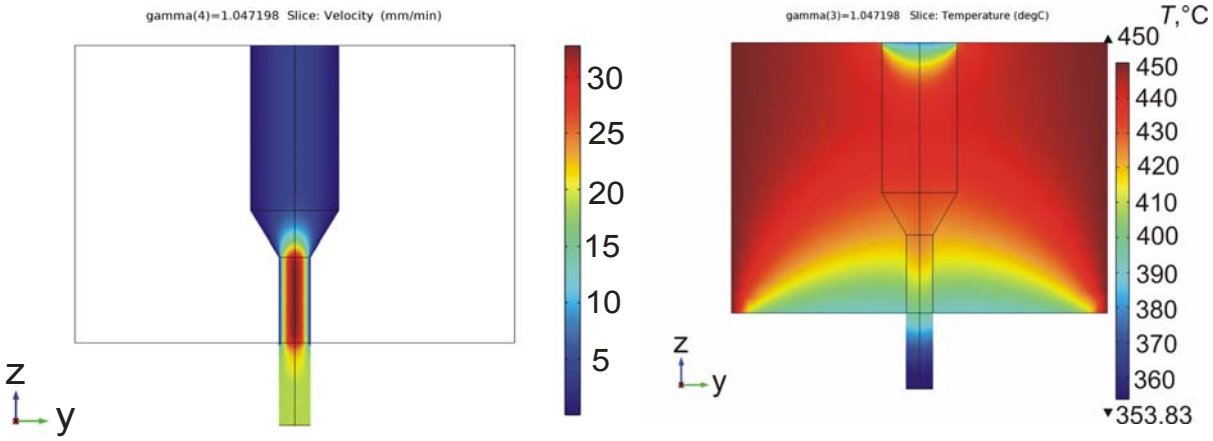

a) *b)*

Fig. 3. Velocity field (a) of thermoelectric material inside the matrix and temperature distribution (b) in material and matrix (γ = 30°)

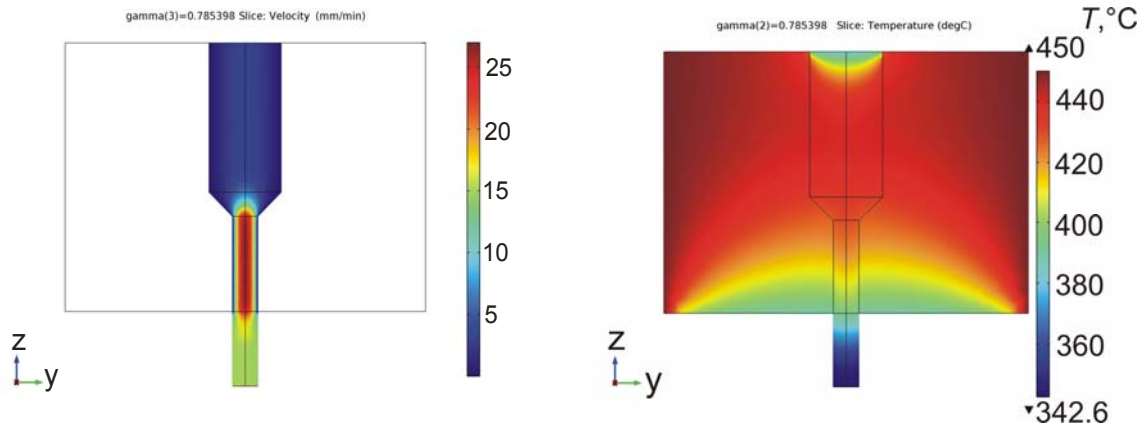

a) *b)*

Fig. 4. Velocity field (a) of thermoelectric material inside the matrix and temperature distribution (b) in material and matrix (γ = 45°)

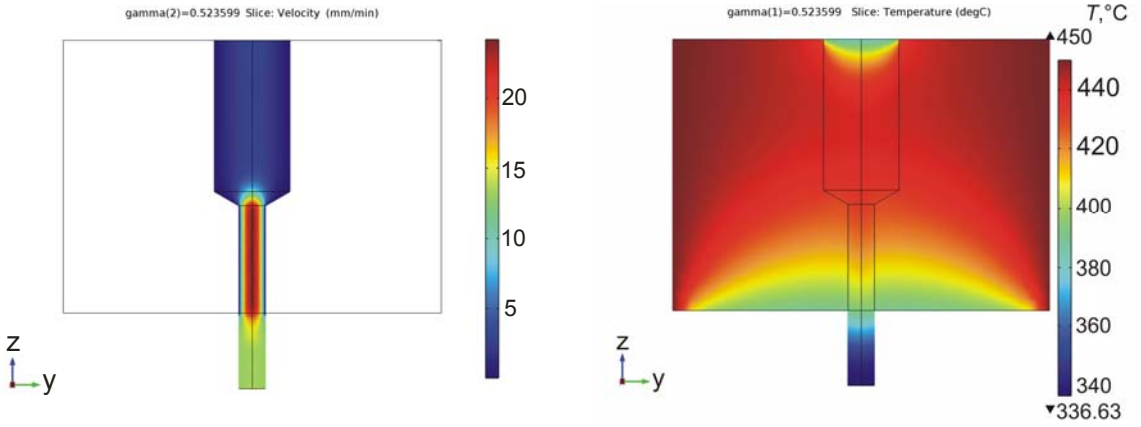

a) *b)*

Fig. 5. Velocity field (a) of thermoelectric material inside the matrix and temperature distribution (b) in material and matrix (γ = 60°)

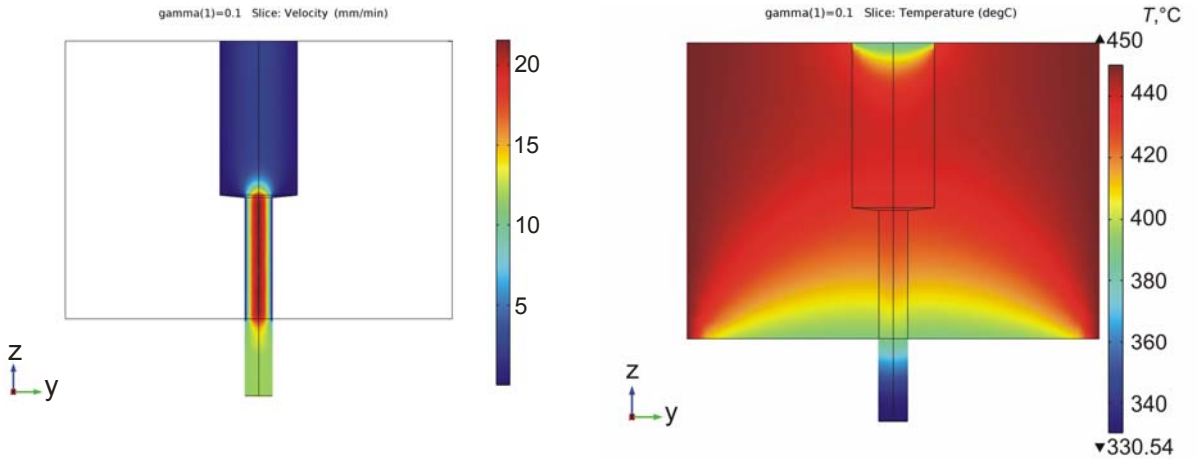

a) *b)*

Fig. 6. Velocity field (a) of thermoelectric material inside the matrix and temperature distribution (b) in material and matrix (γ = 90°)

Matrix configuration for the case of three-stage extrusion is shown in Fig. 7.

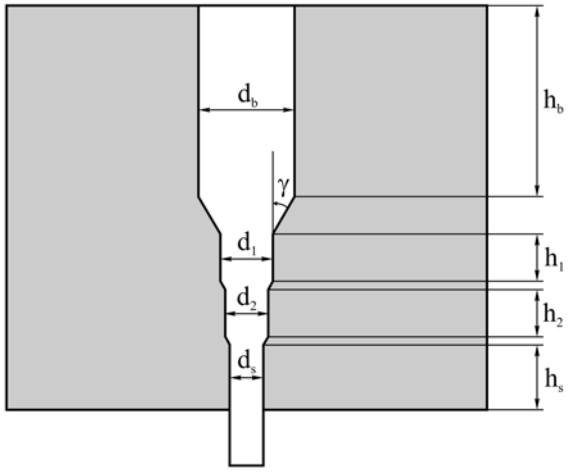

Fig. 7. Matrix for three-stage extrusion of thermoelectric material

Velocity field and temperature distribution for this case are shown in Fig.8.

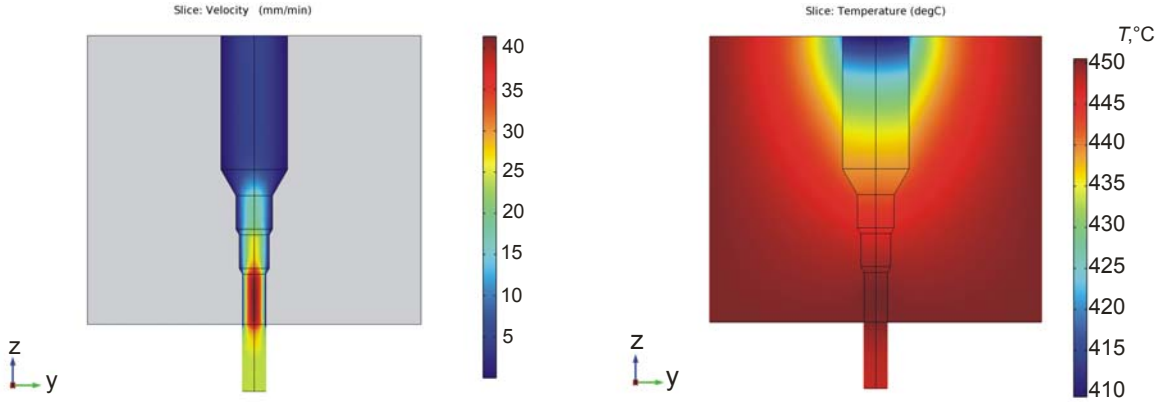

a) *b)*

Fig. 8. Velocity field (a) of thermoelectric material inside the matrix and temperature distribution (b) in material and matrix for the case of three-stage extrusion

The developed computer model can serve the basis for optimizing the design of equipment for extrusion of Bi_2Te_3 based thermoelectric material in order to improve its efficiency and to enhance the quality of the material obtained.

Conclusions

1. A computer model of the hot extrusion process of Bi_2Te_3 based thermoelectric material has been created which can be used to study the distributions of temperature and material flow velocity in the matrix, as well as stress distribution in the matrix due to external pressure and thermal loads.
2. The temperature and velocity field distributions have been obtained depending on matrix configuration for the case of single-stage extrusion of Bi_2Te_3 based thermoelectric material.
3. The behavior of thermoelectric material in its passage through the matrix for the case of multistage extrusion of Bi_2Te_3 based thermoelectric material has been studied.

References

1. Bulat L. P. (2002). *Thermoelectric cooling*. St.-Petersburg: St.-Petersburg State Academy of Cool and Food Technologies.
2. Sabo E. P. (2006). Technology of chalcogenide thermoelements. Physical fundamentals. *J.Thermoelectricity*, 1, 45-66.
3. *Patent of RF 2475333 C1* (2011). Sorokin A.I., Parkhomenko Yu.N., Osvenskyi V.B., Lavrentiev M.G., Karataiev V.V., Drabkin I.A. Extrusion process of thermoelectric material based on bismuth and antimony chalcogenides [in Russian]. .
4. Lavrentiev M.G., Osvenskyi V.B., Mezhennyi M.V., Prostomolotov A.I., Bublik V.T., Tabachkova N,Yu. (2012). Teoreticheskoie i eksperimentalnoie issledovaniie formirovaniia struktyry termoelektricheskogo materiala na osnove tverdykh rastvorov (Bi, $Sb)_2Te_3$ poluchennogo metodom goriachei ekstruzii [Theortical and experimental research on the formation of structure of thermoelectric material based on (Bi, $Sb)_2Te_3$ solid solutions obtained by hot extrusion method. XIII Interstate Workshop “Thermoelectrics and Their Applications” (St.Petersburg, Russia, 2012).
5. Fluid-structure interaction in aluminum extrusion (2008). *Structural Mechanics Module Model Library.* COMSOL AB, p. 301-316.

Submitted 25.02.2019

Лисько В.В. *канд. фіз.– мат. наук* [1,2]

[1]Інститут термоелектрики НАН і МОН України,
вул. Науки, 1, Чернівці, 58029, Україна, *e-mail: anatych@gmail.com*;
[2]Чернівецький національний університет імені Юрія Федьковича,
вул. Коцюбинського 2, Чернівці, 58012, Україна

НАБЛИЖЕННЯ В’ЯЗКОЇ РІДИНИ ПРИ МОДЕЛЮВАННІ ПРОЦЕСУ ЕКСТРУЗІЇ ТЕРМОЕЛЕКТРИЧНОГО МАТЕРІАЛУ НА ОСНОВІ Bi_2Te_3

У процесі екструзії заготовки матеріалу деформуються в практично ідеально пластичних умовах. Такий процес може бути змодельований з використанням теорії гідродинаміки, де матеріал розглядається як рідина з дуже високою в'язкістю, що залежить від швидкості й температури. Внутрішнє тертя шарів, що рухаються, матеріалу є також джерелом тепла, тому необхідно використовувати також рівняння переносу тепла в сукупності з гідродинамічною частиною задачі. Такий підхід є особливо ефективним для моделювання процесу екструзії термоелектричних матеріалів, коли присутні більші деформації. У даній роботі наведено результати об'єктно-орієнтованого комп'ютерного моделювання процесу гарячої екструзії термоелектричного матеріалу на основі Bi_2Te_3. Розглянуто випадки одержання циліндричних зразків круглого перерізу для різних конфігурацій матриці у процесах одноступінчастої та багатоступінчастої екструзії. Отримані розподіли температури й швидкості течії матеріалу в матриці, а також розподіл напруг у матриці за рахунок зовнішнього тиску й теплових навантажень лягли в основу оптимізації устаткування для одержання екструдованого термоелектричного матеріалу. Бібл. 5, рис. 8, табл. 1.
Ключові слова: екструзія, термоелектричний матеріал,моделювання

Лысько В.В., *канд. физ – мат. наук,*[1,2]

[1]Институт термоэлектричества НАН и МОН Украины,
вул. Науки, 1, Черновцы, 58029, Украина;
[2]Чернивецький национальный университет
им. Юрия Федьковича, ул. Коцюбинского 2,
Черновцы, 58000, Украина, *e-mail: anatych@gmail.com*

ПРИБЛИЖЕНИЕ ВЯЗКОЙ ЖИДКОСТИ ПРИ МОДЕЛИРОВАНИИ ПРОЦЕССА ЭКСТРУЗИИ ТЕРМОЭЛЕКТРИЧЕСКОГО МАТЕРИАЛА НА ОСНОВЕ Bi_2Te_3

В процессе экструзии заготовки материала деформируются в практически идеальных пластических условиях. Такой процесс может быть смоделирован с использованием теории гидродинамики, где материал рассматривается как жидкость с очень высокой вязкостью, зависящей от скорости и температуры. Внутреннее трение движущихся слоев материала служит в качестве источника тепла, поэтому необходимо использовать также уравнения переноса тепла в совокупности с гидродинамической стороной задачи. Такой подход является особенно эффективным для моделирования процесса экструзии термоэлектрических материалов, когда присутствуют большие деформации. В настоящей работе приведены результаты объектно-ориентированного компьютерного моделирования процесса горячей экструзии термоэлектрического материала на основе Bi_2Te_3. Рассмотрены случаи получения цилиндрических образцов круглого сечения для различных конфигурации матрицы при одноступенчатой и многоступенчатой экструзии. Получены распределения температуры и скорости течения материала в матрице, а также распределения напряжений в матрице за счет внешнего давления и тепловых нагрузок, которые легли в основу оптимизации оборудования для получения экструдированного термоэлектрического материала. Библ. 5, рис. 8, табл. 1.
Ключевые слова: экструзия, термоэлектрический материал, моделирование.

References

1. Bulat L. P. (2002). *Thermoelectric cooling*. St.-Petersburg: St.-Petersburg State Academy of Cool and Food Technologies.
2. Sabo E. P. (2006). Technology of chalcogenide thermoelements. Physical fundamentals. *J.Thermoelectricity*, 1, 45-66.
3. *Patent of RF 2475333 C1* (2011). Sorokin A.I., Parkhomenko Yu.N., Osvenskyi V.B., Lavrentiev M.G., Karataiev V.V., Drabkin I.A. Extrusion process of thermoelectric material based on bismuth and antimony chalcogenides [in Russian]. .
4. Lavrentiev M.G., Osvenskyi V.B., Mezhennyi M.V., Prostomolotov A.I., Bublik V.T., Tabachkova N,Yu. (2012). Teoreticheskoie i eksperimentalnoie issledovaniie formirovaniia struktyry termoelektricheskogo materiala na osnove tverdykh rastvorov (Bi, $Sb)_2Te_3$ poluchennogo metodom goriachei ekstruzii [Theortical and experimental research on the formation of structure of thermoelectric material based on (Bi, $Sb)_2Te_3$ solid solutions obtained by hot extrusion method. XIII Interstate Workshop “Thermoelectrics and Their Applications” (St.Petersburg, Russia, 2012).
5. Fluid-structure interaction in aluminum extrusion (2008). *Structural Mechanics Module Model Library.* COMSOL AB, p. 301-316.

Submitted 25.02.2019

V.A.Romaka, *doc. techn. sciences, professor*[1]
Yu.V. Stadnyk, *cand. chem. of science*[2]
L.P. Romaka, *cand. chem. of science*[2]
V.Ya.Krayovskyy, *doc. technic sciences*[1],
V.V.Romaka, *doc. techn. sciences, cand. chem. of science, dochent* [1,3]
A.M. Horyn, *cand. chem. of science*[3],
M. B. Konyk, *cand. chem. of science, dochent*[2],
I.M. Romaniv[2], **M. V. Rokomanuk**[1]

[1]National University "Lvivska Politechnika", 12, S. Bandera Str., Lviv, 79013, Ukraine;
e-mail: vromaka@polynet.lviv.ua
[2]Ivan Franko National University of Lviv, 6, Kyryla and Mefodiya Str., Lviv, 79005, Ukraine;
e-mail: lyubov.romaka@lnu.edu.ua,
[3]Institute for Solid State Research, IFW-Dresden, Helmholtzstr. 20, 01069 Dresden, Germany.

FEATURES OF STRUCTURAL, ENERGY, ELECTROKINETIC AND MAGNETIC CHARACTERISTICS OF $Ti_{1-x}Sc_xCoSb$ THERMOELECTRIC MATERIAL

The crystalline and electronic structures, electrokinetic, energy and magnetic characteristics of the $Ti_{1-x}Sc_xCoSb$ thermoelectric material were investigated in the ranges T=80–400 K, x=0.005–0.15. Mechanisms of simultaneous generation of structural defects of the acceptor and donor nature were established. It was shown that the structure of TiCoSb basic compound is defective, comprising defects of the donor and acceptor nature as a result of location in the tetrahedral voids of additional Co atoms and the presence of vacancies at the 4a position of Ti atoms. The introduction of impurity Sc atoms into TiCoSb compound by substitution at the 4a position of Ti atoms generates the acceptor defects, and the ratio of concentrations of available donors and generated acceptors determines the position of the Fermi level ε_F, type, and the mechanisms of conduction for $Ti_{1-x}Sc_xCoSb$. Bibl. 12, Fig. 8.*
Key words: electronic structure, electrical resistivity, Seebeck coefficient.

Introduction

Semiconductor thermoelectric materials based on the *TiCoSb* half-Heusler phase have high efficiency of thermal energy into electrical energy conversion [1 – 8]. In the above mentioned works, the optimization of the parameters of thermoelectric materials to obtain the maximum values of thermoelectric figure of merit [9] was performed by doping the *TiCoSb* semiconductor, owing to which the resulting materials become heavilydoped and strongly compensated semiconductors [10].

The authors of [1–8] predicted that structural defects of the donor nature will be generated in the crystals of $TiCo_{1-x}Ni_xSb$, $TiCo_{1-x}Cu_xSb$, $Ti_{1-x}V_xCoSb$ and $Ti_{1-x}Mo_xCoSb$ semiconductor solid solutions, since *Ni*($3d^8 4s^2$) and *Cu* ($3d^{10}4s^1$) atoms have more 3*d*-electrons than *Co*($3d^7 4s^2$), and *V* ($3d^3 4s^2$) and *Mo*($4d^5 5s^1$) atoms have more 3*d*-electrons than *Ti* ($3d^2 4s^2$). However, in the course of experimental studies, it was found that the results of simulating the energy and kinetic characteristics of the above materials do not agree with the

(experimental) measurement results. Such a discrepancy does not allow predicting and obtaining material with pre-assigned characteristics, due to which they were excluded from the number of promising thermoelectric materials. Inparticular, introductionof *V*, *Mo* and *Ni* atoms in to the structure of *TiCoSb* compound was accompanied by a simultaneous generation of structural defects of the acceptor and donor nature whose ratios determine the kinetic properties of thermoelectric material.

The question arises as to thenature of the acceptors in the above semiconductors.

The authors of [5] assumed that the structure of *TiCoSb* basic semiconductor is defective and comprises at the 4*a* position of *Ti* atoms the vacancies which will be further denoted by, which, in fact, generates acceptors.Moreover, it was notex cluded that impurity atoms will occupy other positions which will also generate acceptors. For instance, on introducing to the structure of *TiCoSb* compound of *V* atoms by substituting at the 4*a* position of *Ti* atoms, which generates donors, there may beal so a simultaneous partial occupation by *V* atoms of the 4*c* crystallographic position of *Co* atoms, which will result in generating structural defects of the acceptor nature (*V* atom has a smaller number of 3*d*-electrons than *Co* atom).

The importance of understanding the structural and energy features of *TiCoSb* basic semiconductor is crucial because it gives a vision of ways to optimize the characteristics of a thermoelectric material by doping with a certain type and concentration of impurities. After all, a prerequisite for achieving maximum efficiency of thermal into electrical energy conversion is doping of material with a type of impurity that coincides with the type of majority carriers of the basic semiconductor array, when the Fermi level ε_F approaches the percolation level of the continuous energy band [11].

In this context, it is interesting to investigate $Ti_{1-x}Sc_xCoSb$ thermoelectric material obtained by substituting *Ti* atoms with *Sc* atoms ($3d^14s^2$) at the 4*a* position. In this case, structural defects of the acceptor nature must be generated in the crystal, since *Sc* atom has fewer *3d*-electrons. In turn, electrokinetic studies will confirm whether a solid substitutional solution is being realized, that is, whether the conductivity type of $Ti_{1-x}Sc_xCoSb$semiconductor will change from electron to hole. The investigations pursued will give insight into the nature of defects of *TiCoSb*basic semiconductor, which will make the process of optimization of the characteristics of thermoelectric material predictable.

Investigation procedures

The object to be investigated included crystalline structure, electronic density distribution (DOS), the magnetic, thermodynamic, kinetic and energy characteristics of $Ti_{1-x}Sc_xCoSb$. The samples of $Ti_{1-x}Sc_xCoSb$ so lid solution were sun the sized by melting the chargeo finitial components in the electrical coven in the inerter go at most here with subsequent homogenizing annealing for 720 hours at a temperature of 1073 K. Diffraction data arrays were obtained with the use of Guinier-Huberpowder diffractometer (imageplatesystem, $CuK\alpha_1$ radiation). Crystallographic parameters were calculated by means of Fullprof program [12]. The chemical and phase compositions of the samples were controlled by microprobe analyzer (EPMA, energy-dispersive *X* – ray analyzer). The electronic structure of $Ti_{1-x}Sc_xCoSb$ was simulated by the Green-function method (the Korringa-Kohn-Rostoker (KKR) method) in coherent potential approximation (CPA) and local density approximation (LDA) [13]. For calculations by KKR method use was made oflicensed soft ware AkaiKK at the 4*a* position R and SPR-KKR in LDA for Moruzzi-Janak-Williams (MJW) exchange-correlation potential with parameterization [14]. The Brillouin zone was broken into 1000 *k*-points which were used for simulation of energy characteristics by calculating DOS. The width of the energy window was 22 e *V* and was chosen to capture all semi-corestates of *p*-elements. For calculations by linear muffin-tin orbital (LMTO) use was made of full potential (FP) in the representation of plane waves. The LDA approximation with MJW parameterization was also use dasex change-correlation potential. The accuracy of calculating the position of the Fermi level ε_F= ±6meV. The

temperature and concentration dependences of the electrical resistivity (ρ) and the Seebeck coefficient (α) with respect to copper and magnetic susceptibility (χ) (Faraday's method) of $Ti_{1-x}Sc_xCoSb$ samples in the ranges: T = 80–400 K, $N_A^V \approx 9.5 \cdot 10^{19}$ cm^{-3}–$1.9 \cdot 10^{21} \cdot$cm^{-3} (x = 0.005–0.10).

However, at temperatures T> 400 K, the solubility of *Sc* atoms increases, and the change in the free energy values ΔG *(x)* (Helmholtz potential) at a temperature T = 800 K passes through the minimum in the concentration range x≈0.35 (Fig. 1*a*, curve 5). Therefore, the compositions of $Ti_{1-x}Sc_xCoSb$, x = 0–0.15 samples under study are within the solubility range, as also evidenced by the absence of extraneous phases therein.

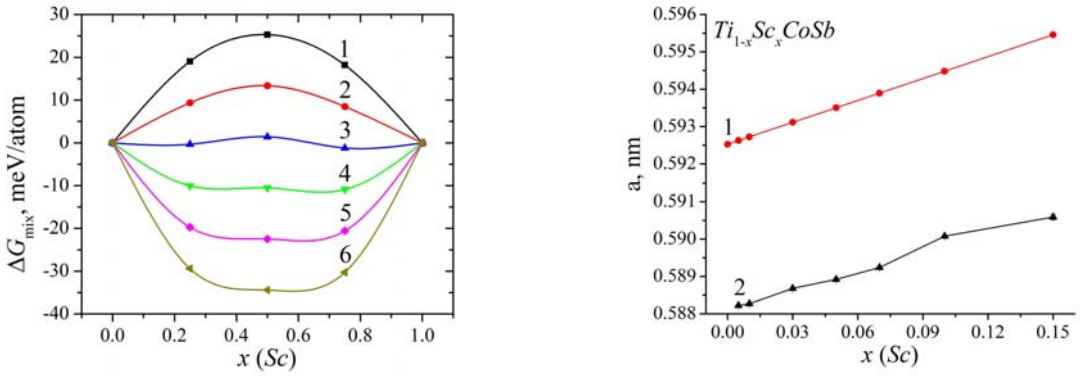

a) *b)*

Fig. 1. Change in the values of thermodynamic potential ΔG(x) at different temperatures (a): 1 – 0 K; 2 – 200 K; 3 – 400 K; 4 – 600 K; 5 – 800 T; 6 – 1000Kand unit cell period a(x) of $Ti_{1-x}Sc_xCoSb$: 1 – simulation, 2 – experiment(b)

Taking into account that the atomic radius of *Sc* (*rSc* = 0.164 nm) is larger than that of *Ti* (*rTi* = 0.146 nm), it is logical to increase the values of the elementary cell period *a*(*x*) of $Ti_{1-x}Sc_xCoSb$ (Fig. 1b). Such a behavior of the value of period *a(x)* may indicate the realization of a solid $Ti_{1-x}Sc_xCoSb$ substitutional solution and at the 4*a* position of *Ti* atoms structural defects of the acceptor nature will be generated. In so doing, in the band gap ε_g of semiconductor solid solution $Ti_{1-x}Sc_xCoSb$ the impurity acceptor zone ε_A^{Sc} ε_A^{Sc} will be formed.

The refinement of the crystalline structure of the $Ti_{1-x}Sc_xCoSb$ in vestigated phases allowed us to obtain the values of the Bragg discrepancy factor (R_{Br}) between the model representation of the structure and the experimental results, which showed high accuracy and quality of the simulation process, in particular: R_{Br}= 3 % for x = 0.005, R_{Br} = 1.5 % for x = 0.03, R_{Br} = 2.6 % for x = 0.05, R_{Br} = 3.5 % for x = 0.07 and R_{Br} = 3.7 % for x = 0.10. With regard to the small number of impurity *Sc* atoms dissolved in the *TiCoSb* compound array, and the low accuracy of the X-ray method, we were unable to detect any other structural changes in structural studies, such as the occupation by impurity atoms of other crystallographic positions or vacancies.

We also simulated a change in the values of the unit cell period *a*(*x*) of $Ti_{1-x}Sc_xCoSb$ provided that all crystallographic positions of *TiCoSb* compound are occupied in accordance with the structural type *MgAgAs* [15], and impurity *Sc* atoms will displace *Ti* atom sat the 4*a* position. If we compare the experimentally obtained change in the values of period *a*(*x*) of $Ti_{1-x}Sc_xCoSb$(Fig. 1b, curve 2) with the course of dependence *a(x)* obtained by calculations (Fig. 1*b*, curve 1), then the curves are close to parallel. The result, at first glance, is amazing. If the course of the calculated and experimentally obtained dependences *a*(*x*) of $Ti_{1-x}Sc_xCoSb$ do not coincide, then this may indicate the inability to take into account all the features of the structure when modeling. This is normal! However, the values of the periods *a*(*x*) for

TiCoSb basic compound, to which the impurity *Sc* atoms are introduced, do not essentially coincide, forming $Ti_{1-x}Sc_xCoSb$ semiconductor solid solution.

What is the reason for this and why are the experimentally obtained $a(x)$ values of *TiCoSb* less than the calculated ones?

We believe that the difference in the values of period $a(x)$ is a manifestation of vacancies in the structure of *TiCoSb* compound, which reduces its volume and, accordingly, the value of period $a(x)$. This conclusion is consistent with that previously obtained in [5]. If we conventionally combine the values of the period $a(x)$ of *TiCoSb* compound obtained experimentally (Fig. 1b, curve 2) with the value obtained by the simulation (Fig. 1b, curve 1), then the dependences $a(x)$ of $Ti_{1-x}Sc_xCoSb$ coincide within the experiment accuracy.

Consequently, structural studies of $Ti_{1-x}Sc_xCoSb$ semiconductor solid solution suggest the ordering of its crystalline structure, and substitution at the 4*a*position of *Ti* atoms with *Sc* will generate structural defects of the acceptor nature.

Research on the electronic structure of $Ti_{1-x}Sc_xCoSb$

To predict the behavior of the Fermi level ε_F, the band gap ε_g and the kinetic characteristics of $Ti_{1-x}Sc_xCoSb$, the electron density (DOS) distribution (Fig. 2) was calculated for an ordered variant of the structure in which *Ti* atoms at the 4*a*position are substituted with *Sc.*

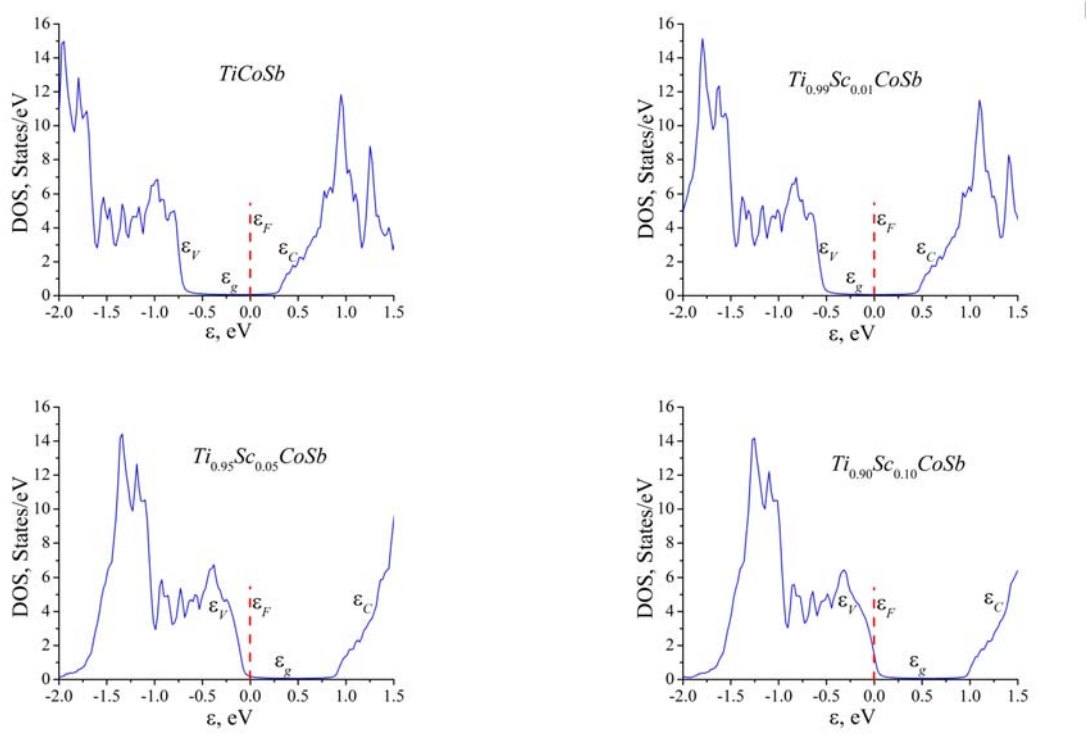

Fig. 2. Distribution of the electron density of states DOSof $Ti_{1-x}Sc_xCoSb$for the ordered structure

As can be seen from Fig. 2, in the *TiCoSb* half-Heusler phase, the Fermi level ε_F (dashed line) is located in the band gap ε_g near its middle, but closer to the percolation level of the conduction band ε_C. Since the replacement of *Ti* atoms with *Sc* generates structural defects of the acceptor nature, already at $Ti_{0.99}Sc_{0.01}CoSb$ concentration, the Fermi level ε_F will drift from the conduction band ε_C and take a position in the mid gap ε_g. At higher concentrations of the acceptor impurity, the concentration of acceptors will increase, and the Fermi level ε_F will approach and subsequently intersect the percolation level of the

valence band ε_V of $Ti_{1-x}Sc_xCoSb$: there will be a dielectric-metal conductivity transition, which is the Anderson transition [16]. Approximation of the Fermi level ε_F to the percolation level of the valence band ε_V will change the sign of the Seebeck coefficient $\alpha\ (T, x)$ from negative to positive, and the intersection by the Fermi levels ε_F of the percolation level of the valence band ε_V will change the conductivity of $Ti_{1-x}Sc_xCoSb$ semiconductor from activation to metallic [10,16]: the activation regions will disappear on the dependences ln(ρ (1 / T) and the resistance values ρ will increase with temperature. The change in the density of states at the Fermi level $g(\varepsilon_F)$ is slower.

The distribution of the electron localization function *(elf)* in $Ti_{1-x}Sc_xCoSb$ solid solution (Fig. 3) indicates that there is a strong localization in *TiCoSb* compound between *Co* and *Sb* atoms, whereas around *Ti* atoms there is a more closed spherical shell. Substitution at the 4*a*position of *Ti* atoms with *Sc* reduces the localization of the electron density around *Co* atoms in the direction of *Sc* atoms and slightly affects the electron density distribution between *Co* and *Sb* atoms.

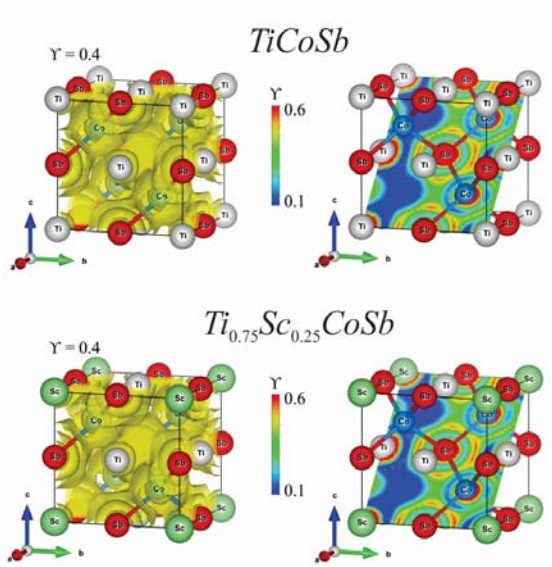

Fig. 3. Distribution of the values of electron localization function (γ=0,4) in plane [101] and electron density isosurface(0,053 e/(103 nm^3)) forTiCoSbandTi$_{0.75}$Sc$_{0.25}$C0Sb

The DOS electronic state density distribution for the ordered $Ti_{1-x}Sc_xCoSb$ structure allows simulating the behavior of the resistivity, the Seebeck coefficient α(*x*, *T*), thermoelectric power Z*, etc. (Figs. 4, 5*a*). Simulating the behavior of the Seebeck coefficient α(x,T) yields, as expected, positive values at all concentrations and temperatures, and maximum values of α(x,T) are achieved at concentration $x \approx 0.08$. In the range of concentrations of *Sc* atoms, $x \approx 0.08$–0.11, maximum values of the thermoelectric power factor Z* calc are predicted (Fig. 4*b*).

Fig. 5*a* shows a dependence inverse to the density of states at the Fermi level $g(\varepsilon_F)$, whose values are proportional to the electrical resistivity of the thermoelectric material $Ti_{1-x}Sc_xCoSb$. It can be seen that the dependence $1/g(\varepsilon_F)$ passes through the maximum at the concentrations of *Sc* atoms, x≈0.01, and then decreases rapidly and reaches quasi-saturation at x > 0.10.This behavior of $1/g(\varepsilon_F)$ is understandable, since the increase in the dependence on the plot x = 0–0.10 is related to the intersection by the Fermi level ε_F of the mid gap, which causes the smallest values of $g(\varepsilon_F)$ and the maximum values of the semiconductor electrical resistance. At higher concentrations of *Sc*, x > 0.01, the Fermi level ε_F will approach the percolation level of the valence band ε_V, leading to the appearance and growth of the concentration of free holes, as well as the density of states at the Fermi level $g(\varepsilon_F)$. Experimental studies of the magnetic, kinetic, and energy characteristics of a $Ti_{1-x}Sc_xCoSb$ solid solution will show the correspondence of these

calculations to the real processes in thermoelectric material.

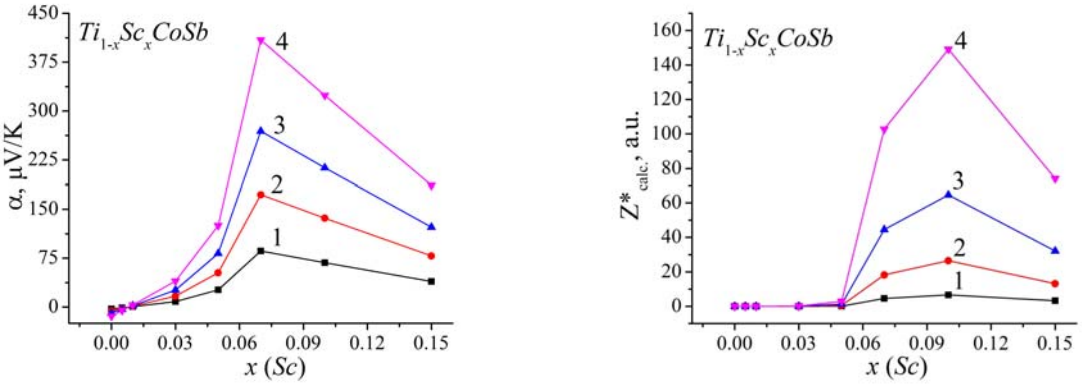

a *b*

Fig. 4. Simulation of change in the values of the Seebeck coefficient α(x,T) at temperatures: 1 – 80 K; 2 – 160 K; 3 – 250 K; 4 – 380 K(a) and thermoelectric power factor $Z^*_{calc.}$(b) of $Ti_{1-x}Sc_xCoSb$for the ordered structure

Research on magnetic susceptibility of $Ti_{1-x}Sc_xCoSb$

Interesting are the results of measuring magnetic susceptibility χ of thermoelectric material $Ti_{1-x}Sc_xCoSb$ (Fig. 5*b*), which are basically consistent with the results of simulating the electronic structure of a semiconductor. Studies have shown that $Ti_{1-x}Sc_xCoSb$ samples, x > 0.005, are Pauli paramagnetics in which the magnetic susceptibility χ is determined solely by electron gas and is proportional to the Fermi density of states $g(\varepsilon_F)$.

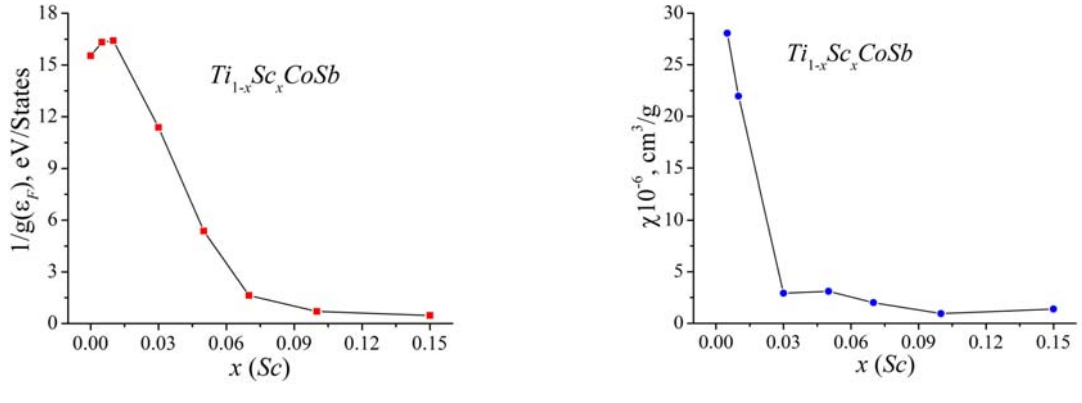

a) *b)*

Fig. 5. Simulation of change in the values $1/g(\varepsilon_F)$ (a) and experimental dependence of magnetic susceptibility χ(x) at temperature T=300 K(b) of $Ti_{1-x}Sc_xCoSb$

As can be seen from Fig. 5*b*, the dependence χ (*x*) at *x* > 0.03 rapidly changes the slope, enters the plateau and is almost unvaried up to *x* = 0.15. That is, the increase in the concentration of the acceptor impurity and the possible increase in the concentration of free holes little changes the value of the state density at the Fermi level $g(\varepsilon_F)$. Such behavior of χ (*x*) (χ ~ *g* (ε_F)) is possible, provided that the Fermi level ε_F intersects the percolation level of valence band $\varepsilon_V Ti_{1-x}Sc_xCoSb$ with subsequent drift over the continuous energy band, as shown by the DOS simulation results (Fig. 2).

Researchon the electrokinetic and energy characteristics of $Ti_{1-x}Sc_xCoSb$

The temperature and concentration dependences of the resistivity ρ and the Seebeck coefficient α of $Ti_{1-x}Sc_xCoSb$ are shown in Figs. 6 and 7.

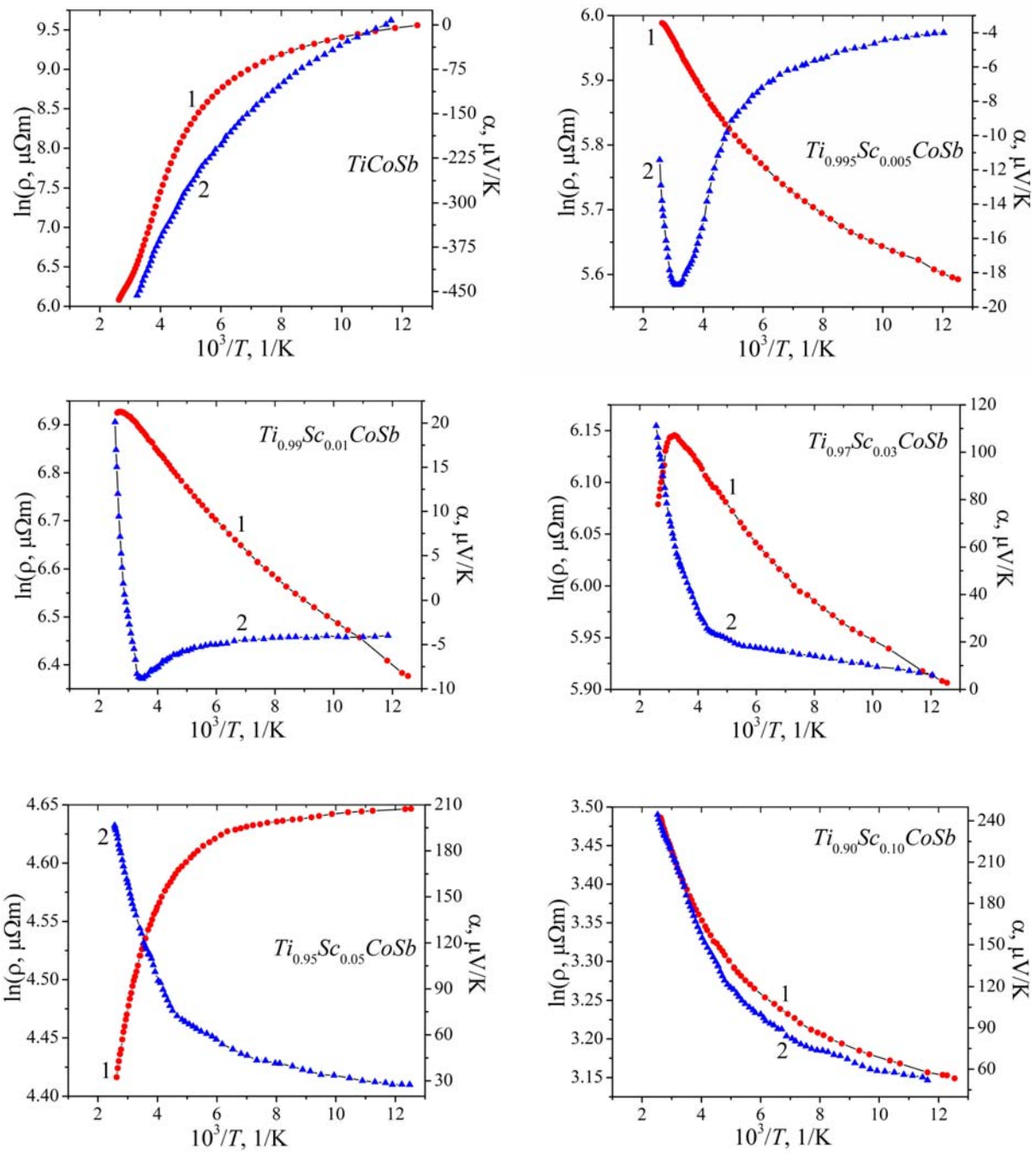

Fig. 6. Temperature dependences of electrical resistivity ln(ρ(1/T)) and the Seebeck coefficient α(1/T) of thermoelectric material$Ti_{1-x}Sc_xCoSb$.

The dependence ln(ρ(1/*T*)) of *TiCoSb* is approximated using the well-known relation [10]:

$$\rho^{-1}(T) = \rho_1^{-1} \exp\left(-\frac{\varepsilon_1^{\rho}}{k_B T}\right) + \rho_3^{-1} \exp\left(-\frac{\varepsilon_3^{\rho}}{k_B T}\right), \quad (1)$$

where the first high-temperature term describes the activation of current carriers ε_1^{ρ}=100.6 mcV from the

Fermi level ε_F to the percolation level of continuous energy bands, and the second, low-temperature term, the hopping conductivity through impurity donor states ε_3^{ρ} = 5.1 mcV. In turn, the temperature dependence of the Seebeck coefficient $\alpha(1/T)$ *TiCoSb* is approximated using the expression [16]:

$$\alpha = \frac{k_B}{e}\left(\frac{\varepsilon_i^{\alpha}}{k_B T} - \gamma + 1\right), \tag{2}$$

where γ is a parameter depending on the nature of scattering. The activation energy ε_1^{α}=214.1 mcV was calculated from the high-temperature region of the α (1/*T*) dependence, which, as shown in [17], is proportional to the amplitude of large-scale fluctuation of continuous-energy bands, and from the low-temperature region, the value of activation energy ε_3^{α}=10.2 mcV, proportional to the modulation amplitude of small-scale fluctuations of heavily doped and strongly compensated semiconductors [10, 17].

The results obtained for *TiCoSb* coincide with those previously obtained in [1–8]. Strong compensation, i.e. close concentration of ionized acceptors and donors, is indicated by the results of studies of the Seebeck coefficient α (Fig. 6). Thus, in the temperature range *T*=80–90 K, *TiCoSb* is a hole-type semiconductor, as evidenced by the positive values of the Seebeck coefficient: $\alpha_{80\ K}$=7.75 mcV/K and α_{90K}=0.71mcV/K. At higher temperatures, the sign of the Seebeck coefficient α ($\alpha_{95\ K}$ = -6.33 mcV/K) changes and electrons become the majority carriers.

Obviously, in the crystal of the *TiCoSb* compound, both donor and acceptor defects are present, generating corresponding donor and acceptor energy levels (zones) in the forbidden zone. At low temperatures, the electron energy is insufficient to flow into the conduction band ε_C (for donor ionization), and impurity acceptor states are small. A temperature of 80 K or less is sufficient for ionization of the acceptors and the holes become the majority carriers. With a rise in temperature, when donor ionization becomes possible, the concentration of electrons and their contribution to conductivity increases. Under these conditions, the Seebeck coefficient changes from positive to negative, and the Fermi level ε_F at $T_{inv.}$≈90 K crosses the mid gap ε_g.

Addition to the *TiCoSb* of the lowest concentration of *Sc* atoms in the experiment by replacing the *Ti* atoms radically changes the behavior of the resistivity *ρ* and the Seebeck coefficientα of $Ti_{0.995}Sc_{0.005}CoSb$. In the 80–350 K temperature range, the resistivity values ρ increase with a rise in temperature, and the conductivity of $Ti_{0.995}Sc_{0.005}CoSb$ is metallic. That is, the addition of the lowest concentration of *Sc* atoms in the experiment (x = 0.005) to be generated by the acceptors changed the position of the Fermi level ε_F in a way that can only cause the appearance of donors in a semiconductor. Thus, if in *TiCoSb* the Fermi level ε_F was in the band gap, then the metallization of the conductivity of $Ti_{0.995}Sc_{0.005}CoSb$ indicates that it not only approached the conduction band, but also crossed its percolation level, and electrons remain the majority carriers. This is indicated by the negative values of the Seebeck coefficient α of $Ti_{0.995}Sc_{0.005}CoSb$. This is only possible if donors of so far unknown nature are generated in a semiconductor.

The metallization of the conductivity of $Ti_{0.995}Sc_{0.005}CoSb$ does not correspond to the results of the simulation of the electronic structure. After all, it was predicted that at the smallest concentration of *Sc* acceptor impurity, the Fermi level ε_F would drift from the conduction band ε_C to the mid gap ε_g.. Therefore, in the high-temperature region of dependence $\ln(\rho(1/T))$ there must be an activation region associated with the thermal throw of electrons from the Fermi level ε_F into the conduction band ε_C, and the value of the electron activation energy ε_1^{ρ} should be greater than in the case of *TiCoSb*.

The discrepancy between the simulation results and the experimental studies of the kinetic characteristics of the semiconductor at the lowest concentration of impurity *Sc*(x = 0.005) can be the result of both the low quality of the synthesized sample and the incomplete consideration of the features of the crystalline structure of $Ti_{0.995}Sc_{0.005}CoSb$ when simulating the characteristics. However, metallographic studies of the $Ti_{1-x}Sc_xCoSb$ samples [18] established their homogeneity and correspondence between the sample composition on the surface and the charge components before synthesis.

On the other hand, the presence of extremes at the temperature of ~ 350 K on the dependences $\ln(\rho(1/T))$ and $\alpha(1/T)$ of $Ti_{0.995}Sc_{0.005}CoSb$ indicates the appearance and participation in semiconductor conduction of free holes, which caused the Fermi level ε_F to return to the band gap ε_g This result is consistent with the simulation results, which provided for the generation of acceptors in the $Ti_{1-x}Sc_xCoSb$ crystal.

At a higher acceptor concentration in the $Ti_{0.99}Sc_{0.01}CoSb$ sample, the dependence $\ln(\rho\ (1/T))$ is similar to that for the $Ti_{0.995}Sc_{0.005}CoSb$ sample, but fundamental changes occurred in the behavior of the Seebeck coefficient $\alpha(1/T)$, which reflects the dynamics of changing the ratio of electrons and holes in the conductivity of a semiconductor. Thus, in the temperature range of 80-350 K, the sign of the Seebeck coefficient is negative, and hence electrons are the majority carriers. However, as can be seen from Fig. 6, the dependence of $\alpha(1/T)$ has a minimum at a temperature of ~ 300 K, following which, with a rise in temperature, the values of the Seebeck coefficient α rapidly decrease in the absolute value and change sign at temperatures $T \geq 340$ K: holes become the majority carriers in $Ti_{0.99}Sc_{0.01}CoSb$. The positive values of the Seebeck coefficient α indicate to this.

This behavior of the Seebeck coefficient is understandable and predictable, since the substitution of *Ti* atoms by *Sc* atoms generates in the crystal structural defects of the acceptor nature. In *TiCoSb* at high temperatures, when all structural defects of both the donor and acceptor nature are ionized, the sign of the Seebeck coefficient α was negative, indicating the predominance of defects of the donor nature over the acceptor. Thus, the substitution of *Ti* atoms with *Sc* at $x = 0.005$ did not radically alter the ratio of donors and acceptors in favor of the latter. However, even at $x = 0.01$ and all higher concentrations of impurity *Sc* atoms introduced into the structure of the *TiCoSb* compound, the number of structural defects of the acceptor nature is outweighed by the number of donors, as indicated by the positive values of the Seebeck coefficient α of $Ti_{1-x}Sc_xCoSb$ at temperatures of 80–400 K. Hence, in $Ti_{0.995}Sc_{0.005}CoSb$ and $Ti_{0.99}Sc_{0.01}CoSb$ semiconductors, electrons and holes are simultaneously involved in electrical conductivity, the relationship between which (compensation ratio) varies with temperature.

The dependences $\ln(\rho\ (1/T))$ of $Ti_{1-x}Sc_xCoSb$ reflect the dynamics of changing the position of the Fermi level ε_F with respect to the continuous energy bands. Thus, in $Ti_{0.97}Sc_{0.03}CoSb$ in the temperature range T= 80–320, the Fermi level ε_F is in the valence band ε_V, as evidenced by both the positive values of the Seebeck coefficient α and the metallic type of conductivity (the resistivity values increase with a rise in temperature). The presence of an extremum on the dependence $\ln(\rho\ (1/T))$ at the temperature $T \approx 320$ K and the formation of the activation region with its growth shows that the Fermi level ε_F left the valence band ε_V and settled in the band gap ε_g of the semiconductor. This may occur if the donors present in the crystal are ionized, but their concentration is insufficient to change the type of conductivity.

At even higher concentrations of *Sc*($x \geq 0.05$), the number of structural defects of the acceptor nature generated in the crystal far exceeds the number of donors, which leads to the entry of the Fermi level ε_F into the valence band ε_V. This is indicated by positive values of the Seebeck coefficient α - free holes are the majority carriers, and the conductivity is metallic in nature.

Changes in the values of the resistivity $\rho(x,T)$ and the Seebeck coefficient $\alpha(x, T)$ of the $Ti_{1-x}Sc_xCoSb$ semiconductor at different temperatures (Fig. 7) complement the considerations regarding the nature of the current carriers.

The increase in the concentration of impurity *Sc* atoms in the structure of the *TiCoSb* compound from $x = 0.005$ to $x = 0.01$ is accompanied by an increase in the resistivity values, for example, at a temperature $T = 80$ K, from $\rho\ (x = 0.005) = 268.4$ mcΩm to $\rho\ (x = 0.01) = 587.8$ mcΩm (which does not correspond to the data in Fig. 8a, this data seems to be for $T = 380$ K). This behavior of $\rho\ (x, T)$ is caused by a decrease in the concentration of free electrons upon their "freezing" into impurity acceptor states, which would logically lead to an increase in resistance values. In so doing, the majority carriers up to temperatures $T \leq 350$ K are electrons, as indicated by the negative values of the Seebeck coefficient $\alpha(x, T)$.At higher temperatures, the concentration of free holes in the $Ti_{0.99}Sc_{0.01}CoSb$ sample becomes larger

than of electrons, and the sign of the Seebeck coefficient α(*x*, *T*) is positive (Fig. 7). It can be stated that the $Ti_{0.99}Sc_{0.01}CoSb$ semiconductor is heavily doped and fully compensated when the concentrations of ionized donors and acceptors are close, and the Fermi level ε_F is located in the mid gap ε_g. This conclusion is in complete agreement with the results of the electronic structure calculation for the case of the $Ti_{0.99}Sc_{0.01}CoSb$ semiconductor (Fig. 2).

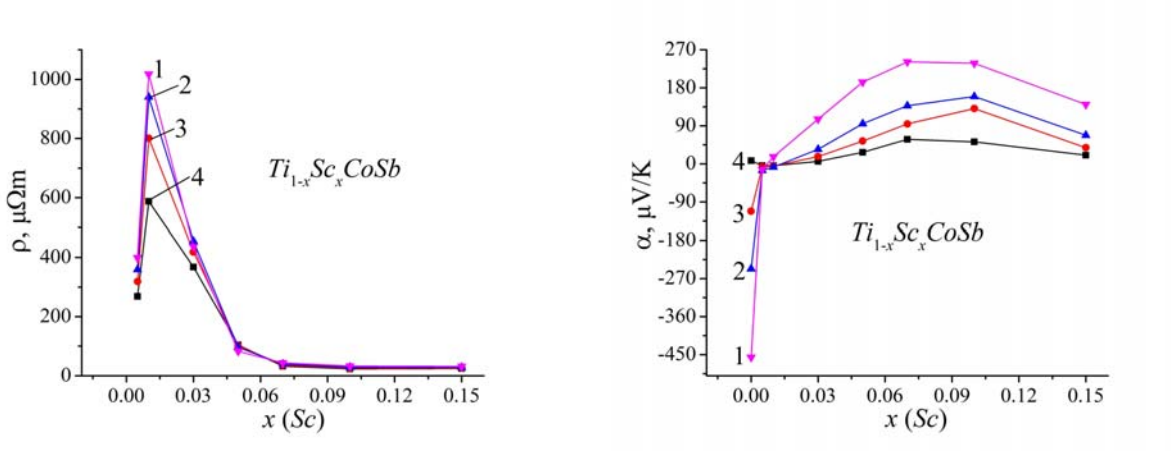

a) *b)*

Fig. 7. Change in the values of electrical resistivity ρ(x,T) (a) and the Seebeck coefficientα (x,T) (b) of $Ti_{1-x}Sc_xCoSb$ atdifferent temperatures: 1 – 80 K, 2 –160 K, 3 –250 K, 4 –380 K

At higher concentrations of impurity *Sc*, the values of the resistivity *ρ(x,T) of Ti1-xScxCoSb* decrease rapidly, and at concentrations $x \geq 0.06$ this change is already insignificant. At these $Ti_{1-x}Sc_xCoSb$ concentrations, the majority carriers are free holes, as indicated by the positive values of the Seebeck coefficient α(*x*,*T*) (Fig. 7).Therefore, a sharp decrease in the values of ρ(*x*,*T*) in the concentration range $0.01 \leq x \leq 0.08$ is associated with the intersection by the Fermi level ε_F of the mid gap ε_g and the approach to the percolation level of valence band ε_V, which will be crossed at $x \approx 0.08$, causing a fast increase in the concentration of free holes as the ionization energy of acceptors decreases. The intersection by the Fermi level ε_F of the percolation level of the valence band ε_V and the motion in this zone make no significant contribution to the change in the concentration of holes, which causes quasi saturation of the dependence ρ(*x*, *T*) at concentrations $x \geq 0.08$.

Thermoelectric power factor of $Ti_{1-x}Sc_xCoSb$

We mentioned above that in thermoelectric semiconductor material a prerequisite for achieving maximum efficiency of thermal into electrical energy conversion is doping the material with a type of impurity that coincides with the type of majority carriers of the basic semiconductor array, and the Fermi level ε_F approaches the band of continuous energies. In this case, the values of electrical conductivity σ(*x*,*T*) will be already high due to the appearance of a large number of free current carriers, and the values of the Seebeck coefficient α(*x*,*T*) will be even higher.

As can be seen from Fig. 8, in the case of thermoelectric material $Ti_{1-x}Sc_xCoSb$, the above conditions are achieved at concentrations $x \approx 0.08$–0.10, and the values of thermoelectric power factor Z* are maximum. In this context, it is appropriate to refer to the results of simulating the behavior of the thermoelectric power factor Z* calc. $Ti_{1-x}Sc_xCoSb$ (Fig. 4*b*), which almost coincide with the results of experimental measurements. The obtained result confirms the promising outlook of thermoelectric material $Ti_{1-x}Sc_xCoSb$, and further studies of thermal conductivity processes will allow establishing the conditions for obtaining the maximum efficiency of thermal into electrical energy conversion.

Therefore, kinetic studies of the $Ti_{1-x}Sc_xCoSb$ semiconductor solid solution showed that, at low concentrations of impurity *Sc* atoms, there is a discrepancy between the results of electronic structure simulation and experimental measurements. Since we optimize thermoelectric characteristics by doping the *TiCoSb* basic semiconductor, it is crucial to understand the characteristics of its crystalline and electronic structures. After all, any compound or semiconductor solid solution only then becomes a thermoelectric material when their structural, energy, kinetic, etc. the characteristics will be clear and predictable. In other words, when investigating $Ti_{1-x}Sc_xCoSb$, we are required to identify the causes that cause unpredictable behavior of the characteristics.

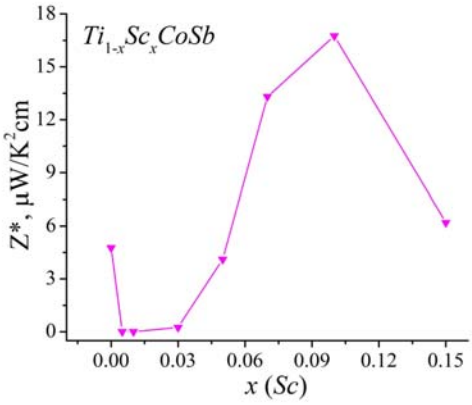

Fig. 8. Change in the values of thermoelectric power factor Z of $Ti_{1-x}Sc_xCoSb$ at T=380 K*

It can be assumed that the discrepancy in the results observed in $Ti_{1-x}Sc_xCoSb$ thermoelectric material is due to an incomplete understanding of the spatial arrangement of atoms and their impurity energy levels generated in the *TiCoSb* source compound. Below we examine this problem in more detail.

Features of the electronic and crystal in structures of *TiCoSb* compound

In order to refine the crystalline and electronic structure of *TiCoSb* compound, electron density distribution (DOS) simulations were carried out under different variants of occupying by atoms of crystallographic positions, as well as occupying by atoms of tetrahedral voids in the structure (Fig. 9), which make up ~ 24% of the unit cell volume [6,7]. After all, there is a cause-effect relationship between the crystalline and electronic structures. Thus, to calculate the energy of an electron in the first Brillou in zone, one must know the spatial location of the atoms or their absence (vacancies) at the unit cell nodes. On the other hand, the slightest structural changes affect the local symmetry and DOS values. Therefore, the adequacy of the results of simulating the electronic structure of a semiconductor and the results of experimental studies, such as kinetic and/or energy characteristics implies that the model of its structure is adequate to spatial arrangement of atoms in the crystal. That is why the results of the calculation of the electronic structure in comparison with simulation results make it possible to obtain information about the crystal structure, which is not available for x-ray methods of investigation [6].

Let us analyze the results of calculating DOS of *TiCoSb* compound for several variants (Fig. 9).

a). In the case when vacancies are present at the 4*a*crystallographic position of *Ti* atoms, which are ~ 1 at. % of all *Ti* atoms, the compound formula takes the form: $(Ti_{0.99(0.01)})CoSb$. The resulting structural defect has an acceptor nature, and an impurity acceptor level (band) ε_A, appears in the band gap ε_g of the semiconductor near the valence band ε_V, which fixes the position of the Fermi level ε_F (Fig. 9). We will obtain a model of the electronic structure of a doped hole-type semiconductor with a conductivity type.

This conclusion coincides with the results of [5]. Adding *Sc* ($3d^14s^2$) impurity atoms to the structure of the semiconductor ($Ti_{0.99(0.01)}$)*CoSb* by occupying the 4*a* crystallographic position of *Ti*($3d^24s^2$) will have the following consequences:

- generation of structural defects of the acceptor nature as a result of substitution of *Ti* atoms, since the *Sc* atom has a smaller number of 3*d* electrons;

- a decrease in the concentration of structural defects of the acceptor nature present in the crystal upon occupation by *Sc* atoms of vacancies.

As a result, we obtain a hole-type conductivity semiconductor $Ti_{1-x}Sc_xCoSb$.This variant of the spatial arrangement of atoms does not correspond to the given experimental results.

b). If additional *Co** atoms (~ 1 at.%) occupy the tetrahedral voids of the structure (internode) of the *TiCoSb* compound, its formula will take the form $TiCo(Co^*_{0.01})Sb$. We obtain a classical doped semiconductor of electronic conductivity type, in the band gap of which an impurity donor level (band) ε_D appeared, which fixes the position of the Fermi level ε_F (Fig. 9).Now the addition of *Sc* impurity atoms to the structure of the $TiCo\ (Co^*_{0.01})\ Sb$ semiconductor in the manner described above will generate structural defects in the acceptor nature. As the concentration of impurity *Sc* atoms increases, the degree of compensation increases, and the Fermi level εF drifts from the conduction band ε_C through the middle of the band gap ε_g to the valence band ε_V.. This will change the conductivity type of the semiconductor from electron to hole.

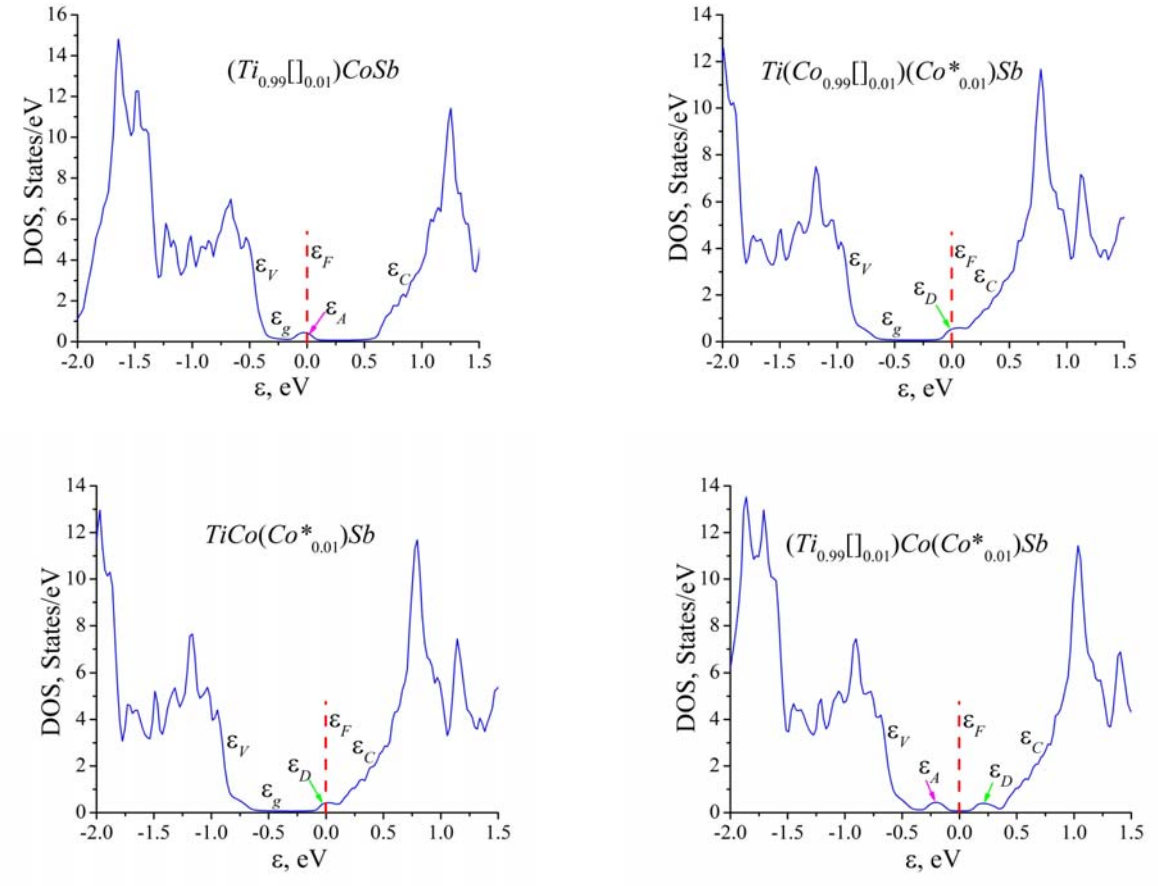

Fig. 9. Calculation of the distribution electron density of states (DOS) of TiCoSb compound for different variants of spatial arrangement of atoms.

This variant of the crystalline and electronic structures of the *TiCoSb* compound does not fully reflect the results of the experiment because it does not answer the question of the absence of activation sites on the dependence ln(ρ(1/*T*)) at concentrations when the Fermi level ε_F departs from the conduction band ε_C and approaches the valence band ε_V.

c). The presence of 1% of vacancies at the *4c* position of *Co* atoms and the location of 1% additional *Co** atoms in tetrahedral voids of the structure is described by the formula $Ti(Co_{0.99(0.01)})(Co^*_{0.01})Sb$ (Fig. 9). In this case, structural defects of the donor nature are generated in the crystal due to the arrangement of *Co* atoms in the voids of the structure. Since *Co* atoms are involved in the formation of both the conduction band and the valence band of the semiconductor, in the presence of 1% of vacancies at the 4*c* position of *Co* atoms, there is a mutual compensation of the donor-acceptor energy levels, which explains their absence in the band gap ε_g.. That is why the energy scheme of such a spatial arrangement of atoms in their own crystallographic positions (or lack thereof) contains only the impurity donor level and is identical to the previous case *(b)* and the conclusions drawn.

d). The closest to the results of the experiment is a variant of the simultaneous presence of 1% of vacancies at the 4*a* position of *Ti* atoms and 1% of additional *Co** atoms in the tetrahedral voids of the structure, which can be described by the formula $(Ti_{0.99(0.01)})Co(Co^*_{0.01})Sb$ (Fig. 9). In this case, vacancies at the position of *Ti* atoms generate structural defects of the donor nature, and the corresponding acceptor level (zone) ε_A appears in the band gap ε_g. In turn, additional *Co** atoms in the voids of the structure generate a structural defect of the donor nature, and in the band gap ε_g the corresponding donor level (zone) ε_D will appear. It is quite logical to locate the Fermi level ε_F between the generated energy states of the donor and acceptor nature. The slightest changes in the ratio between defects in the acceptor and donor nature of the semiconductor, generated, for example, by different modes of thermal annealing of the samples and their cooling, the purity of the initial components during synthesis, etc., will cause a change in the position of the Fermi level ε_F relative to energy levels inε_g. For this reason, in the temperature range T = 80–90 K *TiCoSb* is a semiconductor of the hole type of conductivity, as evidenced by the positive values of the Seebeck coefficient α, and at higher temperatures its sign changes and electrons are now the majority carriers (Fig. 6,7*b*).

The addition of impurity *Sc* atoms to such a semiconductor by substitution at the 4*a* position of the *Ti* atoms generates structural defects of the acceptor nature, which initially will increase the degree of compensation and, as a consequence, lead to an increase in the resistivity ρ (x, T) (Fig. 7a). And only at concentrations of impurities *Sc*, $x \geq 0.03$, the Fermi level ε_F is located in the impurity acceptor zone ε_A^{Sc}, as indicated by the positive values of the Seebeck coefficient$\alpha(x,T)$ (Fig. 7*b*) at all temperatures and the presence of high-temperature of the activation region on the dependence of ln(ρ (1 / *T*)) (Fig. 6).

Therefore, doping the *TiCoSb* semiconductor with *Sc* acceptor impurities introduced into the structure by substitution at the 4*a* position of the *Ti* atoms made it possible to detect defects of the donor nature in the structure of the *TiCoSb* base compound as a result of the occupation by *Co** atoms of tetrahedral voids in the structure, which gave rise to a corresponding donor level (zone) ε_D in the band gap ε_g. The ratio of concentrations of the donor and acceptor levels present in the *TiCoSb* compound structure determines the location of the Fermi ε_F level in the semiconductor, and doping with its acceptor impurities will change the mechanisms and type of conductivity of $Ti_{1-x}Sc_xCoSb$.

Conclusions

1. The result of a comprehensive study of crystalline and electronic structures, kinetic, energy, and magnetic characteristics of the *Ti1-xScxCoSb* thermoelectric material is establishment of the nature of structural defects of the donor and acceptor nature. It is shown that structural defects of the donor and

acceptor nature are present in the *TiCoSb* base compound as a result of the location in the tetrahedral voids of the structure of additional *Co** atoms and the presence of vacancies at the 4*a*crystallographic position of *Ti* atoms. Introduction to *TiCoSb* compound of impurity *Sc* atoms by substitution at the 4*a* position of *Ti* atoms generates structural defects of the acceptor nature, and the ratio in $Ti_{1-x}Sc_xCoSb$ of concentrations of available defects of the donor and acceptor nature determines the location of the Fermi level ε_F and the mechanisms of conductivity.

2. The work was performed in the frame work of grant of the Ministry of Education and Science of Ukraine № 0118U003609.

References

1. Romaka L. P., Shelyapina M. G., Stadnyk Yu. V., Fruchart D.,Hlil E. K., Romaka V. A. (2006). Peculiarity of metal – insulator transition due to composition change in semiconducting $TiCo_{1-x}Ni_xSb$ solid solution. I. Electronic structure calculations.*J. Alloys Compd.*, 414, 46–50.
2. Stadnyk Yu. V., Romaka V. A., Shelyapina M. G., Gorelenko Yu. K., Romaka L. P., Fruchart D., Tkachuk A. V., Chekurin V. F. (2006). Impurity band effecton $TiCo_{1-x}Ni_xSb$ conduction. Donorimpurities. *J. Alloys Compd.*, 421, 19–23.
3. Romaka V. A., Stadnyk Yu. V., Frushart D., Tobola J., Gorelenko Yu. K., Romaka L. P., Chekurin V. F., Horyn A. M. (2007). Features of doping the *p-TiCoSb* in termetallic semiconductor with a *Cu* donorimpurity. 1. Calculation of electron structure. *Ukr. J. Phys*., 52(№5), 453–457.
4. Romaka V. A., Stadnyk Yu. V., Frushart D., Tobola J., Gorelenko Yu. K., Romaka L. P., Chekurin V. F., Horyn A. M. (2007). Specific features of doping the *p-TiCoSb* in termetallic semiconductor with a *Cu* donorimpurity. 2. Experimental studies. *Ukr. J. Phys*., 52 (№7), 650–656.
5. Romaka V. A., Stadnyk Yu. V., Akselrud L. G., Romaka V. V., Frushart D., Rogl P., Davydov V. N., Gorelenko Yu. K. (2008). Mechanism of local am or phization of a heavily doped $Ti_{1-x}V_xCoSb$ in termetallic semiconductor. *Semiconductors*, 42(№7), 753–760.
6. Romaka V. A., Romaka V. V., Stadnyk Yu. V. (2011). *Intermetalichni napivprovidnyky: vlastyvosti ta zastosuvannia [Intermetallic semiconductors]*.Lviv: LvivskaPolitechnica [in Ukrainian].
7. Romaka V. V., Rogl P.F., Carlini R. and Fanciulli C. (2017).Prediction of the thermoelectric properties of half-Heuslerphases from the density functional theory. In *Alloys and Intermetallic Compounds*, Artini C. (Ed.). London–NY: Taylor & Francis Group.
8. Horyn A., Romaka V.A., Stadnyk Yu., Romaka L., RokomanukM., Krayovskyy V. (2019). *Features of Electrical Conductivity Mechanisms of the $Ti_{1-x}Mo_xCoSb$ Solid Solution*. XIV International Conference on Crystal Chemistry of Intermetallic Compounds, Collected Abstracts (Lviv, Ukraine, September 22–26, 2019).
9. Anatychuk L. I. (1979). *Termoelementy i termoelektricheskiie ustroistva. Spravochnik [Thermoelements and thermoelectric devices. Handbook]*.Kyiv: Naukovadumka [in Russian].
10. Shklovskii B.I. and Efros A.L. (1979).*Electronic properties ofdoped semiconductors.*NY: Springer, 1984; Moscow:Nauka1979 [in Russian].
11. RomakaV.A., FrushartD., StadnykYu.V., Tobola J., GorelenkoYu.K.,ShelyapinaM.G., RomakaL.P., ChekurinV.F. (2006). A condition of maximum power characteristic to intermetallic semiconductors of the *MgAgAs* structure tupe. *Semiconductors*, 40(№ 11), 1289–1395.
12. Roisnel T., Rodriguez-Carvajal J. (2001). WinPLOTR: a Windows Tool for Powder Diffraction Patterns analysis, Mater. Sci. Forum, Proc. EPDIC7 378–381, 118–123.
13. Schruter M., Ebert H., Akai H., Entel P., Hoffmann E., Reddy G.G. (1995). First-principles investigations of atomic disorder effects on magnetic and structural instabilities in transition-metal alloys.*Phys. Rev*. B 52, 188–209.

14. Moruzzi V.L., Janak J.F., Williams A.R. (1978). *Calculated electronic properties of metals (1978).* NY:PergamonPress.
15. Romaka V.V., Romaka L.P., KrayovskyyV.Ya., StadnykYu.V. (2015). *Stannides of rare earth and transition metals.*Lviv: LvivskaPolytechnika [in Ukrainian].
16. Mott N.F., Davis E.A. (1979). *Electron processes in non-crystalline materials*.Oxford: Clarendon Press.
17. RomakaV.A.,FruchartD., HlilE.K., GladyshevskiiR.E., GignouxD., RomakaV.V., KuzhelB.S. andKrayovskiiR.V. (2010). Feature so fan in termetallic *n-ZrNiSn* semiconductor heavily doped with atoms of rare-earth metals. *Semiconductors*, 44(№ 3), 293–302.
18. Stadnyk Yu., Romaka V. V.,Romaka L., Orovchik L., Horyn A. (2019). Synthesis, electrical transport, magnetic properties and electronic structure of $Ti_{1-x}Sc_xCoSb$ semiconducting solid solution. *J. Alloys Compd.*, 805, 840–846.

Submitted 18.03.2019

Ромака В.А.[1], *док. тех. наук*, *профессор*
Стадник Ю.В[2], *канд. хім. наук*
Ромака Л.П.[2], *канд. хім. наук*
Стадник Ю.В[2], *канд. хім. наук*
Крайовський В.Я.[1], *док. тех. наук*
Ромака В.В.[1,3], *док. тех. наук, канд. хім. наук, доц.*
Горинь А.М.[2], *канд. хім. наук*
Коник М.Г.[2], *канд. хім. наук, доц.*
Романів І.М.[2], Рокоманюк М.В.[1]

[1]Національний університет "Львівська політехніка",
вул. С. Бандери, 12, Львів, 79013, Україна; *e-mail: vromaka@polynet.lviv.ua*
[2]Львівський національний університет ім. І. Франка,
вул. Кирила і Мефодія, 6, Львів, 79005, Україна;
e-mail: lyubov.romaka@lnu.edu.ua,
[3]Інститут досліджень твердого тіла, IFW-Drezden, Гельмгольц
штрасе, 20, 01069 Дрезден, Німеччина

ДОСЛІДЖЕННЯ ТЕРМОЕЛЕКТРИЧНОГО МАТЕРІАЛУ $Zr_{1-x}V_xNiSn$

Досліджено кристалічну та електронну структури, кінетичні та енергетичні характеристики термоелектричного матеріалу $Zr_{1-x}V_xNiSn$ у діапазонах: T=80–400 K, x=0.01–0.10. Встановлено механізми одночасного генерування структурних дефектів акцепторної та донорної природи, які визначають електропровідність матеріалу. Показано, що енергетично доцільним є одночасне часткове зайняття атомами V ($3d^34s^2$) позиції 4c атомів Ni ($3d^84s^2$), що генерує структурні дефекти акцепторної природи та домішкову акцепторну зону ε^1_A, а також позиції 4a атомів Zr ($4d^25s^2$), генеруючи структурні дефекти донорної природи та домішкову донорну зону ε^2_D. Бібл. 12, Рис.8.

Ключові слова: електронна структура, електроопір, коефіцієнт термоЕРС.

Ромака В.А.[1], *док. тех. наук*, *профессор*
Стадник Ю.В[2], *канд. хим. наук*
Ромака Л.П.[2], *канд. хим. наук*
Крайовский В.Я.[1], *док. тех. наук*
Ромака В.В.[1,3], *док. тех. наук, канд. хим. наук, доц.*
Горынь А.М.[2], *канд. хим. наук,*
Коник М.Г.[2], *канд. хим. наук, доц.*
Романив И.М.[2], *V.V.Romaka,*
Рокоманюк М.В.[1]

[1]Национальный университет "Львовская политехника", ул. С. Бандеры, 12,
Львов, 79013, Украина, *e-mail: vromaka@polynet.lviv.ua*,
[2]Львовский национальный университет им. И. Франко,
ул. Кирилла и Мефодия, 6, Львов, 79005, Украина,
e-mail: lyubov.romaka@lnu.edu.ua,
[3]Институт исследований твердого тела, IFW-Drezden,
Гельмгольц штрассе, 2001069 Дрезден, Германия

ИССЛЕДОВАНИЕ ТЕРМОЭЛЕКТРИЧЕСКИХ МАТЕРИАЛОВ $Zr_{1-x}V_xNiSn$

Исследованы кристаллическая и электронная структуры, кинетические и энергетические характеристики термоэлектрического материала $Zr_{1-x}V_xNiSn$ в диапазонах: T = 80-400 K, x = 0.01-0.10. Установлены механизмы одновременного генерирования структурных дефектов акцепторной и донорной природы, которые определяют электропроводность материала. Показано, что энергетически целесообразно одновременное частичное занятие атомами V ($3d^34s^2$) позиции 4c атомов Ni ($3d8^4s^2$), генерирующий структурные дефекты акцепторной природы и примесную акцепторную зону, ε^1_A а также позиции 4a атомов Zr ($4d^25s^2$), генерируя структурные дефекты донорной природы и примесную донорных зону ε^2_D. Библ. 12, Рис.8.
Ключевые слова: электронная структура, электросопротивление, коэффициент термоЭДС.

References

1. Romaka L. P., Shelyapina M. G., Stadnyk Yu. V., Fruchart D.,Hlil E. K., Romaka V. A. (2006). Peculiarity of metal – insulator transition due to composition change in semiconducting $TiCo_{1-x}Ni_xSb$ solid solution. I. Electronic structure calculations.*J. Alloys Compd.*, 414, 46–50.
2. Stadnyk Yu. V., Romaka V. A., Shelyapina M. G., Gorelenko Yu. K., Romaka L. P., Fruchart D., Tkachuk A. V., Chekurin V. F. (2006). Impurity band effecton $TiCo_{1-x}Ni_xSb$ conduction. Donorimpurities. *J. Alloys Compd.*, 421, 19–23.
3. Romaka V. A., Stadnyk Yu. V., Frushart D., Tobola J., Gorelenko Yu. K., Romaka L. P., Chekurin V. F., Horyn A. M. (2007). Features of doping the *p-TiCoSb* in termetallic semiconductor with a *Cu* donorimpurity. 1. Calculation of electron structure. *Ukr. J. Phys*., 52(№5), 453–457.
4. Romaka V. A., Stadnyk Yu. V., Frushart D., Tobola J., Gorelenko Yu. K., Romaka L. P., Chekurin V. F., Horyn A. M. (2007). Specific features of doping the *p-TiCoSb* in termetallic semiconductor with a *Cu* donorimpurity. 2. Experimental studies. *Ukr. J. Phys*., 52 (№7), 650–656.

5. Romaka V. A., Stadnyk Yu. V., Akselrud L. G., Romaka V. V., Frushart D., Rogl P., Davydov V. N., Gorelenko Yu. K. (2008). Mechanism of local am or phization of a heavily doped $Ti_{1-x}V_xCoSb$ in termetallic semiconductor. *Semiconductors*, 42(№7), 753–760.
6. Romaka V. A., Romaka V. V., Stadnyk Yu. V. (2011). *Intermetalichni napivprovidnyky: vlastyvosti ta zastosuvannia [Intermetallic semiconductors]*.Lviv: LvivskaPolitechnica [in Ukrainian].
7. Romaka V. V., Rogl P.F., Carlini R. and Fanciulli C. (2017).Prediction of the thermoelectric properties of half-Heuslerphases from the density functional theory. In *Alloys and Intermetallic Compounds*, Artini C. (Ed.). London–NY: Taylor & Francis Group.
8. Horyn A., Romaka V.A., Stadnyk Yu., Romaka L., RokomanukM., Krayovskyy V. (2019). *Features of Electrical Conductivity Mechanisms of the $Ti_{1-x}Mo_xCoSb$ Solid Solution*. XIV International Conference on Crystal Chemistry of Intermetallic Compounds, Collected Abstracts (Lviv, Ukraine, September 22–26, 2019).
9. Anatychuk L. I. (1979). *Termoelementy i termoelektricheskiie ustroistva. Spravochnik [Thermoelements and thermoelectric devices. Handbook]*.Kyiv: Naukovadumka [in Russian].
10. Shklovskii B.I. and Efros A.L. (1979).*Electronic properties ofdoped semiconductors*.NY: Springer, 1984; Moscow:Nauka1979 [in Russian].
11. RomakaV.A., FrushartD., StadnykYu.V., Tobola J., GorelenkoYu.K.,ShelyapinaM.G., RomakaL.P., ChekurinV.F. (2006). A condition of maximum power characteristic to intermetallic semiconductors of the *MgAgAs* structure tupe. *Semiconductors*, 40(№ 11), 1289–1395.
12. Roisnel T., Rodriguez-Carvajal J. (2001). WinPLOTR: a Windows Tool for Powder Diffraction Patterns analysis, Mater. Sci. Forum, Proc. EPDIC7 378–381, 118–123.
13. Schruter M., Ebert H., Akai H., Entel P., Hoffmann E., Reddy G.G. (1995). First-principles investigations of atomic disorder effects on magnetic and structural instabilities in transition-metal alloys.*Phys. Rev*. B 52, 188–209.
14. Moruzzi V.L., Janak J.F., Williams A.R. (1978). *Calculated electronic properties of metals (1978)*. NY:PergamonPress.
15. Romaka V.V., Romaka L.P., KrayovskyyV.Ya., StadnykYu.V. (2015). *Stannides of rare earth and transition metals*.Lviv: LvivskaPolytechnika [in Ukrainian].
16. Mott N.F., Davis E.A. (1979). *Electron processes in non-crystalline materials*.Oxford: Clarendon Press.
17. RomakaV.A.,FruchartD., HlilE.K., GladyshevskiiR.E., GignouxD., RomakaV.V., KuzhelB.S. andKrayovskiiR.V. (2010). Feature so fan in termetallic *n-ZrNiSn* semiconductor heavily doped with atoms of rare-earth metals. *Semiconductors*, 44(№ 3), 293–302.
18. Stadnyk Yu., Romaka V. V.,Romaka L., Orovchik L., Horyn A. (2019). Synthesis, electrical transport, magnetic properties and electronic structure of $Ti_{1-x}Sc_xCoSb$ semiconducting solid solution. *J. Alloys Compd.*, 805, 840–846.

Submitted 18.03.2019

Anatychuk L.I. *acad. National Academy of sciences of Ukraine*[1,2]**,**
Kobylianskyi R.R. *cand. phys.– math. sciences*[1,2]**, Fedoriv R.V.**[2]

[1]Institute of Thermoelectricity of the NAS and MES of Ukraine,
1, Nauky str., Chernivtsi, 58029, Ukraine;
[2]Yu.Fedkovych Chernivtsi National University,
2, Kotsiubynskyi str., Chernivtsi, 58012, Ukraine

METHOD FOR TAKING INTO ACCOUNT THE PHASE TRANSITION IN BIOLOGICAL TISSUE DURING COMPUTER-AIDED SIMULATION OF CRYODESTRUCTION PROCESS

The paper presents a method for taking into account the phase transition in biological tissue during computer-aided simulation of cryodestruction process. The physical, mathematical and computer models of biological tissue are constructed with regard to thermophysical processes, blood circulation, heat transfer, metabolic processes and the phase transition. As an example, we consider the case when there is a cooling element on the surface of biological tissue at a temperature of -50 ° C. The temperature and heat flux distributions in biological tissue are determined in cooling mode. The results obtained make it possible to predict the depth of freezing of biological tissue at a given temperature exposure. Bibl. 28, Fig. 7, Table. 1.
Key words: biological tissue, temperature exposure, cryodestruction, phase transition, computer simulation.

Introduction

It is well known in medical practice that temperature exposure is an important factor in the treatment of many diseases of the human body [1-3]. One of the promising areas is cryodestruction, i.e. a set of surgical treatment methods based on local freezing of the human body biological tissue. To perform cryodestruction, it is necessary to cool a certain part of the human body to a temperature of -50 ° C. Today, such cooling is realized with the help of special cryotools using liquid nitrogen [4 8]. However, the use of liquid nitrogen has a number of disadvantages, namely nitrogen does not provide cooling with the required accuracy of maintaining the temperature, and there are risks of overcooling with negative consequences. Moreover, liquid nitrogen is a very dangerous substance and requires proper care when used, and delivery of liquid nitrogen is not always available, which limits the possibility of using this method. This opens up prospects for the use of thermoelectric cooling for cryodestruction, which can be used for cooling to a temperature of (0 ÷ -80) ° C. Thermoelectric medical devices make it possible to precisely set the required temperature of the working tool, the time of temperature exposure on the corresponding part of the human body and provide a cyclic change of cooling and heating modes [1 – 2, 9 – 12].

Computer models of biological tissue created so far, on the surface of which there is a cooling element, make it possible to simulate thermophysical processes with regard to blood circulation, heat transfer and metabolic processes [13 19]. However, the existing computer models do not take into account the phase transition in biological tissue when it is cooled to a temperature below 0 ° C, which leads to errors in computer simulation of temperatures and heat fluxes.

Therefore, *the purpose of this paper* is to develop a method for taking into account the phase transition in biological tissue during computer simulation of the cryodestruction process.

Physical model

We constructed a physical 2*D* model with axial symmetry (Fig. 1) of the human body biological tissue 1 on the surface of which there is a cooling element 2. This model is a structure of two homogeneous rectangular bars and is characterized by the following thermophysical properties: thermal conductivity κ, specific heat C, density ρ, blood perfusion rate ω_b, blood density ρ_b, blood temperature T_b, specific heat of blood C_b, specific heat release Q_{met} due to metabolic processes and latent phase transition heat L (table 1). The corresponding section of biological tissue 1 is considered as a volumetric heat source q, where:

$$q = Q_{met} + \rho_b \cdot C_b \cdot \omega_b \cdot (T_b - T). \quad (1)$$

The geometric dimensions of biological tissue 1 are *a, b*, and, accordingly, of cooling element 2 - *c, d*. The temperatures at the boundaries of biological tissue 1 and cooling element 2 are T_1, T_2, T_3, T_4. The temperature inside biological tissue is T_1 = +37 ° C. The temperature of cooling element is T_4 = -50 ° C. The ambient temperature is T_5 = +22 ° C. The upper surface of biological tissue with temperature T_3 is in a state of heat exchange with the environment (coefficient of heat exchange α and emissivity ε) at temperature T_5. The lateral surface of biological tissue is adiabatically isolated.

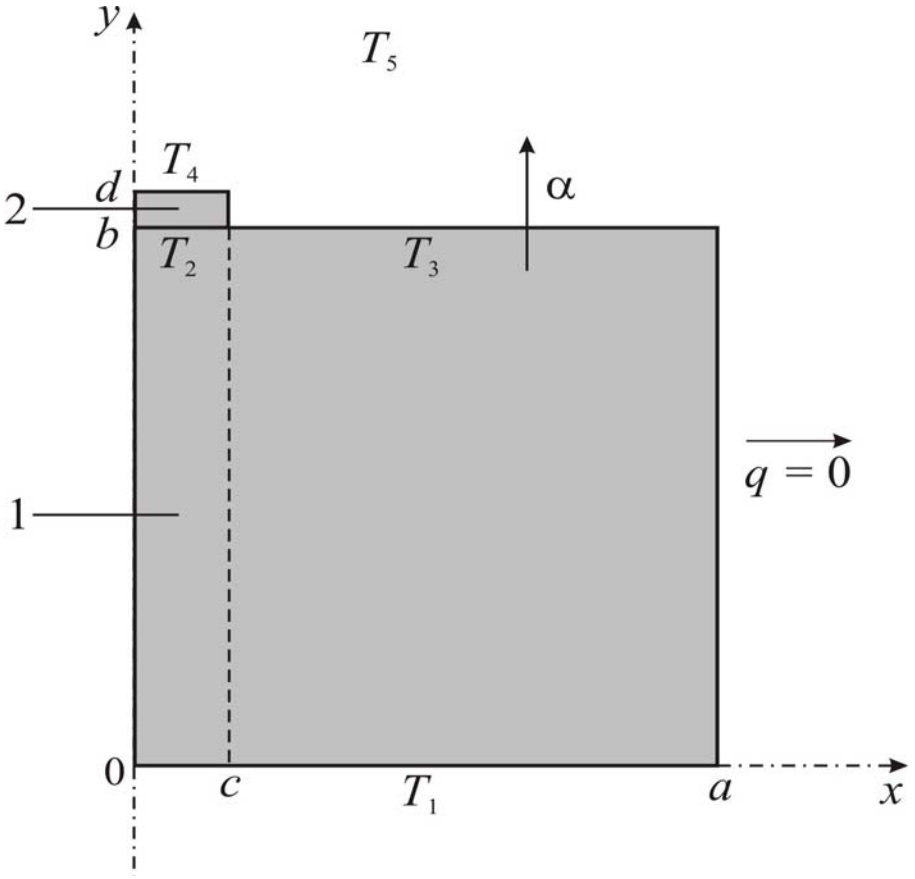

Fig.1. Physical 2D model with axial symmetry:
1 – biological tissue, 2 – cooling element.

Table 1.

Thermophysical properties of the human body biological tissue in normal [20-25] and frozen states [26, 27]

Thermophysical properties of biological tissue	Value	Measurement units
Heat capacity of normal biological tissue (C_1)	3600	J/m^3 ·°C
Heat capacity of frozen biological tissue (C_2)	1800	J/m^3 ·°C
Blood heat capacity (C_b)	3600	J/m^3 ·°C
Blood density (ρ_b)	1000	kg/m^3
Thermal conductivity of normal biological tissue (κ_1)	0.5	W/m ·°C
Thermal conductivity of frozen biological tissue (κ_2)	2	W/m ·°C
Latent heat of phase transition (L)	$250 \cdot 10^3$	J/m^3
Blood temperature (T_b)	37	°C
Upper temperature of phase transition (T_1)	-1	°C
Lower temperature of phase transition (T_2)	-8	°C
Blood perfusion in biological tissue (ω_b)	0.0005	ml/s·ml
Metabolism in biological tissue (Q_{met})	4200	W/m^3

Mathematical model

In general, the heat transfer equation in biological tissue is given by [20-27]:

$$C \cdot \frac{\partial T}{\partial t} = \nabla \cdot (\kappa \cdot \nabla T) + \rho_b \cdot C_b \cdot \omega_b \cdot (T_b - T) + Q_{met}, \quad (2)$$

where C, κ are specific heat and thermal conductivity of biological tissue, ρ_b is blood density, C_b is specific heat of blood, ω_b is blood perfusion, T_b is blood temperature, T is temperature of biological tissue; Q_{met} is heat which is released due to metabolic processes.

The term on the left side of equation (2) is the rate of change of thermal energy contained in a unit volume of biological tissue. The three terms on the right side of this equation represent, respectively, the rate of change of thermal energy due to thermal conductivity, blood perfusion, and heat metabolism.

The equation of heat transfer in biological tissue (2) is solved with the corresponding boundary conditions. The temperature on the surface of cooling element is T_4 = -50°C. The temperature inside

biological tissue is T_1 = + 37 ° C. The lateral surfaces of biological tissue are adiabatically isolated (q = 0), and the upper surface is in a state of heat exchange (heat transfer coefficient α and emissivity ε) with the environment at a temperature of T_5.

$$q(x,y,t)\Big|_{\substack{c\le x\le a\\ y=b}} = \alpha\cdot(T_5 - T_3) + \varepsilon\cdot\sigma\cdot(T_5^4 - T_3^4)\,, \tag{3}$$

where α is coefficient of convective heat exchange of the surface of biological tissue with the environment, ε is emissivity, σ is the Boltzmann constant, T_3 is temperature of biological tissue surface, T_5 is ambient temperature (T_5=+22°C).

At the initial time t = 0 s, it is believed that the temperature in the entire volume of biological tissue is T = +37 ° C, that is, the initial conditions for solving equation (2) are as follows:

$$T(x,y,0) = T_b. \tag{4}$$

As a result of solving the initial boundary value problem (2) - (4), the temperature distributions $T\ (x,\ y,\ t)$ and heat fluxes in biological tissue are determined at an arbitrary time. As an example, in this paper we consider a case in which the temperature of cooling element is T_4 = -50 ° C. However, it should be noted that the proposed method allows considering cases where the temperature of cooling element $T_f(t)$ changes in any temperature range or according to a predetermined function.

During the freezing, the cells will undergo a phase change at the freezing point, with the loss of latent heat of the phase transition (L) occurring and the temperature in these cells will not change. The phase transition in biological cells occurs in the temperature range (-1 ÷ -8) ° C. The properties of biological tissue in normal and frozen states are shown in Table 1. In the temperature range (-1 ÷ -8) ° C, when cells are frozen, the latent heat of the phase transition is absorbed, which can be simulated by adding an appropriate value to the heat capacity [26, 27].

When biological tissue is frozen, the vessels in the capillaries are narrowed to freeze all blood in the capillaries, and the value tends to zero. In addition, the cells will not be able to generate metabolic heat when frozen and Q_{met} will be zero at a temperature below zero.

In the frozen state the properties of biological tissue will have the following values (5)-(8):

$$C = \begin{cases} C_1 & T \ge -1°C \\ \dfrac{L}{-1-(-8)} + \dfrac{C_1 + C_2}{2} & -8°C \le T \le -1°C \\ C_2 & T \le -8°C \end{cases} \tag{5}$$

$$\kappa = \begin{cases} \kappa_1 & T \ge -1°C \\ \dfrac{\kappa_1 + \kappa_2}{2} & -8°C \le T \le -1°C \\ \kappa_2 & T \le -8°C \end{cases} \tag{6}$$

$$Q_m = \begin{cases} 4200 & T \ge -1°C \\ 0 & -8°C \le T \le -1°C \\ 0 & T \le -8°C \end{cases} \tag{7}$$

$$\omega_b = \begin{cases} 0,0005 & T \geq -1°C \\ 0 & -8°C \leq T \leq -1°C \\ 0 & T \leq -8°C \end{cases} \quad (8)$$

Computer model

A computer model of biological tissue was created with a cooling element on its surface. Comsol Multiphysics software package [28] was used to build the computer model, which enables simulating thermophysical processes in biological tissue taking into account blood circulation, heat exchange, metabolism processes and phase transition.

The distribution of temperatures and heat fluxes in biological tissue was calculated by the finite element method, the essence of which is that the object under study is divided into a large number of finite elements and in each of them a function value is searched that satisfies given second-order differential equations with the corresponding boundary conditions. The accuracy of solving the formulated problem depends on the level of partitioning and is ensured by the use of a large number of finite elements [28].

As an example, Figs.2 - 3 show the distributions of temperature and isothermal surfaces in the bulk of the human body biological tissue on the surface of which there is cooling element at a temperature of T = -50°C.

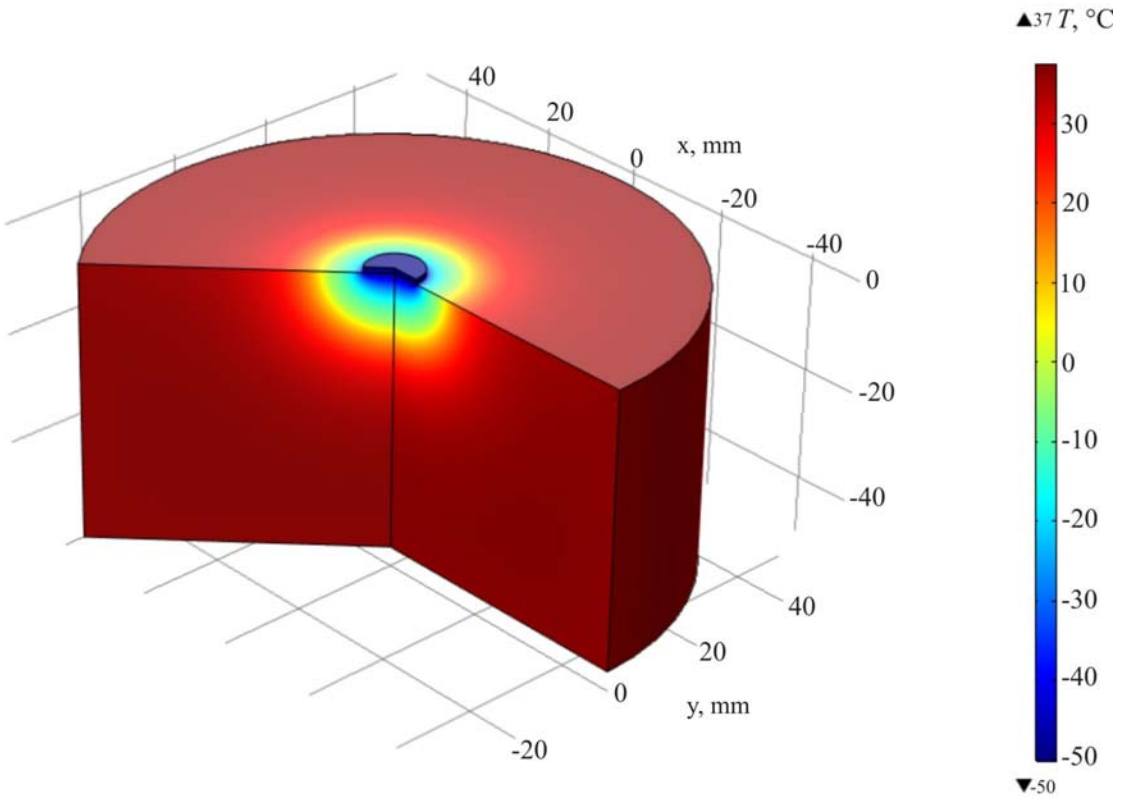

Fig.2. Temperature distribution in the bulk of biological tissue on the surface of which there is a cooling element at a temperature of T = -50°C.

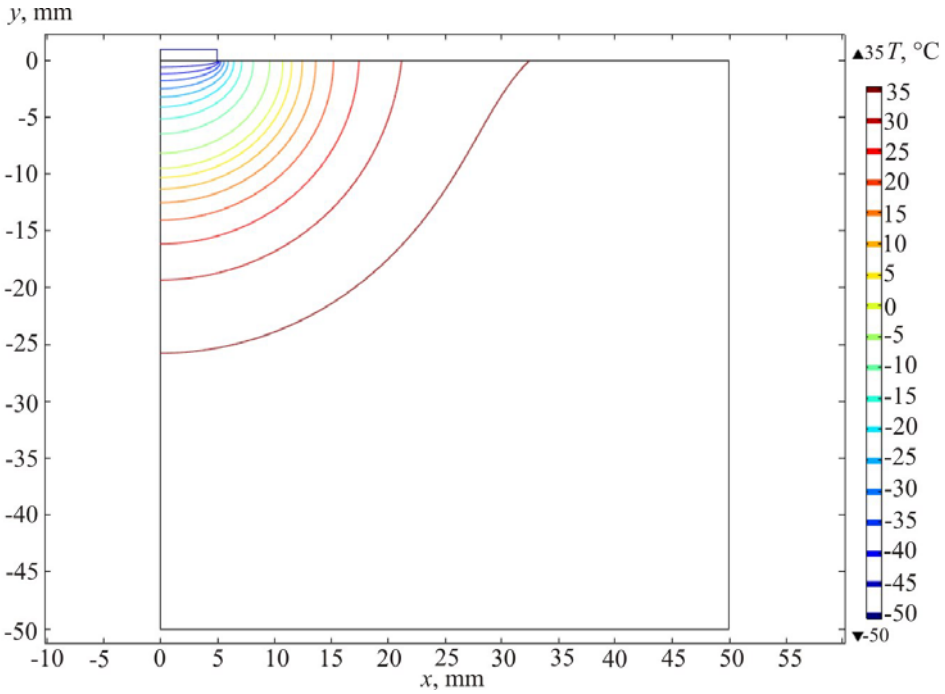

Fig. 3. Isothermal surfaces in the bulk of biological tissue on the surface of which there is a cooling element at a temperature T = -50°C.

Computer simulation results

Fig. 4 shows temperature distribution in the section of biological tissue on the surface of which there is a cooling element at temperature T = -50°C at time moment t = 500 s. In this case, l_1 is temperature level T = -8°C and l_2 is temperature level T = -1°C.

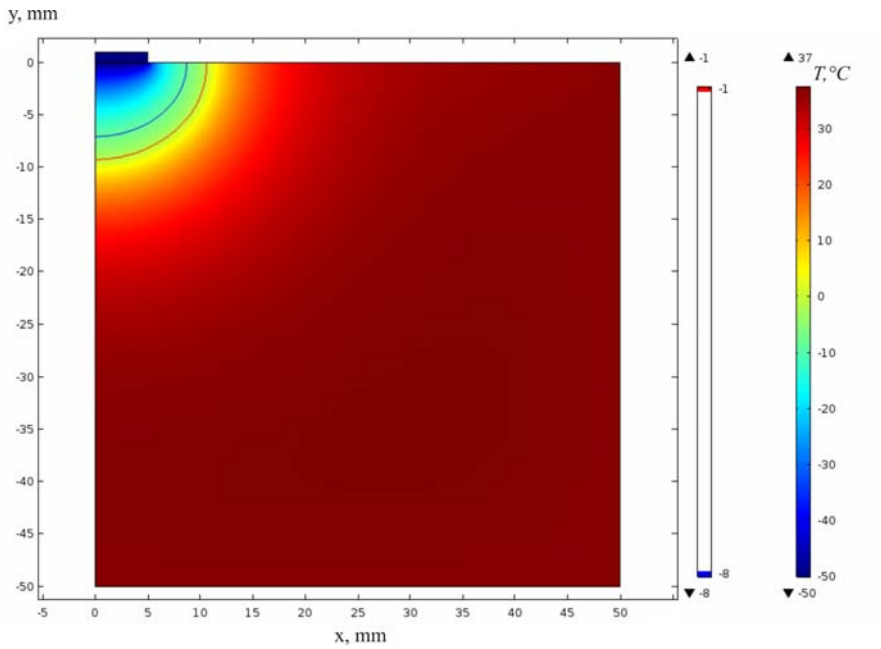

Fig. 4. Temperature distribution in the section of biological tissue on the surface of which there is a cooling element at a temperature T = -50°C at time moment t = 500 s:
l_1 – temperature level T = -8°C and l_2 is temperature level T = -1°C.

Fig. 5 shows the dependence of the motion of phase transition zone (crystallization zone of biological tissue) on the time of temperature exposure. From Fig.5 it is seen that maximum freezing depth of biological tissue is about $l \approx 10$ mm at a temperature of cooling element T = -50°C.

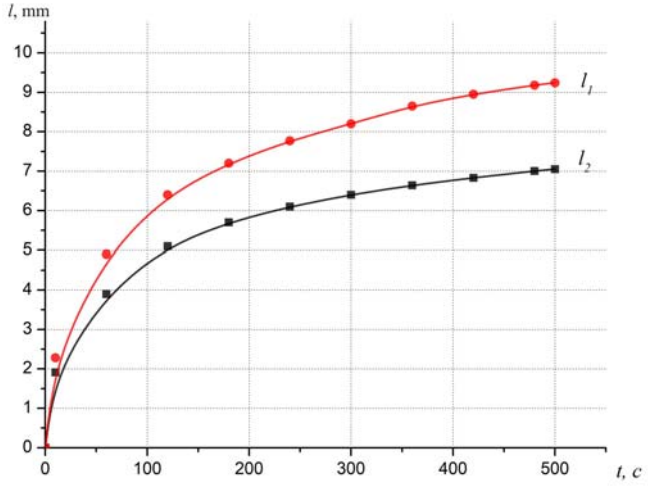

Fig. 5. Dependence of the motion of phase transition zone (crystallization zone of biological tissue) on the time of temperature exposure at a cooling element temperature T = -50°C: l_1 – temperature level T = -8°C and l_2 – temperature level T = -1°C.

Computer simulation was used to determine the dependence of the freezing depth of biological tissue on temperature at different time intervals (Fig. 6) and on the time of temperature exposure at a cooling element temperature T = -50 ° C (Fig. 7).

Figs. 6 and 7 show that at t = 60 s the biological tissue is cooled to a temperature of T = 10 ° C at a depth of l ≈ 4 mm, and at t = 180 s - at a depth of l ≈ 5 mm and at t = 480 s - at a depth of l ≈ 7 mm.

It is established that with increasing temperature exposure, a deeper cooling of biological tissue is attained. That is, with prolonged temperature exposure (T = -50 ° C), destruction of the corresponding section of biological tissue can be achieved.

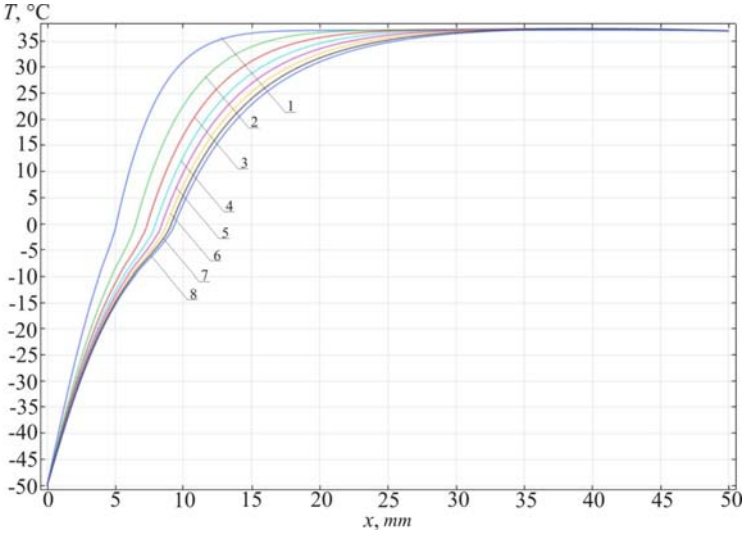

Fig.6. Temperature distribution in biological tissue at different time moments of temperature exposure: 1 – t = 60 s; 2 – t = 120 s; 3 – t = 180 s; 4 – t = 240 s; 5 – t = 300 s; 6 – t = 360 s; 7 – t = 420 s; 8 – t = 480 s.

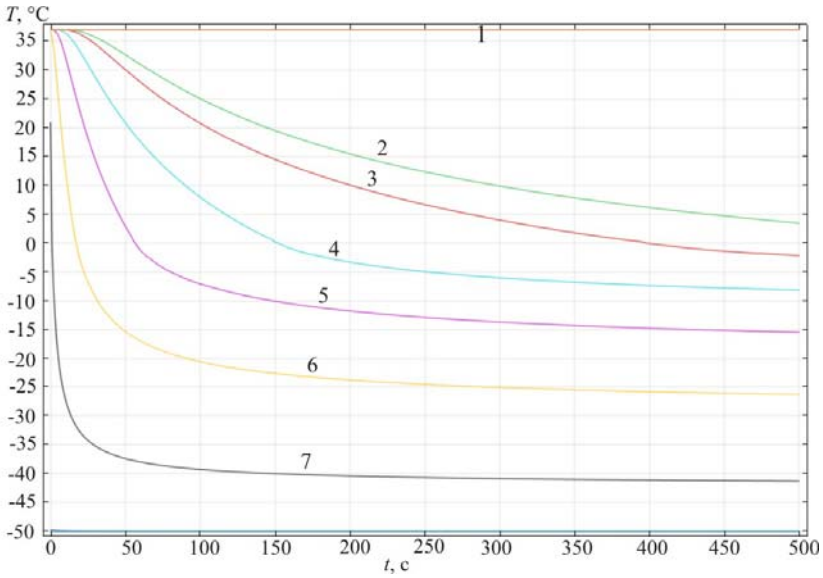

Fig. 7. Time dependence of temperature at different depth h of biological tissue at cooling element temperature T = -50°C: 1 – h = 0; 2 – h = 1 mm; 3 – h = 3 mm; 4 – h = 5 mm; 5 – h = 7 mm; 6 – h = 9 mm; 7 – h = 10 mm.

Thus, a technique was developed for taking into account the phase transition in biological tissue during computer –aided simulation of cryodestruction process, which makes it possible to predict the results of local temperature effect on biological tissue and to determine the temperature and heat flux distributions at any given time with a predetermined arbitrary time function of change in the temperature of cooling element $T_f(t)$.

It should be noted that the obtained results make it possible to predict the depth of freezing of biological tissue at a given temperature exposure, taking into account the phase transition to achieve the maximum effect during cryodestruction.

Conclusion

1. A technique was developed for taking into account the phase transition in biological tissue during computer-aided simulation of the cryodestruction process, which makes it possible to predict the results of local temperature effect on biological tissue and to determine the temperature and heat flux distributions at any given time with a predetermined arbitrary time function of change in the temperature of cooling element $T_f(t)$.
2. Physical, mathematical and computer models of biological tissue on the surface of which there is a cooling element at a temperature of T = -50°C have been created with regard to thermophysical processes, blood circulation, heat transfer, metabolic processes and phase transition.
3. Using computer simulation, the distribution of temperature and heat fluxes inside the biological tissue was determined in cooling mode at a cooling element temperature T = 50 °C. The dependence of the freezing depth of biological tissue on the temperature of cooling element and the time of temperature exposure was established. The maximum freezing depth of biological tissue was determined, which is $l \approx$ 7-10 mm at a cooling element temperature T = 50 °C.

References

1. Anatychuk L.I. (1979). *Termoelementy i termoelektricheskiie ustroistva. Spravochnik [Thermo-*

elements and thermoelectric devices. Reference book]. Kyiv: Naukova Dumka [in Russian].
2. Kolenko E.A. (1967). *Termoelektricheskiie okhlazhdaiushchiie pribory [Thermoelectric cooling devices. 2nd ed.* Leningrad: Nauka [in Russian].
3. Anatychuk L.I., Denisenko O.I., Kobylianskyi R.R., Kadeniuk T.Ya., Perepichka M.P. (2017). Modern methods of cryotherapy in dermatological practice. *Klinichna ta eksperymental'na patologiia - Clinical and experimental pathology*, XVI, (59), 150-156.
4. Denkov V. (1988). At the edge of life. Moscow: Znaniie [Russian transl.]
5. Maruyama S., Nakagawa K., Takeda H. (2008). The flexible cryoprobe using Peltier effect for heat transfer control. *Journal of Biomechanical Science and Engineering*, 138-150.
6. Kochenov V.I. (2000). *Kriokhirurgicheskaia profilakticheskaia onkologiia [Cryosurgical preventive oncology]*. Nizhnii Novgorod [in Russian].
7. Kochenov V.I. (2003). *Kriologicheskaia profilakticheskaia onkologiia: kratkoie uchebnoie I metodicheskooie posibiie dlia vrachei i studentov [Cryological preventive oncology: brief educational and methodological manual for doctors and students]*. 2nd revised ed. Nizhnii Novgorod [in Russian].
8. Kochenov V.I. (1982). Adhesive effect in cryosurgery. *Abstract in the International Abstract Journal*, IV, 8.
9. Moskalyk, I.A., Manyk O.M. (2013). On the use of thermoelectric cooling in cryodestruction practice. *J.Thermoelectricity*, 6, 84-92.
10. Anatychuk L.I., Denisenko O.I., Kobylianskyi R.R., Kadeniuk T.Ya. (2015). On the use of thermoelectric cooling in dermatology and cosmetology. *J.Thermoelectricity*, 3, 57-71.
11. Moskalyk I.A. (2015). On the use of thermoelectric devices in cryosurgery. *Physics and Chemistry of the Solid State,* 4, 742-746.
12. Kobylianskyi R.R., Kadeniuk T.Ya. (2016) Pro perspektyvy vykorystannia termoelektryky dlia likuvannia zakhvoriuvan shkiry kholodom [On the prospects of using thermoelectricity for treatment of skin diseases with cold]. *Naukovy visnyk Chernivetskogo universitetu: zbirnyk naukovykh ptrats. Fizyka. Elektronika - Scientific Bulletin of Chernivtsi University: Collection of Scientific Papers. Physics. Electronics,* 5, 1, 67 – 72 [in Ukrainian].
13. Anatychuk L.I., Vikhor L.M., Kotsur M.P., Kobylianskyi R.R., Kadeniuk T.Ya. (2016). Optimal control of time dependence of cooling temperature in thermoelectric devices. *J.Thermoelectricity*, 5, 5-11.
14. Anatychuk L.I., Kobylianskyi R.R., Kadeniuk T.Ya. (2017). Computer simulation of local thermal effect on human skin. *J.Thermoelectricity*, 1, 69-79.
15. Anatychuk L.I., Vikhor L.M., Kobylianskyi R.R., Kadeniuk T.Ya. (2017). Computer simulation and optimization of the dynamic operating modes of thermoelectric device for treatment of skin diseases. *J.Thermoelectricity*, 2, 44-57.
16. Anatychuk L.I.., Vikhor L.M., Kobylianskyi R.R., Kadeniuk T.Ya., Zvarich O.V. (2017). Computer simulation and optimization of the dynamic operating modes of thermoelectric device for reflexotherapy. *J.Thermoelectricity*, 3, 68-78.
17. Anatychuk L.I., Vikhor L.M., Kobylianskyi R.R., Kadeniuk T.Ya. (2017). Computer simulation and optimization of the dynamic operating modes of thermoelectric device for cryodestruction. *Physics and Chemistry of the Solid State*, 18 (4), 455-459.
18. Anatychuk L., Vikhor L, Kotsur M., Kobylianskyi R., Kadeniuk T. (2018). Optimal control of time dependence of temperature in thermoelectric devices for medical purposes. *International Journal of Thermophysics 3*9:108. https://doi.org/10.1007/s10765-018-2430-z.

19. Anatychuk L.I., Vikhor L.M., Kobylianskyi R.R., Kadeniuk T.Ya. (2018). Kompiuterne modeliuvannia lokalnogo temperaturenogo vplyvu na shkiru liudyny v dynamichnomu rezhymi [Computer simulation of local temperature effect on human skin in the dynamic mode]. *Visnyk Natsionalnogo universitetu "Lvivska Politechnica". Physical and mathematical sciences – Bulletin of National university "Lvivska Politechnica." Physical and mathematical sciences.* Lviv: Lvivska Politechnical Publ., 898, 78-82.
20. Pennes H.H. (1948). Analysis of tissue and arterial blood temperatures in the resting forearm *J. Appl. Physiol*. 1(2), 93 – 122.
21. Jiang S.C., Ma N., Li H.J. and Zhang X.X. (2002). Effects of thermal properties and geometrical dimensions on skin burn injuries. *Burns* 28, 713 – 717.
22. Cetingul M.P., Herman C. (2008). Identification of skin lesions from the transient thermal response using infrared imaging technique. *IEEE*, 1219 – 1222.
23. Ciesielski M., Mochnacki B. and Szopa R. (2011). Numerical modeling of biological tissue heating. Admissible thermal dose. *Scientific Research of the Institute of Mathematics and Computer Science* 1 (10), 11 – 20.
24. Filipoiu Florin, Bogdan Andrei Ioan and Carstea Iulia Maria (2010). Computer-aided analysis of the heat transfer in skin tissue. *Proceedings of the 3rd WSEAS Int. Conference on Finite Differences - Finite Elements - Finite Volumes - Boundary Elements,* 53 – 59.
25. Carstea Daniela, Carstea Ion and Carstea Iulia Maria Carstea (2011). Interdisciplinarity in computer-aided analysis of thermal therapies. *WSEAS Transactions on Systems and Control*, 6 (4), 115 – 124.
26. Deng Z.S., Liu J. (2005). Numerical simulation of selective freezing of target biological tissues following injection of solutions with specific thermal properties. *Cryobiology*, 50, 183-192.
27. Han Liang Lim, Venmathi Gunasekaran. Mathematical modeling of heat distribution during cryosurgery // https://isn.ucsd.edu/last/courses/beng221/problems/2011/project10.pdf.
28. COMSOL Multiphysics User's Guide (2018). COMSOLAB.

Submitted 21.03.2019

Анатичук Л.І. *акад. НАН України*[1,2]
Кобилянський Р.Р. *канд. фіз.– мат. наук* [1,2]**, Федорів Р.В.**[2]

[1]Інститут термоелектрики НАН і МОН України,
вул. Науки, 1, Чернівці, 58029, Україна;
[2]Чернівецький національний університет
ім. Юрія Федьковича, вул. Коцюбинського 2,
Чернівці, 58012, Україна; *e-mail: anatych@gmail.com*

МЕТОДИКА ВРАХУВАННЯ ФАЗОВОГО ПЕРЕХОДУ В БІОЛОГІЧНІЙ ТКАНИНІ ПРИ КОМП'ЮТЕРНОМУ МОДЕЛЮВАННІ ПРОЦЕСУ КРІОДЕСТРУКЦІЇ

У роботі наведено методику врахування фазового переходу в біологічній тканині при комп'ютерному моделюванні процесу кріодеструкції. Побудовано фізичну, математичну та комп'ютерну моделі біологічної тканини з врахуванням теплофізичних процесів, кровообігу, теплообміну, процесів метаболізму та фазового переходу. Як приклад, розглянуто випадок, коли на поверхні біологічної тканини знаходиться охолоджуючий елемент при температурі - 50°С. Визначено розподіли температури і теплових потоків у біологічній тканині в режимі охолодження. Отримані результати дають можливість прогнозувати глибину промерзання біологічної тканини при заданому температурному впливі. Бібл. 28, рис. 7, табл. 1.
Ключові слова: біологічна тканина, температурний вплив, кріодеструкція, фазовий перехід, комп'ютерне моделювання.

Анатичук Л.И. *акад. НАН Украины*[1,2]
Кобылянський Р.Р. *канд. физ.– мат. наук* [1,2]**, Федорив Р.В.**[2]

[1]Институт термоэлектричества НАН и МОН Украины, ул. Науки, 1,
Черновцы, 58029, Украина, *e–mail: anatych@gmail.com;*
[2]Черновицкий национальный университет
им. Юрия Федьковича, ул. Коцюбинского, 2,
Черновцы, 58012, Украина

В работе приведена методика учитывания фазового перехода в биологической ткани при компьютерном моделировании процесса криодеструкции. Построены физическая, математическая и компьютерная модели биологической ткани с учетом теплофизических процессов, кровообращения, теплообмена, процессов метаболизма и фазового перехода. Как пример, рассмотрен случай, когда на поверхности биологической ткани находится охлаждающий элемент при температуре - 50 С. Определенно распределения температуры и тепловых потоков в биологической ткани в режиме охлаждения. Полученные результаты дают возможность прогнозировать глубину промерзания биологической ткани при заданном температурном влиянии. Библ. 28, рис. 7, табл. 1.
Ключевые слова: биологическая ткань, температурное влияние, криодеструкция, фазовый переход, компьютерное моделирование.

References

1. Anatychuk L.I. (1979). *Termoelementy i termoelektricheskiie ustroistva. Spravochnik [Thermoelements and thermoelectric devices. Reference book]*. Kyiv: Naukova Dumka [in Russian].
2. Kolenko E.A. (1967). *Termoelektricheskiie okhlazhdaiushchiie pribory [Thermoelectric cooling devices. 2nd ed.* Leningrad: Nauka [in Russian].
3. Anatychuk L.I., Denisenko O.I., Kobylianskyi R.R., Kadeniuk T.Ya., Perepichka M.P. (2017). Modern methods of cryotherapy in dermatological practice. *Klinichna ta eksperymental'na patologiia - Clinical and experimental pathology*, XVI, (59), 150-156.
4. Denkov V. (1988). At the edge of life. Moscow: Znaniie [Russian transl.]
5. Maruyama S., Nakagawa K., Takeda H. (2008). The flexible cryoprobe using Peltier effect for heat transfer control. *Journal of Biomechanical Science and Engineering*, 138-150.

6. Kochenov V.I. (2000). *Kriokhirurgicheskaia profilakticheskaia onkologiia [Cryosurgical preventive oncology]*. Nizhnii Novgorod [in Russian].
7. Kochenov V.I. (2003). *Kriologicheskaia profilakticheskaia onkologiia: kratkoie uchebnoie I metodicheskooie posibiie dlia vrachei i studentov [Cryological preventive oncology: brief educational and methodological manual for doctors and students]*. 2nd revised ed. Nizhnii Novgorod [in Russian].
8. Kochenov V.I. (1982). Adhesive effect in cryosurgery. *Abstract in the International Abstract Journal*, IV, 8.
9. Moskalyk, I.A., Manyk O.M. (2013). On the use of thermoelectric cooling in cryodestruction practice. *J.Thermoelectricity*, 6, 84-92.
10. Anatychuk L.I., Denisenko O.I., Kobylianskyi R.R., Kadeniuk T.Ya. (2015). On the use of thermoelectric cooling in dermatology and cosmetology. *J.Thermoelectricity*, 3, 57-71.
11. Moskalyk I.A. (2015). On the use of thermoelectric devices in cryosurgery. *Physics and Chemistry of the Solid State,* 4, 742-746.
12. Kobylianskyi R.R., Kadeniuk T.Ya. (2016) Pro perspektyvy vykorystannia termoelektryky dlia likuvannia zakhvoriuvan shkiry kholodom [On the prospects of using thermoelectricity for treatment of skin diseases with cold]. *Naukovy visnyk Chernivetskogo universitetu: zbirnyk naukovykh ptrats. Fizyka. Elektronika - Scientific Bulletin of Chernivtsi University: Collection of Scientific Papers. Physics. Electronics,* 5, 1, 67 – 72 [in Ukrainian].
13. Anatychuk L.I., Vikhor L.M., Kotsur M.P., Kobylianskyi R.R., Kadeniuk T.Ya. (2016). Optimal control of time dependence of cooling temperature in thermoelectric devices. *J.Thermoelectricity*, 5, 5-11.
14. Anatychuk L.I., Kobylianskyi R.R., Kadeniuk T.Ya. (2017). Computer simulation of local thermal effect on human skin. *J.Thermoelectricity*, 1, 69-79.
15. Anatychuk L.I., Vikhor L.M., Kobylianskyi R.R., Kadeniuk T.Ya. (2017). Computer simulation and optimization of the dynamic operating modes of thermoelectric device for treatment of skin diseases. *J.Thermoelectricity*, 2, 44-57.
16. Anatychuk L.I.., Vikhor L.M., Kobylianskyi R.R., Kadeniuk T.Ya., Zvarich O.V. (2017). Computer simulation and optimization of the dynamic operating modes of thermoelectric device for reflexotherapy. *J.Thermoelectricity*, 3, 68-78.
17. Anatychuk L.I., Vikhor L.M., Kobylianskyi R.R., Kadeniuk T.Ya. (2017). Computer simulation and optimization of the dynamic operating modes of thermoelectric device for cryodestruction. *Physics and Chemistry of the Solid State*, 18 (4), 455-459.
18. Anatychuk L., Vikhor L, Kotsur M., Kobylianskyi R., Kadeniuk T. (2018). Optimal control of time dependence of temperature in thermoelectric devices for medical purposes. *International Journal of Thermophysics 3*9:108. https://doi.org/10.1007/s10765-018-2430-z.
19. Anatychuk L.I., Vikhor L.M., Kobylianskyi R.R., Kadeniuk T.Ya. (2018). Kompiuterne modeliuvannia lokalnogo temperaturenogo vplyvu na shkiru liudyny v dynamichnomu rezhymi [Computer simulation of local temperature effect on human skin in the dynamic mode]. *Visnyk Natsionalnogo universitetu "Lvivska Politechnica". Physical and mathematical sciences – Bulletin of National university "Lvivska Politechnica." Physical and mathematical sciences.* Lviv: Lvivska Politechnical Publ., 898, 78-82.
20. Pennes H.H. (1948). Analysis of tissue and arterial blood temperatures in the resting forearm *J. Appl. Physiol*. 1(2), 93 – 122.
21. Jiang S.C., Ma N., Li H.J. and Zhang X.X. (2002). Effects of thermal properties and geometrical

dimensions on skin burn injuries. *Burns* 28, 713 – 717.
22. Cetingul M.P., Herman C. (2008). Identification of skin lesions from the transient thermal response using infrared imaging technique. *IEEE*, 1219 – 1222.
23. Ciesielski M., Mochnacki B. and Szopa R. (2011). Numerical modeling of biological tissue heating. Admissible thermal dose. *Scientific Research of the Institute of Mathematics and Computer Science* 1 (10), 11 – 20.
24. Filipoiu Florin, Bogdan Andrei Ioan and Carstea Iulia Maria (2010). Computer-aided analysis of the heat transfer in skin tissue. *Proceedings of the 3rd WSEAS Int. Conference on Finite Differences - Finite Elements - Finite Volumes - Boundary Elements,* 53 – 59.
25. Carstea Daniela, Carstea Ion and Carstea Iulia Maria Carstea (2011). Interdisciplinarity in computer-aided analysis of thermal therapies. *WSEAS Transactions on Systems and Control*, 6 (4), 115 – 124.
26. Deng Z.S., Liu J. (2005). Numerical simulation of selective freezing of target biological tissues following injection of solutions with specific thermal properties. *Cryobiology*, 50, 183-192.
27. Han Liang Lim, Venmathi Gunasekaran. Mathematical modeling of heat distribution during cryosurgery // https://isn.ucsd.edu/last/courses/beng221/problems/2011/project10.pdf.
28. COMSOL Multiphysics User's Guide (2018). COMSOLAB.

Submitted 21.03.2019

T.V.Zakharchuk[1],
I.A. Konstantynovych *cand. phys.– math. sciences, dochent*[1,2]**,**
A.V. Konstantynovych *doc. phys.– math. sciences, dochent*[1]**,**
A.V.Forbatiuk[1]

[1]Chernivtsi National University, 2 Kotsiubynskyi Str.,
Chernivtsi, Ukraine, 58012
[2]Institute of Thermoelectricity of the NAS and MES of Ukraine,
1, Nauky str., Chernivtsi, 58029, Ukraine;
aconst@ukr.net, dj_kneo@ukr.net

ON THE EFFICIENCY OF SPIRAL GYROTROPIC THERMOELEMENTS IN COOLING MODE

In this paper, the characteristics of BiSb, Ag_2Te and InSb materials in constant magnetic field were considered. Analytical and numerical methods were used to study the basic relations for the calculation of optimal parameters of spiral gyrotropic thermoelements in cooling mode. The dependences of maximum temperature difference for gyrotropic thermoelements of various shapes were obtained. It was shown that at constant magnetic fields the use of BiSb is more reasonable in the temperature range of 80-120 K, whereas in the range of 200 – 300 K it is worthwhile to use Ag_2Te. Bibl. 25, Tabl. 2, Fig. 14.
Key words: gyrotropic medium, magnetic field induction, spiral gyrotropic thermoelement.

Introduction

Thermoelectric devices are known to be widely used in power engineering, refrigeration and measurement techniques. However, the possibilities of practical application of thermoelectricity depend on the progress in physics of thermoelectric power conversion, since the main feature of thermoelectric devices is their ability to use interconversion of the electrical and thermal energies [1–12]. Advances of thermoelectricity in the area of instrument engineering are mainly achieved on the basis of physics of thermocouple elements. The generalized theory of thermoelectricity afforded an opportunity to develop methods for devising new types of thermoelements. Their application in anisotropic media helped to discover, create and research a variety of basically new types of thermoelements with unique features which significantly expanded the potential of thermoelectricity. Searching for new types of thermoelements based on the gyrotropic media is one of the best lines in the development of thermoelectric applications. These opportunities of thermoelectricity are little studied, and their implementation will make it possible to expand the element basis of thermoelectricity, create thermoelectric products of enhanced performance and increase the competitiveness of such power converters.

Of vital importance is the avenue for increasing the efficiency and reliability of power converters for their application in instrument engineering. Another advantage offered by gyrotropic thermoelements is the absence of internal junctions, assuring reliability and ease of manufacture, possibility of junction-free connection of rings into a space spiral structure, which sufficiently increases the functionality of thermoelements, especially when used in refrigeration and measurement technique.

The purpose of the work is to evaluate the efficiency of spiral gyrotropic thermoelements in cooling mode for their subsequent use in refrigeration and measurement technique.

Mathematical model

Thermal conductivity equation for homogeneous gyrotropic medium is given by

$$\kappa\Delta T + \rho_0 j^2 + 2\alpha_B\left(j_y\frac{\partial T}{\partial x} - j_x\frac{\partial T}{\partial y}\right) = 0, \tag{1}$$

де T – temperature, ρ_0 is electrical resistivity in gyrotropic medium; κ is thermal conductivity; j is modulus of electric current density vector; j_x, j_y are projections of j vector in the Cartesian coordinate system; $\alpha_B = Q_\perp B$ is asymmetric part of thermoEMF tensor; $Q_\perp$ is the Nernst –Ettingshausen coefficient; B is magnetic field induction.

ThermoEMF tensor in gyrotropic medium is of the form

$$\alpha = \begin{pmatrix} \alpha_0 & \alpha_B & 0 \\ -\alpha_B & \alpha_0 & 0 \\ 0 & 0 & \alpha_\perp \end{pmatrix}, \tag{2}$$

In the polar coordinate system, with regard to the system axial symmetry, we have

$$\kappa\Delta T + \rho_0 j^2 + 2Q_\perp B\left(j_\varphi\frac{\partial T}{\partial r} - \frac{j_r}{r}\frac{\partial T}{\partial \varphi}\right) = 0, \tag{3}$$

where r is the thermoelement radius; j_r, j_φ are the radial and azimuthal components of the current density vector.

Cooling mode

There is a variety of references describing the properties of gyrotropic materials [1–8]. For *BiSb, Ag_2Te* and *InSb* materials subject to constant magnetic field the temperature dependences of the figure of merit were built [1–4].

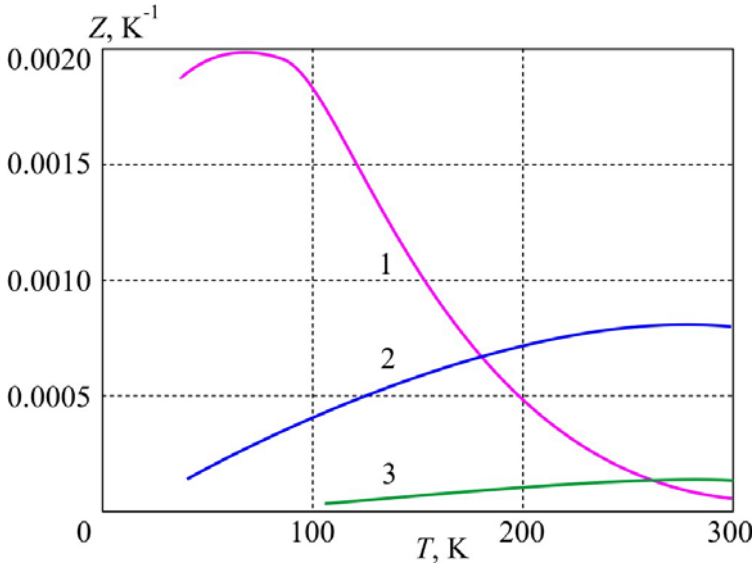

Fig. 1. Figure of merit Z shown as a function of temperature T (1 – BiSb, 2 – Ag_2Te, 3 – InSb) [1–4].

The simulation of gyrotropic thermoelements for Ag_2Te material was carried out. The thermoelements were exposed to the magnetic field with induction of $B = 1$ T. Fig. 2 shows a three-dimensional model of temperature distribution in the spiral gyrotropic thermoelement (round section) [13].

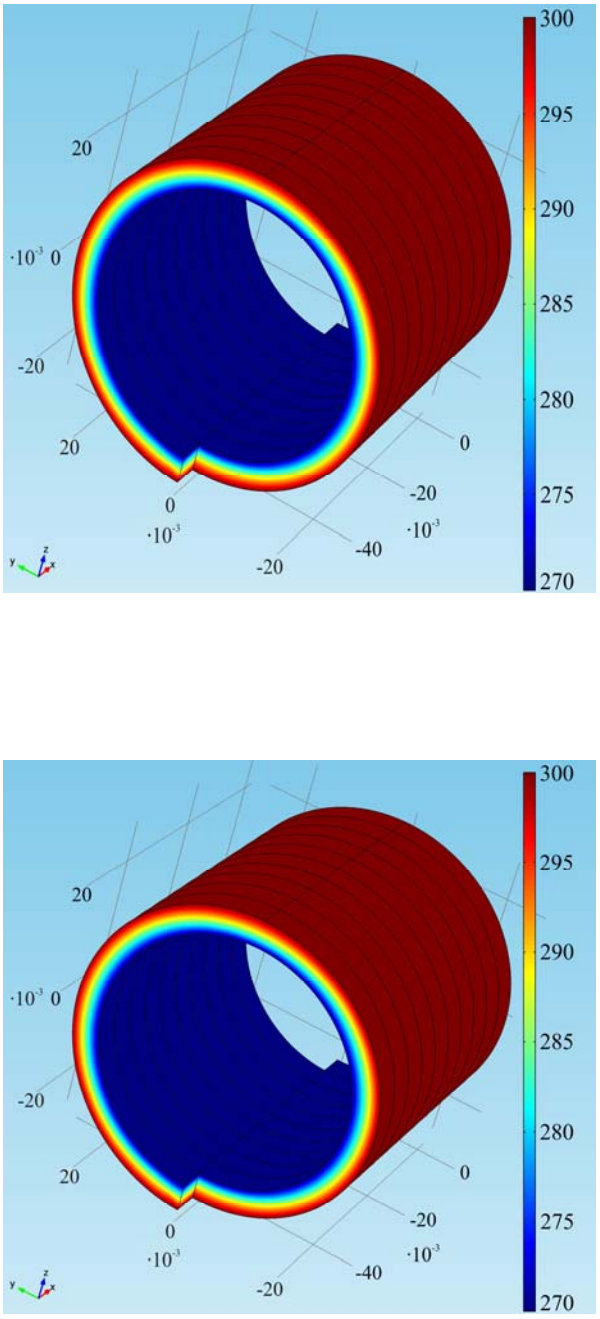

Fig. 2. Model of temperature distribution in the spiral gyrotropic thermoelement (round section)

Fig. 3 shows a three-dimensional model of temperature distribution in the spiral gyrotropic thermoelement (square section).

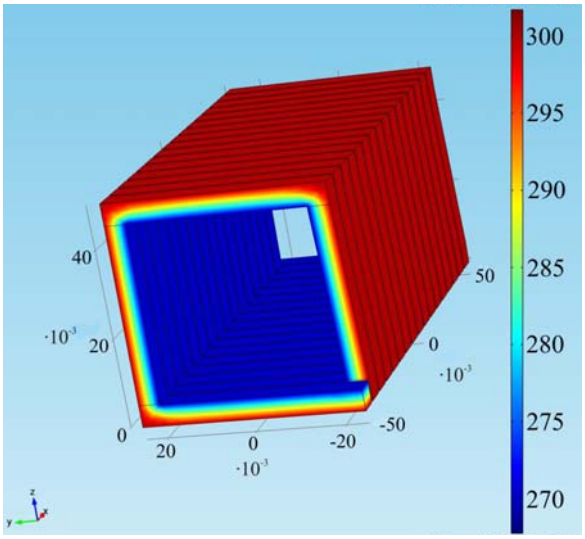

Fig. 3. Model of temperature distribution in the spiral gyrotropic thermoelement (square section)

Assuming that the hot side of spiral gyrotropic thermoelement is adiabatically isolated and ignoring the losses through the side surfaces of the thermoelement, one can use the formula for calculating maximum temperature difference ΔT_{max} between the sides of spiral gyrotropic thermoelement [5]. Using the data presented in Fig. 1, it is possible to obtain the dependence of maximum temperature difference on the hot side temperature of thermoelement for *BiSb, Ag_2Te* and *InSb* (Fig. 4).

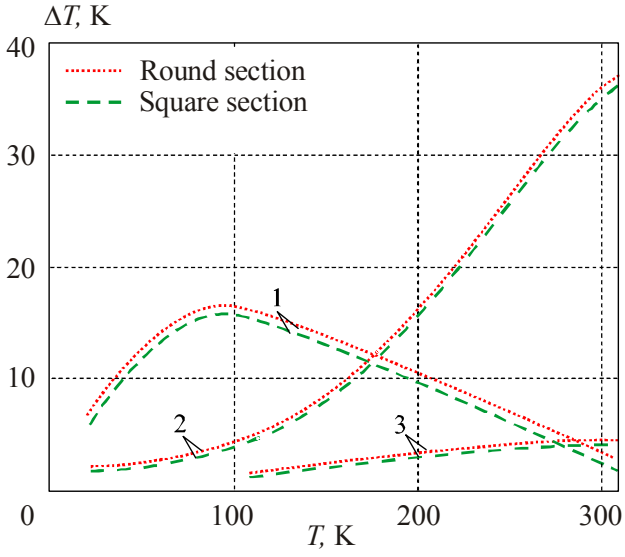

Fig. 4. ΔT_{max} shown as a function of T_1 (1 – BiSb, 2 – Ag_2Te, 3 – InSb)

From Fig. 4 it can be seen that the use of Ag_2Te material in the temperature range of 200 – 300 K yields the highest values of $(\Delta T)_{max}$, at $T_2 = 300$ K the value of $(\Delta T)_{max} \approx 37$ K. It means that the use of Ag_2Te is more reasonable in the temperature range of 200-300 K, and in the temperature range of 80 – 120 K it is worthwhile to use *BiSb* – $(\Delta T)_{max} \approx 17$ K for round section.

Conclusions

1. The analytical and numerical methods were used to study the basic relations for the calculation of optimal parameters of gyrotropic thermoelements in cooling mode. For Ag_2Te material, computer simulation was performed and the temperature distributions in gyrotropic thermoelements were obtained.
2. It was shown that the use of Ag_2Te material is more reasonable in the temperature range of 200 – 300 K, when $(\Delta T)_{max} \approx 37$ K, and in the range of 80 – 120 K it is worthwhile to use *BiSb* – $(\Delta T)_{max} \approx 17$ K for round section.

References

1. Anatychuk L.I. (1979). *Termoelementy i termoelektricheskiie ustroistva. Spravochnik. [Thermoelements and thermoelectric devices. Reference Book]*. Kyiv: Naukova Dumka [in Russian].
2. Osipov E.V., Varich N.I., Mikitey P.P. (1971). Study of the Ettingshausen effect in $Bi_{1-x}Sb_x$ single crystals. *Semiconductors*, 5(11), 2202 – 2204.
3. Aliev S.A., Aliev M.I., Agaev Z.F., Arasli D.G. (1981). Material for Ettingshausen's cooler. *Certificate of Authorship №828269.*
4. Aliev S.A., Zulfigarov E.I. (2009). *Termomagnitnyie i termoelektricheskiie effekty v nauke i tekhnologii [Thermomagnetic and thermoelectric effects in science and technology]*. Baku: Elm Publ. [in Russian].
5. Samoilovich A.G. (2006*). Termoelektricheskiie i termomagnitnyie metody preobrazonaniia energii [Thermoelectric and thermomagnetic energy conversion methods]*. Chernivtsi: Ruta [in Russian].
6. Anatychuk L.I. (2003). *Termoelektrichestvo, T.2, Termoelektricheskiie preobrazovateli energii [Thermoelectricity, Vol.2, Thermoelectric Power Converters]*. Kyiv, Chernivtsi: Naukova Dumka [in Russian].
7. Samoilovich A.G., Korenblit L.L. (1953). Current status of theory of thermoelectric and thermomagnetic effects in semiconductors. *Advances in Physical Sciences*, 49(2), 243 – 272.
8. Nakamura H., Ikeda K., and Yamaguchi S. (1997). Transport coefficients of InSb in a strong magnetic field. *Proc. of XVI International Conference on Thermoelectrics* (Dresden, Germany, 1997).
9. Anatychuk L.I., Luste O.J., Fedoruk Ya.G., Shinkaruk S.M. (2004). Eddy thermoelectric currents in gyrotropic medium with a radial temperature distribution. *J.Thermoelectricity* 1, 19 – 24.
10. Luste O.J., Fedoruk Ya.G. (2006). Gyrotropic thermoelement in the inhomogeneous magnetic field. *J.Thermoelectricity*, 1, 16 – 22.
11. Luste O.J., Fedoruk Ya.G. (2008). Optimization of materials for gyrotropic thermoelements. *J.Thermoelectricity*, 4, 21 – 26.
12. Konstantynovych I.A., Rendigevych O.V. (2016). On the efficiency of gyrotropic thermoelements in generation mode *J.Thermoelectricity*, 1, 64 – 69.
13. Konstantynovych I.A. (2016). On the efficiency of gyrotropic thermoelements in cooling mode. *J.Thermoelectricity*, 3, 46 –50.

Submitted 07.02.2019

Захарчук Т.В.[1], Константинович І.А *канд. фіз.– мат. наук, доцент*[1,2],
Константинович А.В. *док. фіз.– мат. наук, доцент* [1], **Форбатюк А.В.[1]**

[1]Чернівецький національний університет
ім. Юрія Федьковича, вул. Коцюбинського 2,
Чернівці, 58012, Україна
[2]Інститут термоелектрики НАН і МОН України,
вул. Науки, 1, Чернівці, 58029, Україна;
e-mail: anatych@gmail.com

ПРО ЕФЕКТИВНІСТЬ СПІРАЛЬНИХ ГІРОТРОПНИХ ТЕРМОЕЛЕМЕНТІВ У РЕЖИМІ ОХОЛОДЖЕННЯ

Розглянуто характеристики матеріалів BiSb, Ag_2Te й InSb в постійному магнітному полі. Досліджено основні співвідношення для розрахунку оптимальних параметрів спіральних гіротропних термоелементів у режимі охолодження, аналітичними та числовими методами. Отримано залежності максимальної різниці температір для гіротропних термоелементів різних форм. Показано, що при постійних магнітних полях доцільно використовувати BiSb в температурному діапазоні 80 – 120 К, а Ag_2Te для 150 – 300 К.
Ключові слова: гіротропне середовище, індукція магнітного поля, спіральний гіротропний термоелемент.

Захарчук Т.В.,[1] **Константинович І.А.** *канд. физ.– мат. наук*[1,2]
Константинович А.В. *док. физ.– мат. наук, доцент*[1]
Форбатюк А.В.[1]

[1]Черновицкий национальный университет
имени Юрия Федьковича, ул. Коцюбинского,
2, Черновцы, 58012, Украина;
[2]Институт термоэлектричества НАН и МОН Украины, ул. Науки,
1, Черновцы, 58029, Украина, *e-mail: anatych@gmail.com*;

ОБ ЭФФЕКТИВНОСТИ СПИРАЛЬНЫХ ГИРОТРОПНЫХ ТЕРМОЭЛЕМЕНТОВ В РЕЖИМЕ ОХЛАЖДЕНИЯ

Рассмотрены характеристики материалов BiSb, Ag_2Te и InSb в постоянном магнитном поле. Исследованы основные соотношения для расчетов оптимальных параметров спиральных гиротропных термоэлементов в режиме охлаждения, аналитическими и числовыми методами. Получены зависимости максимального перепада температур для гиротропных термоэлементов различной формы. Показано, что при постоянных магнитных полях целесообразно использовать BiSb в температурном диапазоне 80 – 120 К, а Ag_2Te для 150 – 300 К. Библ. 13, рис. 4.

Ключевые слова*:* гиротропная среда, индукция магнитного поля, спиральный гиротропный термоэлемент.

References

1. Anatychuk L.I. (1979). *Termoelementy i termoelektricheskiie ustroistva. Spravochnik. [Thermoelements and thermoelectric devices. Reference Book]*. Kyiv: Naukova Dumka [in Russian].
2. Osipov E.V., Varich N.I., Mikitey P.P. (1971). Study of the Ettingshausen effect in $Bi_{1-x}Sb_x$ single crystals. *Semiconductors*, 5(11), 2202 – 2204.
3. Aliev S.A., Aliev M.I., Agaev Z.F., Arasli D.G. (1981). Material for Ettingshausen's cooler. *Certificate of Authorship №828269.*
4. Aliev S.A., Zulfigarov E.I. (2009). *Termomagnitnyie i termoelektricheskiie effekty v nauke i tekhnologii [Thermomagnetic and thermoelectric effects in science and technology]*. Baku: Elm Publ. [in Russian].
5. Samoilovich A.G. (2006*). Termoelektricheskiie i termomagnitnyie metody preobrazonaniia energii [Thermoelectric and thermomagnetic energy conversion methods]*. Chernivtsi: Ruta [in Russian].
6. Anatychuk L.I. (2003). *Termoelektrichestvo, T.2, Termoelektricheskiie preobrazovateli energii [Thermoelectricity, Vol.2, Thermoelectric Power Converters]*. Kyiv, Chernivtsi: Naukova Dumka [in Russian].
7. Samoilovich A.G., Korenblit L.L. (1953). Current status of theory of thermoelectric and thermomagnetic effects in semiconductors. *Advances in Physical Sciences*, 49(2), 243 – 272.
8. Nakamura H., Ikeda K., and Yamaguchi S. (1997). Transport coefficients of InSb in a strong magnetic field. *Proc. of XVI International Conference on Thermoelectrics* (Dresden, Germany, 1997).
9. Anatychuk L.I., Luste O.J., Fedoruk Ya.G., Shinkaruk S.M. (2004). Eddy thermoelectric currents in gyrotropic medium with a radial temperature distribution. *J.Thermoelectricity* 1, 19 – 24.
10. Luste O.J., Fedoruk Ya.G. (2006). Gyrotropic thermoelement in the inhomogeneous magnetic field. *J.Thermoelectricity*, 1, 16 – 22.
11. Luste O.J., Fedoruk Ya.G. (2008). Optimization of materials for gyrotropic thermoelements. *J.Thermoelectricity*, 4, 21 – 26.
12. Konstantynovych I.A., Rendigevych O.V. (2016). On the efficiency of gyrotropic thermoelements in generation mode *J.Thermoelectricity*, 1, 64 – 69.
13. Konstantynovych I.A. (2016). On the efficiency of gyrotropic thermoelements in cooling mode. *J.Thermoelectricity*, 3, 46 –50.

Submitted 07.02.2019

Cherkez R.G.

Cherkez R.G., *cand. phys.– mat. sciences, Acting professor*[1,2]

[1]Institute of Thermoelectricity of the NAS and MES of Ukraine,
1, Nauky str., Chernivtsi, 58029, Ukraine
[2]Yuriy Fedkovych Chernivtsi National University,
2, Kotsiubynsky str., Chernivtsi, 58012, Ukraine

EFFECT OF LEG SEGMENTATION ON THE EFFICIENCY OF PERMEABLE THERMOELEMENT OF *Co-Sb* BASED MATERIALS

The results of computer research on the effect of leg segment length of Co-Sb-based material on energy conversion efficiency are presented. The optimal operating modes of a 2-segment thermoelement are determined whereby the maximum efficiency values are realized. The possibility of 1.1-1.2-fold increase of the electric power generated by using 2-segment permeable thermoelements of Co-Sb-based materials is demonstrated. Bibl. 14, Fig. 2.

Key words: permeable thermoelements, segmented materials, computer design, Co-Sb based materials.

Introduction

This paper contributes to further research started in [1] and is dedicated to the use of thermal waste by means of permeable segmented thermoelements. It is known that the use of segmented legs in thermoelements allows increasing the efficiency and the generated electric power [2]. This is achieved both due to expansion of the operating temperature range at leg segmentation, and due to the choice of materials with maximum figure of merit value over the entire temperature range. At the same time, in the course of recent decades, the researchers' attention has been drawn to promising materials, namely *Co-Sb* based scutterudites [3], which hold much promise for being used in high-temperature legs of thermoelectric generators in the temperature range up to 800 K. They are characterized by rather high values of the Seebeck coefficient and electrical conductivity. Maximum ZT values of such materials are 1-1.1 at a temperature of 700 K [4 – 5].

However, studies on the use of permeable thermoelements of *Co-Sb* based segmented materials have not been encountered in the literature. Therefore, the purpose of the work is to determine the characteristics of permeable segmented thermoelements of *Co-Sb* based materials in electric energy generation mode, as well as to find their optimal operating conditions and parameters whereby maximum efficiency of thermal into electric energy conversion is realized.

Physical model and its mathematical description

A physical model of permeable thermoelement in electric energy generation mode is represented in Fig. 1. The thermoelement consists of *n*- and *p*-type legs whose physical properties are temperature-dependent. Heat input is realized by passing heat carrier along the legs through the channels (pores). Each leg comprises N_n and N_p segments, and the contact resistance of compound is r_0. The lateral surfaces of the legs are adiabatically isolated; heat carrier temperature at thermoelement inlet T_m is assigned. The temperature of cold junctions T_c is thermostated.

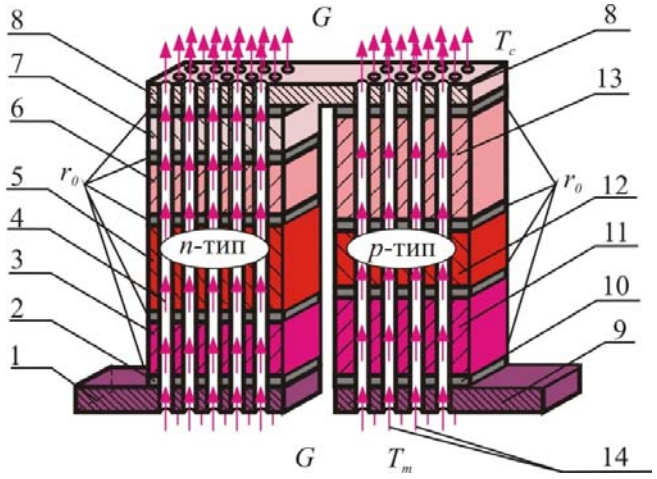

Fig. 1. Physical model of permeable segmented thermoelement.
1, 8, 9 – connecting plates; 2, 10 – connecting layers;
3, 5, 6, 7 – segments of n-type leg; 4,14 – heat carrier;
11, 12, 13 – segments (sections) of p-type leg.

A system of differential equations describing the distribution of temperatures and heat fluxes in a steady-state one-dimensional case, in the infinitely small part *dx* of each *k*-th segment of *n*- and *p*-type legs, in the dimensionless coordinates is given by relations [7]:

$$\left.\begin{aligned}
&\frac{dT}{dx} = -\frac{\alpha_k j}{\kappa_k} T - \frac{j}{\kappa_k} q, \\
&\frac{dq}{dx} = \frac{\alpha_k^2 j}{\kappa_k} T + \frac{\alpha_k j}{\kappa_k} q + j\rho_k + \frac{\alpha_T P_K^1 N_K l_K^2}{(S - S_K) j}(t - T), \\
&\frac{dt}{dx} = \frac{\alpha_T P_K^1 N_K l_k}{G c_P}(t - T),
\end{aligned}\right\}_{n,p} \quad \begin{aligned} &k = 1, \ldots, N_{n,p} \\ &x_{k-1} \le x \le x_k \end{aligned} \tag{1}$$

where $\dot{I}_{\hat{E}}^{1}$ is channel perimeter; N_K is the number of channels, S_K is cross-sectional area of all the channels, S is a section of leg together with the channels, G is heat carrier consumption in the channels, c_P is specific heat of heat carrier, t is heat carrier temperature at point x, T is leg temperature at point x, α_T is heat-transfer coefficient, α, κ, ρ are the Seebeck coefficient, thermal conductivity and resistivity of leg material.

Specific heat fluxes q and the reduced density of electric current j are determined through

$$q = \frac{Q}{I}, \qquad j = \frac{Il}{S}, \tag{2}$$

where Q is power of heat flux passing through thermoelement leg, I is electric current, S is cross-sectional area of thermoelement legs, l – the height of the branch.

The boundary conditions necessary for solving (1) with regard to the Joule-Lenz heat release due to contact resistance r_0 at points of connection of leg segments are formulated as:

$$\begin{aligned}
&T_{n,p}(0) = T_C, \qquad t_{n,p}(1) = T_m, \qquad q_{n,p}(1) = 0, \\
&T_{n,p}(x_k^+) = T_{n,p}(x_k^-), \qquad q_{n,p}(x_k^+) = q_{n,p}(x_k^-) + \frac{r_0}{S_{n,p}} I,
\end{aligned} \tag{3}$$

where indices "-" and "+" denote the values of functions immediately to the left and right of the interface of

segments x_k; $k = 1, \ldots, N$ is the index which determines leg segment number.

For seeking optimal values of doping impurities which determine carrier concentrations in leg segments it is necessary to assign the dependences of material parameters α, κ, ρ on temperature and concentration of carriers (or impurities). The main task in the design of permeable segmented generator thermoelement is to determine such agreed parameters (reduced current density j in the legs, heat carrier consumption in channels G, concentration of doping impurities in materials of each segment) whereby the efficiency of the thermoelement reaches a maximum.

The efficiency will be determined through the relation of electric power P generated by the thermoelement to a change in heat carrier enthalpy:

$$\eta = \frac{P}{\sum\limits_{n,p} Gc_p\left(T_m - T_C\right)}. \tag{4}$$

The maximum efficiency can be conveniently reduced to achievement of functional minimum:

$$J = \ln\left[\sum_{n,p}\left\{Gc_P\left(T_m - T_C\right)\right\}\right] - \ln\left[\sum_{n,p}\left\{Gc_P\left(T_m - t(0)\right) + q(0)\frac{j\left(S - S_K\right)}{l} - I\left(\frac{r_0}{S_n} + \frac{r_0}{S_p}\right)\right\}\right]. \tag{5}$$

This problem was solved through use of the Pontryagin maximum principle [8], yielding the necessary optimality conditions:

1. Optimal values of specific current density in thermoelement legs j must satisfy the equalities

$$-\left[\frac{\partial J}{\partial j}\right]_{n,p} + \sum_{n,p}\int_0^1\left[\psi_1^k\frac{\partial f_1^k}{\partial j_k} + \psi_2^k\frac{\partial f_2^k}{\partial j_k} + \psi_3^k\frac{\partial f_3^k}{\partial j_k}\right]_{n,p} dx = 0, \tag{6}$$

where $\left(f_1^k, f_2^k, f_3^k\right)_{n,p}$ are right-hand sides of equations (1), $\psi = \left(\psi_1^k, \psi_2^k, \psi_3^k\right)_{n,p}$ is pulse vector function [3, 4], which is found from solving the additional system of differential equations

$$\left.\begin{aligned}
\frac{d\psi_1}{dx} &= \frac{\alpha_k j_k}{\kappa_k}R_1\psi_1 - \left(\frac{\alpha_k j_k}{\kappa_k}R_2 - \frac{\alpha_e l_k}{\left(S - S_{\hat{E}}\right)j_k}\right)\psi_2 + \frac{\alpha_T \ddot{I}_K^1 N_K}{Gc_P}\psi_3,\\
\frac{d\psi_2}{dx} &= \frac{j_k}{\kappa_k}\psi_1 - \frac{\alpha_k j_k}{\kappa_k}\psi_2,\\
\frac{d\psi_3}{dx} &= -\frac{\alpha_T \ddot{I}_K^1 N_K l_k}{\left(S - S_{\hat{E}}\right)j_k}\psi_2 - \frac{\alpha_T \ddot{I}_K^1 N_K}{Gc_P}\psi_3,
\end{aligned}\right\}_{n,p} \tag{7}$$

where

$$\left.\begin{aligned}
R_1 &= 1 + \frac{d\ln\alpha}{dT}T - \frac{d\ln\kappa}{dT}\left(T + \frac{q}{\alpha}\right),\\
R_2 &= R_1 + \frac{\kappa}{\alpha^2\sigma}\frac{d\ln\sigma}{dT} + \frac{d\ln\kappa}{dT}\left(T + \frac{q}{\alpha}\right).
\end{aligned}\right\}_{n,p}$$

with the boundary conditions

$$\psi_1^{n,p}(1)=0,$$
$$\psi_2^{n,p}(0)=\frac{\frac{j(S-S_K)}{l}}{\sum_{n,p}\left\{Gc_P(T_m-t(0))+q(0)\frac{j(S-S_K)}{l}-I\left(\frac{r_0}{S_n}+\frac{r_0}{S_p}\right)\right\}}, \quad (8)$$
$$\psi_3^{n,p}(0)=\frac{Gc_P}{\sum_{n,p}\left\{Gc_P(T_m-t(0))+q(0)\frac{j\ (S-S_K)}{l}-I\left(\frac{r_0}{S_n}+\frac{r_0}{S_p}\right)\right\}}.$$

2. Optimal values of heat carrier consumption G in the channels

$$-\left[\frac{\partial J}{\partial G}\right]_{n,p}+\sum_{n,p}\int_0^1\left[\psi_1^k\frac{\partial f_1^k}{\partial G}+\psi_2^k\frac{\partial f_2^k}{\partial G}+\psi_3^k\frac{\partial f_3^k}{\partial G}\right]_{n,p}dx=0\,. \quad (9)$$

3. Optimal values of doping impurities in each segment material C_k are found from the relations

$$\int_0^1\left[\psi_1^k\frac{\partial f_1^k}{\partial C_k}+\psi_2^k\frac{\partial f_2^k}{\partial C_k}+\psi_3^k\frac{\partial f_2^k}{\partial C_k}\right]_{n,p}dx=0, \qquad k=1\ldots, N_{n,p}. \quad (10)$$

In the case of thermoelement design for fixed segment materials the optimality conditions (10) are disregarded. Such a method as applied to thermoelectric power conversion is described in many works, for instance [2, 9], and was used for creation of computer program and research on permeable segmented thermoelement of *Co-Sb* based materials.

Results of computer research on permeable segmented generator thermoelement based on *Co-Sb*

Results of calculations of the efficiency and electric power dependence on leg segment height are represented in Fig.2. This figure shows the dependences for 1- and 2-segment legs of permeable thermoelement for different heat carrier temperatures at the inlet to thermoelement. The data is given for the case when the cross-sectional area of the leg together with the channels was $S = 1$ cm^2, the contact resistance at point of connection of legs was $r_0 = 5\cdot10^{-6}$ Ωm·cm^2. The calculation was made under thermostating of cold junctions at a temperature of T_c=300 K for different values of heat carrier temperature at the inlet to thermoelement T_m = 900 K, 1100 K, 1500 K. In so doing, the temperature of thermoelement hot junctions was program controlled, so as not to exceed 800 K – the boundary value of the temperature dependences of *Co-Sb* based materials.

As a result of calculations, the optimal values *j, G* and doping parameter *x* were found whereby maximum efficiency of thermal into electric energy conversion is realized. The dependences of the efficiency and power on the leg height were determined.

The dependence of maximum efficiency η and specific electric power W of permeable generator thermoelement at optimal values of *j, G* and doping parameter *x* of legs on the leg height l_k for different heat carrier temperatures is shown in Fig. 2. The data is given for channel diameter d_k = 0.1 cm and the number of channels N_k = *25* pcs per 1 cm^2.

It is seen that the generated electric power has a maximum at leg segment height which is in the area of 1.0-1.6cm. A gain in electric power with the use of a 2-segment leg can be 10-20 %. No essential efficiency gain with the use of a 2-segment leg is observed at the value of contact resistance $r_0 = 5\cdot10^{-6}$ Ωm·cm^2.

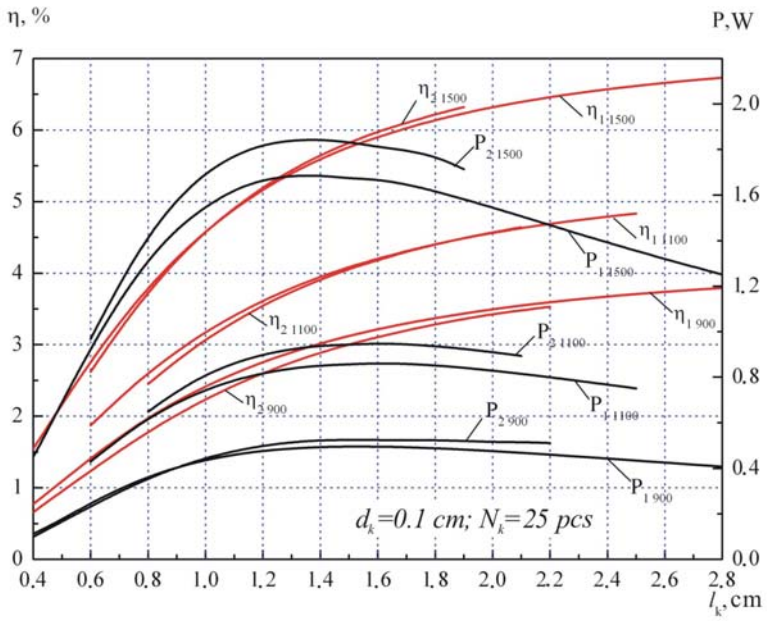

Fig.2. Dependence of efficiency and specific electric power W of permeable generator thermoelement on leg segment height l_k.

This is due to the negative influence of the Joule-Lenz heat at points of connection of leg segments. Higher efficiency values can be achieved with a decrease in contact resistance at points of connection of leg segments.

Conclusions

1. The effect of leg segmentation in permeable thermoelement of *Co-Sb* based materials on the basic power conversion characteristics was determined. Optimal parameters of a 2-segment permeable thermoelement whereby maximum power conversion efficiency is realized were found.
2. It is shown that the electric power generated by a 2-segment permeable thermoelement of *Co-Sb* based materials can be 1.1-1.2 fold higher.

References

1. Cherkez R.G. (2014). Permeable generator thermoelements of Co-Sb based materials. *J.Thermoelectricity*, 3, 75-81.
2. Anatychuk L.I., Vikhor L.N. (2012). *Thermoelectricity. Vol.4. Functionally-graded thermoelectric materials.* Chernivtsi: Bukrek.
3. Uher C. (2006). Skutterudite-based thermoelectrics. In: *Thermoelectrics Handbook. Macro to Nano*. D.M.Rowe (Ed.). Boca-Raton: CRC Press.
4. Jung Jae-Yong, Park Kwan-Ho and Kim Il-Ho (2010). Thermoelectric and transport properties of In-filled and Ni-doped CoSb3 skutterudites. J. of the Korean Physical Society, 57 (4), 773-777.
5. Lamberton G.A., Bhattacharya S., Littleton R.T., Kaeser M.A., Tedstrom R.H., Tritt T.M., Yang J., and Nolas G.S. (2002). High figure of merit in Eu-filled $CoSb_3$-based skutterudites. *Appl. Phys. Lett.* 80, 598.
6. Anatychuk L.I., Cherkez R.G. (2003). Permeable thermoelement in electric energy generation mode. *J.Thermoelectricity*, 2, 35-46.
7. Anatychuk L.I., Cherkez R.G. (2010). Permeable segmented thermoelement in electric energy generation mode. *J.Thermoelectricity*, 3, 5-12.

8. Zhou A.J., Zhu T.J., Zhao X.B., et al. (2010). Improved thermoelectric performance of higher manganese silicides with Ge additions. J.Electronic Materials, 39(9), 2002.
9. Cherkez R.G., Maksimuk M.V., Fenyak P.P. (2013). Design of thermoelectric permeable structures based on Mg and Mn silicides. *J.Thermoelectricity*, 6, 62-70.
10. Bilinsky-Slotylo V.R., Vikhor L.M., Mykhailovsky V.Ya., Mocherniuk R.M., Semizorov O.F. (2013). Efficiency improvement of generator modules based on CoSb through use of segmented and multi-stage structures. *J.Thermoelectricity*, 3, 71-76.
11. Su X., Li H., Guo Q., Tang X., Zhang Q., Uher C. (2011). Structure and thermoelectric properties of Te- and Ge-doped skutterudites $CoSb_{2.875-x}Ge_{0.125}Te_x$. J.Electronic Materials, 40(5), 1286-1291.
12. Zhou Ch., Morelli D., Zhou X., Wang G., Uher C. (2011). Thermoelectric properties of p-type Yb-filled skutterudite $Yb_xFe_yCo_{4-y}Sb_{12}$. Intermetallics, 19(10), 390-1393.
13. Lobunets Yu.N. (1989). Metody raschiota i proektirovaniia termoelektricheskikh preobrazovatelei energii [Methods of calculation and design of thermoelectric power converters]. Kyiv: Naukova dumka [in Russian].
14. Kotyrlo G.K., Schegolev G.M. (1973), Teplovyiie skhemy termoelektricheskikh ustroistv [Heat diagrams of thermoelectric devices]. Kyiv: Naukova dumka [in Russian].

Submitted 04.03.2019

Черкез Р.Г. *док. фіз.– мат. наук, в.о. професора*[1,2]

[1]Інститут термоелектрики НАН України та МОН України,
вул. Науки, 1, Чернівці, 58029, Україна, *e-mail: anatych@gmail.com*;
[2]Чернівецький національний університет ім. Юрія Федьковича,
вул. Коцюбинського, 2, Чернівці, 58012, Україна

ВПЛИВ СЕГМЕНТУВАННЯ ВІТОК НА ЕФЕКТИВНІСТЬ ПРОНИКНОГО ТЕРМОЕЛЕМЕНТА З МАТЕРІАЛІВ НА ОСНОВІ *Co-Sb*

Приведено результати комп'ютерних досліджень впливу довжини сегментів віток з матеріалів на основі Co-Sb на ефективність перетворення енергії. Визначено оптимальні режими роботи 2-сегментного термоелемента, за якої реалізуються максимальні значення ККД. Показано можливість покращення електричної потужності, що генерується при використанні 2-сегментних проникних термоелементів з матеріалів на основі Co-Sb, в 1.1-1.2 рази. Бібл. 14, рис. 2.
Ключові слова: проникні термоелементи, сегментні матеріали, комп'ютерне проектування, матеріали на основі Co-Sb.

Черкез Р.Г, *док. физ.-мат. наук, в.о. профессора*[1,2]

[1]Институт термоэлектричества НАН и МОН Украины,
ул. Науки, 1, Черновцы, 58029, Украина,
e–mail: anatych@gmail.com;
[2]Черновицкий национальный университет имени Юрия Федьковича,
ул. Коцюбинского, 2, Черновцы, 58012, Украина

ВЛИЯНИЕ СЕГМЕНТИРОВАНИЯ ВЕТВЕЙ НА ЭФФЕКТИВНОСТЬ ПРОНИЦАЕМОГО ТЕРМОЭЛЕМЕНТА ИЗ МАТЕРИАЛОВ НА ОСНОВЕ *Co-Sb*

Приведены результаты компьютерных исследований влияния длины сегментов ветвей из материалов на основе Co-Sb на эффективность преобразования энергии. Определены оптимальные режимы работы 2- сегментного термоэлемента, по которым реализуются максимальные значения КПД. Показана возможность улучшения электрической мощности, которая генерируется при использовании 2-сегментных проницаемых термоэлементов из материалов на основе Co-Sb, в 1.1-1.2 раза. Библ. 14, рис. 2.

Ключевые слова: *проницаемые термоэлементы, сегментные материалы, компьютерное проектирование, материалы на основе Co-Sb.*

References

1. Cherkez R.G. (2014). Permeable generator thermoelements of Co-Sb based materials. *J.Thermoelectricity*, 3, 75-81.
2. Anatychuk L.I., Vikhor L.N. (2012). *Thermoelectricity*. *Vol.4. Functionally-graded thermoelectric materials.* Chernivtsi: Bukrek.
3. Uher C. (2006). Skutterudite-based thermoelectrics. In: *Thermoelectrics Handbook. Macro to Nano*. D.M.Rowe (Ed.). Boca-Raton: CRC Press.
4. Jung Jae-Yong, Park Kwan-Ho and Kim Il-Ho (2010). Thermoelectric and transport properties of In-filled and Ni-doped CoSb3 skutterudites. J. of the Korean Physical Society, 57 (4), 773-777.
5. Lamberton G.A., Bhattacharya S., Littleton R.T., Kaeser M.A., Tedstrom R.H., Tritt T.M., Yang J., and Nolas G.S. (2002). High figure of merit in Eu-filled $CoSb_3$-based skutterudites. *Appl. Phys. Lett.* 80, 598.
6. Anatychuk L.I., Cherkez R.G. (2003). Permeable thermoelement in electric energy generation mode. *J.Thermoelectricity*, 2, 35-46.
7. Anatychuk L.I., Cherkez R.G. (2010). Permeable segmented thermoelement in electric energy generation mode. *J.Thermoelectricity*, 3, 5-12.
8. Zhou A.J., Zhu T.J., Zhao X.B., et al. (2010). Improved thermoelectric performance of higher manganese silicides with Ge additions. J.Electronic Materials, 39(9), 2002.
9. Cherkez R.G., Maksimuk M.V., Fenyak P.P. (2013). Design of thermoelectric permeable structures based on Mg and Mn silicides. *J.Thermoelectricity*, 6, 62-70.
10. Bilinsky-Slotylo V.R., Vikhor L.M., Mykhailovsky V.Ya., Mocherniuk R.M., Semizorov O.F. (2013). Efficiency improvement of generator modules based on CoSb through use of segmented and multi-stage structures. *J.Thermoelectricity*, 3, 71-76.
11. Su X., Li H., Guo Q., Tang X., Zhang Q., Uher C. (2011). Structure and thermoelectric properties of Te- and Ge-doped skutterudites $CoSb_{2.875-x}Ge_{0.125}Te_x$. J.Electronic Materials, 40(5), 1286-1291.
12. Zhou Ch., Morelli D., Zhou X., Wang G., Uher C. (2011). Thermoelectric properties of p-type Yb-filled skutterudite $Yb_xFe_yCo_{4-y}Sb_{12}$. Intermetallics, 19(10), 390-1393.
13. Lobunets Yu.N. (1989). Metody raschiota i proektirovaniia termoelektricheskikh preobrazovatelei energii [Methods of calculation and design of thermoelectric power converters]. Kyiv: Naukova dumka [in Russian].
14. Kotyrlo G.K., Schegolev G.M. (1973), Teplovyiie skhemy termoelektricheskikh ustroistv [Heat diagrams of thermoelectric devices]. Kyiv: Naukova dumka [in Russian].

Submitted 04.03.2019

L.I. Anatychuk *acad. National Academy of sciences of Ukraine*[1,2]
P.D. Mykytiuk. *cand. phys.– math. sciences*[1,2]
O.Yu. Mykytiuk. *cand. phys.– math. sciences, Assistant Professor*[3]

[1]Institute of Thermoelectricity of the NAS and MES of Ukraine,
1, Nauky str, Chernivtsi, 58029, Ukraine;
e-mail: anatych@gmail.com;
[2]Yuriy Fedkovych Chernivtsi National University,
2, Kotsiubynsky str., Chernivtsi, 58012, Ukraine;
[3]Higher State Educational Institution of Ukraine
"Bukovinian State Medical University", 2,
Theatre Square, Chernivtsi, 58002, Ukraine

DESIGN OF AN ANNULAR THERMOPILE FOR A SINGLE ACTING CURRENT SOURCE

The results of studies on the creation of an annular thermopile for a current source with a pyrotechnic heat source are presented. The method of computer simulation confirmed the possibility of creating an annular thermopile with predetermined geometric dimensions, providing an output power of 2W at a voltage of 5V. Bibl. 2, Fig. 4, Tabl. 3.
Key words: thermoelectric battery, current source, rated voltage, output power.

Introduction

In connection with a significant expansion of the scope of autonomous control systems at military facilities, the issue of developing electric power supplies intended for various electronic devices becomes urgent.

Such power supplies have increased requirements for their performance and specific energy characteristics. In addition to their small weight and size parameters, they must meet the requirements for the probability of trouble-free operation after long (at least 10 years) storage in warehouses as well as in the field. In addition, they must maintain their performance under conditions of high climatic and mechanical loads.

The combination of these requirements directs developers to create power supplies that work on the principle of direct conversion of one of the types of energy (chemical, mechanical or thermal) into electrical energy. At the same time, special requirements are imposed on the design of current source, the implementation of which requires new technical and technological solutions. From the information given in [1], thermoelectric (TE) current sources are most in line with the requirements for single acting power supplies.

The main parts of TE current sources which determine their efficiency include a heat source in which capacity mixtures based on zirconium and barium chromate are best suitable [1], and a thermoelectric converter of corresponding design.

However, the nature of using the aforementioned power supplies has determined their specifi-

city, and the assessment of the present state of development of TE current sources on the basis of the analysis of scientific and technical information is a problem.

The purpose of this work is research to create a high performance annular thermopile for a single acting TE current source.

Annular thermopile

Ref. [2] provides descriptions of dozens of thermoelectric generators (TEGs) with different heat sources based on gaseous, liquid or solid fuels. Such TEGs can operate for a long time under conditions of climatic and mechanical influences close to normal. Constructive designs of TEGs, as well as their specific energy characteristics cannot be applied in a single acting TE current source. At the same time, the experience of creating thermopiles for such TEGs is the basis for the creation of optimum, both from the point of view of design and from the point of view of technology of manufacturing high performance thermopile for a TE current source. The closest analogue in this regard is a thermopile consisting of 8 series-connected spiral elementary thermopiles located in a circle on the inner surface of the cylindrical body of a TE current source [1]. The space between the spiral thermopiles is filled with a heat-resistant compound to ensure the mechanical strength of the thermopile in a TE current source.

With a number of obvious advantages over the constructions of the well-known TE current sources, the thermopile design described in [1] has a number of disadvantages. In particular, the manufacturing technology of spiral thermopiles is very complicated, which is financially costly for serial production of TE current sources. Besides, spiral thermopiles are made of extruded thermoelectric material with a low thermoelectric figure of merit (Z ~ 2 * 10-3 K). Therefore, an annular thermopile was created, in which the legs of thermoelements are made of high-performance Bi_2Te_3.

Computer design of an annular thermopile for a current source

Taking into account the requirements of the technical specifications under the contract № 3/2019 от 16.04.2019 the thermoelectric converter for a TE current source should be designed with an inner diameter of 39 mm and an outer diameter of 50 mm in the form of an annular thermopile consisting of the calculated number of elementary single-row thermopiles, providing an output voltage of 5V and an electric power of 2W at a working temperature drop of not more than 300K. In turn, thermopiles should consist of a given number of thermoelements connected in series with an optimal combination of weight and size characteristics and thermoelectric properties.

Therefore, for computer design, we used the model of the thermopile structural unit - a thermoelement consisting of n- and p-type legs, connecting materials, and heat-leveling insulating ceramic plates, Fig. 1.

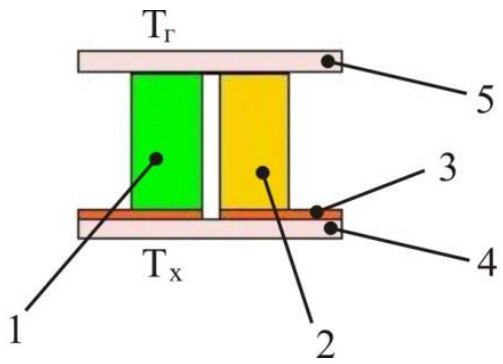

Fig. 1. Physical model of the structural element of thermopile. 1, 2 – thermoelement legs of n- and p-type conductivity; 3 – copper connecting plates; 4 – lower ceramic plate; 5 –upper ceramic plate.

The temperatures on the heat-releasing and heat-absorbing thermoelement surfaces T_h and T_c are fixed, the lateral surface is adiabatically isolated. Parameters of thermoelectric materials are functions of temperature. T_0 determine maximum efficiency and maximum electric power, it is necessary to find the distribution of temperatures and current density in thermoelement legs.

The solution of this problem is realized by the numerical method of successive approximations using the Comsol Multiphysics software environment.

Mathematical description of the model

To describe the flows of heat and electricity in such a thermoelement, we used the laws of conservation of energy:

$$div\vec{W} = 0, \tag{1}$$

and electric charge:

$$div\vec{j} = 0, \tag{2}$$

where:

$$\vec{W} = \vec{q} + U\vec{j}. \tag{3}$$

$$\vec{q} = \kappa\nabla T + \alpha T\vec{j}, \tag{4}$$

$$\vec{j} = -\sigma\nabla U - \sigma\alpha\nabla T, \tag{5}$$

($\vec{W}$ is energy flow density, $\vec{j}$ is electric current density, U is electric potential, T is temperature, α, σ, κ are the Seebeck coefficient, electric conductivity and thermal conductivity of materials).

Taking into account (3) - (5) yields:

$$\vec{W} = -(\kappa + \alpha^2\sigma T + \alpha U\sigma)\nabla T - (\alpha\sigma T + U\sigma)\nabla U. \tag{6}$$

Then the laws of conservation (1), (2) will take on the form:

$$-\nabla\left[(\kappa + \alpha^2\sigma T + \alpha U\sigma)\nabla T\right] - \nabla\left[(\alpha\sigma T + U\sigma)\nabla U\right] = 0, \tag{7}$$

$$-\nabla(\sigma\alpha\nabla T) - \nabla(\sigma\nabla U) = 0. \tag{8}$$

These second-order nonlinear differential equations in partial derivatives (7) and (8) determine the distributions of temperature T and potential U in the materials of thermoelement legs, contact, connecting and insulating layers of the thermoelement.

The boundary conditions for solving equations (7) and (8) were chosen as follows. The temperatures of the heat-absorbing and heat-releasing surface of the thermoelement T_h and T_c were recorded. The potential value on the connecting plate of the n-type leg was set to zero. On the other connecting plate of the *p*-type leg the value of U was set, which is half the thermoEMF generated by the thermoelement. In turn, the value of the generated thermoEMF was determined by the system of equations (7) and (8) in the absence of current flow through the thermoelement.

At the boundaries of the legs of thermoelements and connecting plates, connecting plates and ceramics, the conditions of equality of temperatures and heat flows were taken into account.

The general equation of the "Comsol Multiphysics" program is as follows:

$$\nabla\left(-C\nabla M + \alpha M + \gamma\right) + \delta M + \beta\nabla M = f, \tag{9}$$

where

$$C=\begin{bmatrix} C_{11} & C_{12} \\ C_{21} & C_{22} \end{bmatrix},\ \alpha=\begin{bmatrix} \alpha_{11} & \alpha_{12} \\ \alpha_{21} & \alpha_{22} \end{bmatrix},\ \gamma=\begin{bmatrix} \gamma_{11} & \gamma_{12} \\ \gamma_{21} & \gamma_{22} \end{bmatrix},\ \delta=\begin{bmatrix} \delta_{11} & \delta_{12} \\ \delta_{21} & \delta_{22} \end{bmatrix},$$

$$\beta=\begin{bmatrix} \beta_{11} & \beta_{12} \\ \beta_{21} & \beta_{22} \end{bmatrix},\ f=\begin{bmatrix} f_1 \\ f_2 \end{bmatrix},\ M=\begin{bmatrix} T \\ U \end{bmatrix}. \tag{10}$$

From the analysis of Eqs.(7) - (10) it follows that Eq.(9) can be simplified as:

$$\nabla\left(-C\nabla M\right)=0\,. \tag{11}$$

The differential equation for matrix components is given by:

$$\left.\begin{aligned} \nabla\left(-C_{11}\nabla T\right)+\nabla\left(-C_{12}\nabla U\right)=0 \\ \nabla\left(-C_{21}\nabla T\right)+\nabla\left(-C_{22}\nabla U\right)=0 \end{aligned}\right\}. \tag{12}$$

Comparing the laws of conservation in the form of (7), (8) with equations (12), we obtain coefficients for a computer model:

$$C=\begin{pmatrix} \kappa+\alpha^2\sigma T+\alpha U\sigma & \alpha\sigma T+U\sigma \\ \sigma\alpha & \sigma \end{pmatrix}. \tag{13}$$

Computer research results

Using this method, the energy characteristics of elementary thermopiles for TE power supplies were calculated. The temperature dependences of the thermoelectric parameters α, σ, κ of materials based on bismuth telluride of *n*- and *p*-types of conductivity ((*n*-Bi_2Te_3), and (*p*-Bi_2Te_3) were used as input data, Fig. 2.

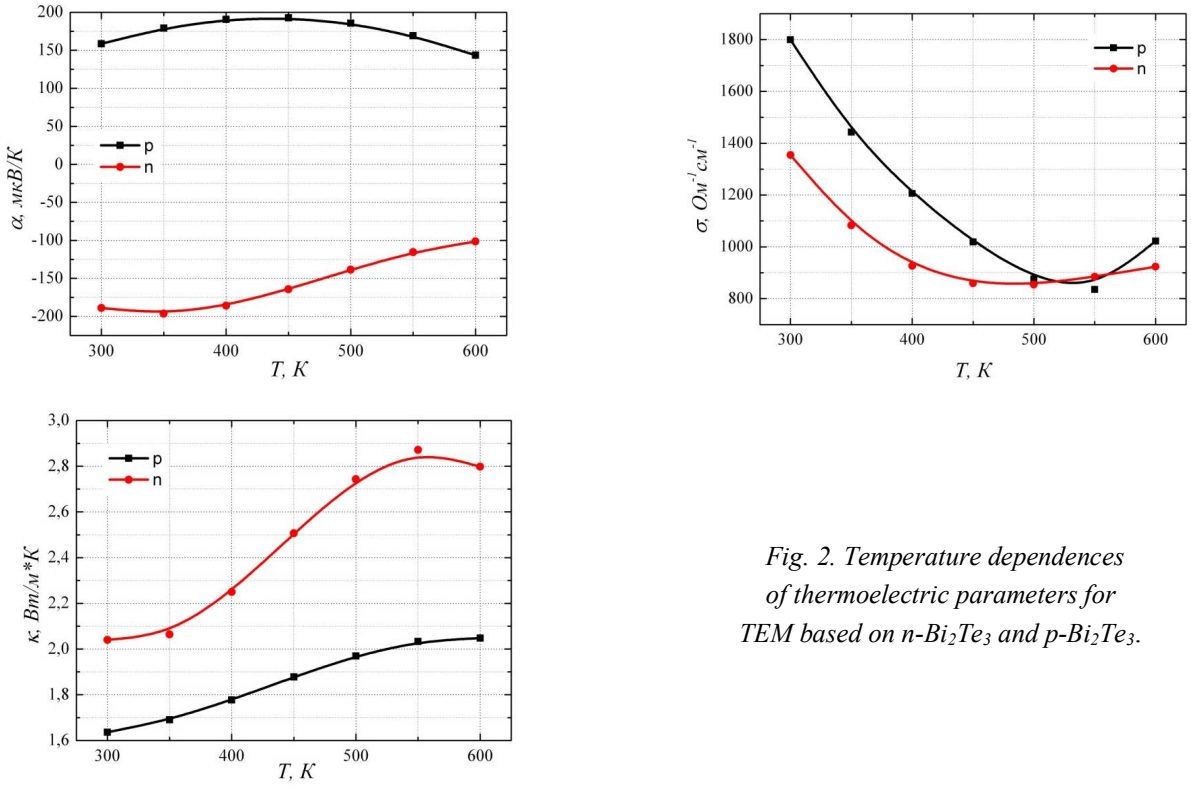

Fig. 2. Temperature dependences of thermoelectric parameters for TEM based on n-Bi_2Te_3 and p-Bi_2Te_3.

The temperature dependences (Fig. 2) were approximated by one-dimensional polynomials in the form of $\alpha^{n,p} = \alpha^{n,p}(T)$, $\sigma^{n,p} = \sigma^{n,p}(T)$, $\kappa^{n,p} = \kappa^{n,p}(T)$, whose coefficients were entered into computer program.

As a result of simulation we obtained the distributions of temperature and electric potential for one of thermoelements which form elementary thermopiles (Fig 3).

The calculated electric parameters of thermoelement (voltage U, power P, efficiency η) at operating temperature gradients ΔT = 473 K, 523 K and 573 K on its surfaces are represented in Table 1.

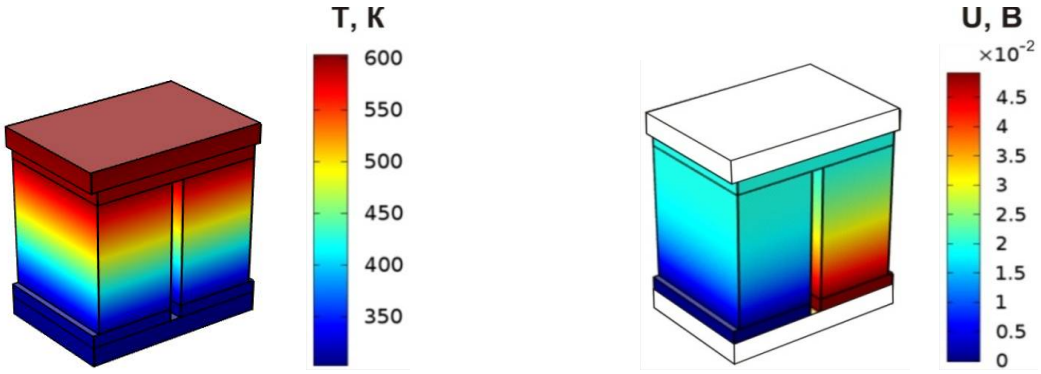

a) *b)*

Fig. 3. The distribution of temperatures (a) and electric potential (σ) in thermoelement

Table 1

Parameters of thermoelement

ΔT, K	U, V	P, W	η, %
473	0.035	0.1	5.8
523	0.045	0.16	6.7
573	0.05	0.18	6.9

Taking into account the above data, the temperature and electric potential distributions were found (Fig. 4), as well as the energy characteristics of elementary thermopile for a TE current source (Table 2).

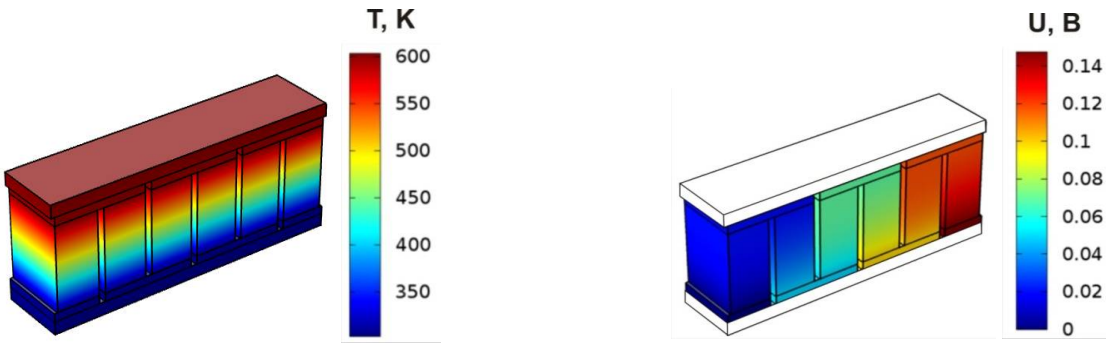

a) *b)*

Fig 4. The distribution of temperatures (a) and electric potential (b) in elementary thermopile.

Table 2

Characteristics of elementary thermopile for a TE current source

ΔT, K	TE current source		
	U, V	P, W	η, %
473	0.105	0.31	6.0
523	0.135	0.48	6.7
573	0.145	0.56	7.0

Based on the data given in Table 2, the electrical characteristics of an annular thermopile were calculated for a TE current source at operating temperature gradients ΔT = 200°C, 250°C and 300°C (Table 3).

Table 3

Calculated electrical characteristics of an annular thermopile

ΔT, K	TE current source	
	U, V	P, W
473	3.78	11.16
523	4.86	17.28
573	5.22	20.16

Thus, taking into account the estimated calculations and the data given in the Tables 2-3 it follows that to achieve the assigned electrical power and voltage of a TE current source, an annular thermopile of each sample must consist of 36 series-connected elementary thermopiles. For a TE current source -1 the optimal number of thermoelements in one elementary thermopile is 3 pcs (6 legs).

It should be noted that computer design of thermoelectric converters was carried out for the maximum power mode, when the resistance of the thermopile is equal to the value of the external load. In fact, the operating mode of a TE current source will be different and a significant power reserve of power supply will ensure the required voltage values.

Moreover, a number of factors that affect the initial characteristics of a TE current source were not considered in computer design. In particular, the influence of contact resistances at the boundaries of thermoelement legs with connecting plates, at the boundaries of connecting plates with ceramics is not taken into account. In addition, heat loss from the side surfaces of the thermopile legs and the layer of heat-conducting glue K - 400 is disregarded.

However, the calculations confirmed the reality of achieving the output characteristics of a TE current source at a given operating temperature difference not exceeding 300K.

Conclusion

Computer simulation and experimental studies confirmed the possibility of creating an annular thermopile with an outer diameter of 50 mm and an inner diameter of 39 mm for a thermoelectric current source, providing an output power of at least 2 W at a voltage of 5V.

References

1. 1.Anatychuk L.I., Mykytiuk P.D. (2012). Small-size thermoelectric current source of single action. J.Thermoelectricity, 1, 56-62.
2. 2.Anatychuk L.I. (1979). Termoelementy i termoelektricheskiie ustroistva. Spravochnik. [Thermoelements and thermoelectric devices. Handbook]. Kyiv: Naukova dumka [in Russian].

Submitted 11.02.2019

Анатичук Л.І., *акад. НАН України*[1,2]
Микитюк П.Д. *канд. фіз.– мат. наук*[1,2]
Микитюк О.Ю. *канд. фіз.– мат. наук, доцент*[3]

[1]Інститут термоелектрики НАН і МОН України,
вул. Науки, 1, Чернівці, 58029, Україна,
e-mail: anatych@gmail.com;
[2]Чернівецький національний університет
імені Юрія Федьковича, вул. Коцюбинського 2,
Чернівці, 58012, Україна,

[3]Вищий державний навчальний заклад України
«Буковинський державний медичний університет»,
Театральна площа, 2, Чернівці, 58012, Україна

ПРОЕКТУВАННЯ КІЛЬЦЕВОЇ ТЕРМОБАТАРЕЇ ДЛЯ ДЖЕРЕЛА СТРУМУ ОДНОРАЗОВОЇ ДІЇ

Приведені результати досліджень по створенню кільцевої термоелектричної батареї для джерела струму з піротехнічним джерелом тепла. Методом комп'ютерного моделювання підтверджена можливість створення кільцевої термобатареї із заданими геометричними розмірами, що забезпечує вихідну потужність 2Вт при напрузі 5В. Бібл. 2, рис. 4, табл. 3.
Ключові слова: термоелектрична батарея, джерело струму, номінальна напруга, вихідна потужність.

Анатычук Л.И., *акад. НАН Украины*[1,2]
Микитюк П.Д. *канд. физ.– мат. наук*[1,2]
Микитюк О.Ю. *канд. физ.– мат. наук, доцент*[3]

[1]Институт термоэлектричества НАН и МОН Украины,
ул. Науки, 1, Черновцы, 58029, Украина,
e-mail: anatych@gmail.com;
[2]Черновицкий национальный университет
имени Юрия Федьковича, ул. Коцюбинского 2,
Черновцы, 58012, Украина
[3]Высшее государственное учебное заведение Украины
«Буковинский государственный медицинский университет»,
Театральная площадь, 2, Черновцы, 58002, Украина

ПРОЕКТИРОВАНИЕ КОЛЬЦЕВОЙ ТЕРМОБАТАРЕИ ДЛЯ ИСТОЧНИКА ТОКА ОДНОРАЗОВОГО ДЕЙСТВИЯ

Приведены результаты исследований по созданию кольцевой термоэлектрической батареи для источника тока с пиротехническим источником тепла.
Методом компьютерного моделирования подтверждена возможность создания кольцевой термобатареи с заданными геометрическими размерами, обеспечивающая выходную мощность 2Вт при напряжении 5В. Библ. 2, рис. 4, табл. 3.
Ключевые слова*:* термоэлектрическая батарея, источник тока, номинальное напряжение, выходная мощность.

References

1. Anatychuk L.I., Mykytiuk P.D. (2012). Small-size thermoelectric current source of single action. J.Thermoelectricity, 1, 56-62.
2. Anatychuk L.I. (1979). Termoelementy i termoelektricheskiie ustroistva. Spravochnik. [Thermoelements and thermoelectric devices. Handbook]. Kyiv: Naukova dumka [in Russian].

Submitted 11.02.2019


L.I. Anatychuk

L.I. Anatychuk, *acad. National Academy of sciences of Ukraine*[1,2]
A.V. Prybyla, *cand. phys.– math. sciences*[1,2]

[1]Institute of Thermoelectricity
of the NAS and MES of Ukraine,
e-mail: anatych@gmail.com
1, Nauky str., Chernivtsi, 58029, Ukraine;
[2]Yu.Fedkovych Chernivtsi National University,
2, Kotsiubynskyi str., Chernivtsi, 58000, Ukraine


A.V. Prybyla

ON THE EFFICIENCY OF THERMOELECTRIC AIR-CONDITIONERS FOR VEHICLES

The paper presents the results of calculations and comparative analysis of the integral efficiency of thermoelectric and compression air-conditioners, subject to their use for air conditioning in vehicles during the whole year in different climatic conditions. Bibl. 25, Tabl. 2, Fig. 14.
Key words: thermoelectric air-conditioner, compression air-conditioner, efficiency.

Introduction

General characterization of the problem. The upward trend in the number of cars is well known. Already in 2010, their number exceeded 1 billion [1] and this figure is growing rapidly. Along with this, the requirements for safety, ecology and comfort in vehicles are growing. So, there is a need to create effective, reliable and environmentally friendly devices to ensure comfortable conditions in vehicles, i.e. air conditioners [2 – 8].

The literature mentions the possibility of air conditioning in vehicles by various methods [2 – 8]. Particular attention is paid to the use of compression air-conditioners. This is due to their relatively high performance. However, they also have a number of disadvantages, in particular the presence of environmentally hazardous refrigerants, which significantly reduces the attractiveness of such air-conditioners. This situation is intensified by the transition to environmentally friendly modes of transport, in particular electric cars [6 – 14].

The works [4, 8, 9] describe the use of thermoelectric converters for air conditioning in vehicles. Such air conditioners have a number of advantages over compression, namely: the absence of harmful refrigerants (environmentally safe), lower overall dimensions, high reliability and ease of maintenance [15, 16].

In addition, despite the higher maximum efficiency indicators of compression air-conditioners in cooling mode, during their operation in vehicles throughout the year, one should use the integral efficiency indicators (for both cooling and heating modes) in different time and geographical conditions, which can significantly change the understanding of the energy situation of air conditioners. Such indicators will become a true criterion for the energy efficiency of air conditioners in the real conditions of their operation.

The purpose of the proposed work is to determine the integral energy efficiency indicators of thermoelectric and compression air-conditioners of vehicles in different operating conditions.

Peculiarities of functioning of automobile air-conditioners in different climatic conditions in the course of a year

To obtain full picture of the operating conditions of air-conditioners in different climatic zones [17], we used data on the daily and monthly fluctuations of air temperature in different geographical regions of the planet [18]. The work considers temperature conditions in 10 cities which correspond to the most characteristic climatic regions of the Earth (Fig. 1): Kuala Lumpur (Malaysia) – equatorial climate; Mumbai (India) – tropical monsoon climate; Aswan (Egypt) – tropical dry climate; Athens (Greece) – Mediterranean climate; Ashgabat (Turkmenistan) – subtropical dry climate; Plimuth (Great Britain) – moderate maritime climate; Kyiv (Ukraine) – moderate continental climate; Harbin (China) – moderate monsoon climate; Point Hope (Alaska, USA) – subarctic climate; Tiksi (Russian Federation) – arctic climate.

Using the information obtained, you can determine the energy efficiency of the use of vehicle air-conditioners in almost all regions of our planet.

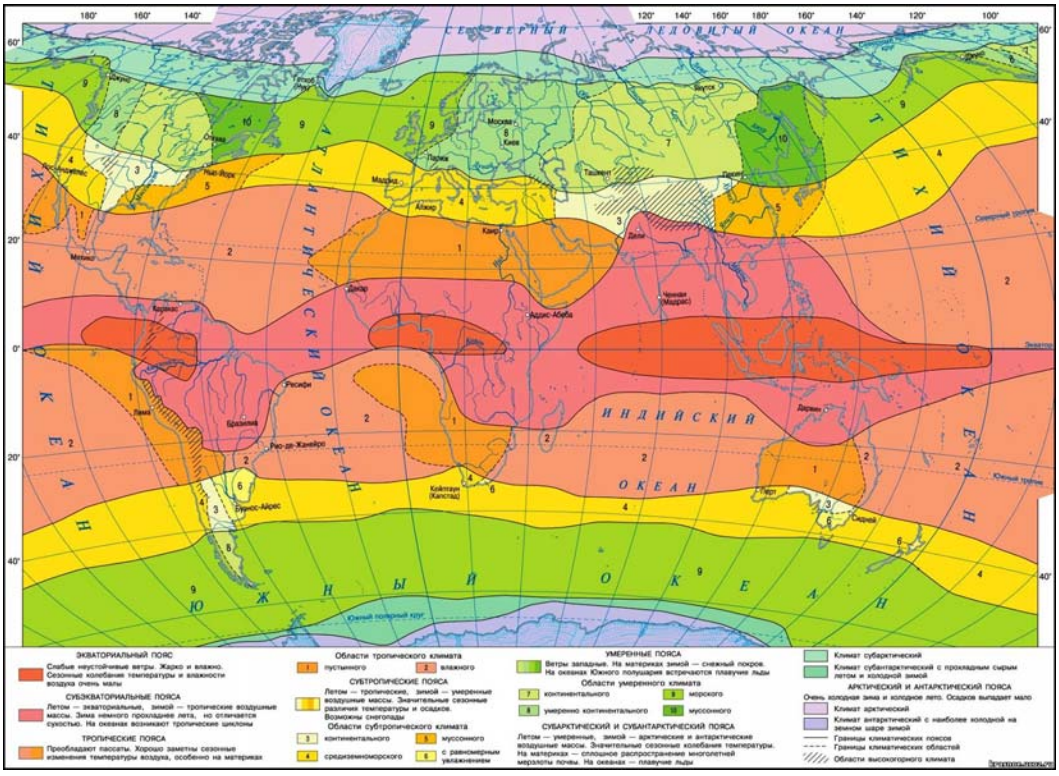

Fig.1. Climatic zones [17].

Figs. 2 - 11 show diagrams of annual temperature changes in different zones of the Earth. The line shows the change in average air temperature during the year and the outline indicates its maximum deviations. Analysis of these diagrams allows one to see the most general patterns of changes in temperature conditions in climatic zones during the year. Thus, it can be seen from Fig. 2 that the equatorial climate is characterized by virtually unchanged average air temperature during the year at +26 °C; tropical monsoon climate is characterized by average temperatures of January +20 °C and July +30 °C (Fig. 3); tropical dry climate is characterized by a more abrupt change in temperature during the year - average January temperature +12 °C and July +35 °C (Fig. 4); the Mediterranean climate is characterized by an average temperature of January +7 ° C and July +22 °C (Fig. 5); subtropical dry climate is notable for the most dramatic change in temperatures during the year - average January temperature is 0 °C and July +40 °C (Fig. 6); temperate marine climate is characterized by slight temperature changes - average January temperature +2 °C and July +17 °C (Fig. 7); temperate continental

climate characterized by average temperatures in January -15 ° C and July +20 °C (Fig. 8); temperate monsoon climate is characterized by average temperatures of January -20 °C and July +23 °C (Fig. 9); subarctic climate is characterized by average temperatures of January -25 °C and July +8 °C (Fig. 10); the arctic climate is characterized by very severe average temperatures of January – 40 °C and July 0 °C (Fig. 11).

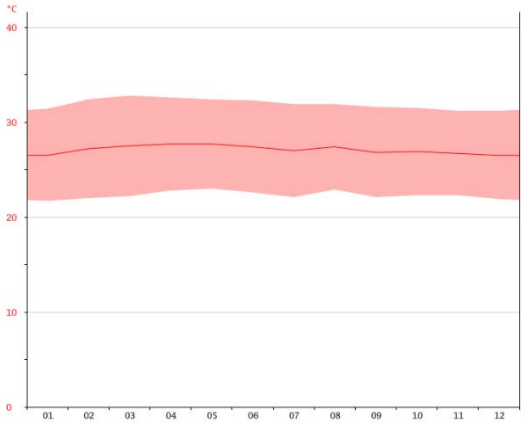

Fig.2. Diagram of annual change of air temperature in Kuala Lumpur, Malaysia [18]

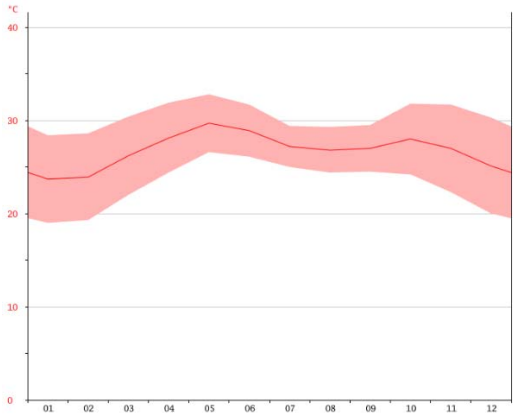

Fig.3. Diagram of annual change of air temperature in Mumbai, India [18]

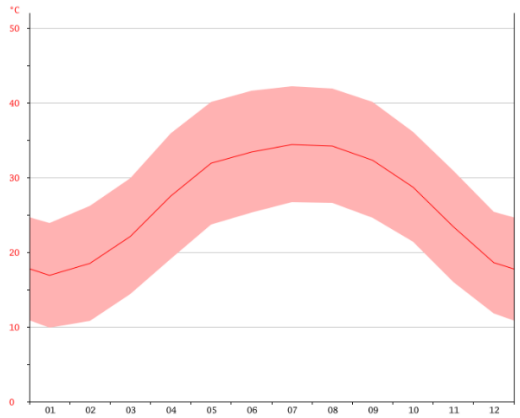

Fig.4.Diagram of annual change of air temperature in Aswan, Egypt [18]

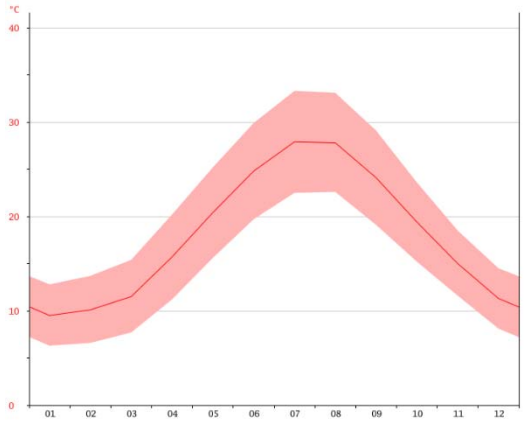

Fig.5. Diagram of annual change of air temperature in Athens, Greece [18]

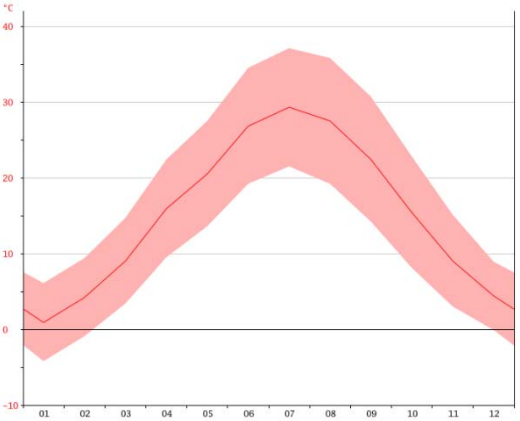

Fig.6. Diagram of annual change of air temperature in Ashgabat, Turkmenistan [18]

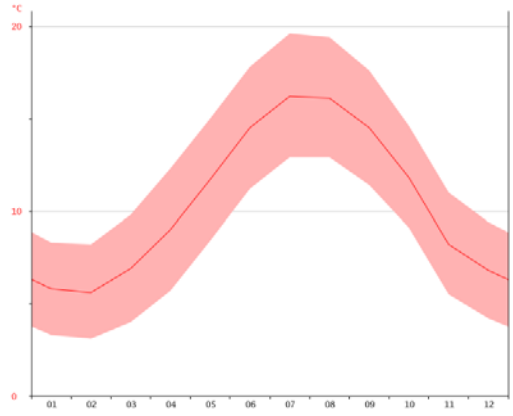

Fig.7. Diagram of annual change of air temperature in Plimuth, Great Britain [18]

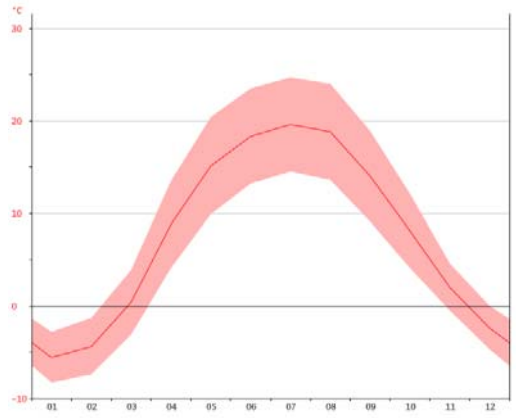

Fig.8. Diagram of annual change of air temperature in Kyiv, Ukraine [18]

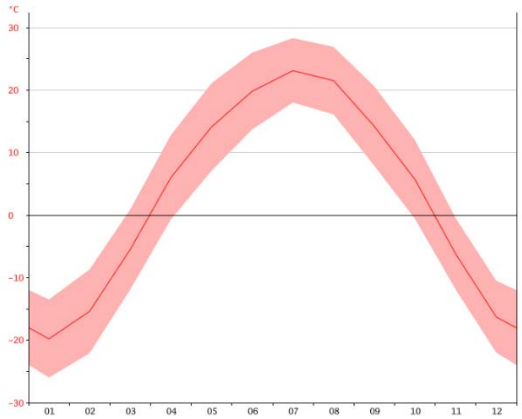

Fig.9. Diagram of annual change of air temperature in Harbin, China [18]

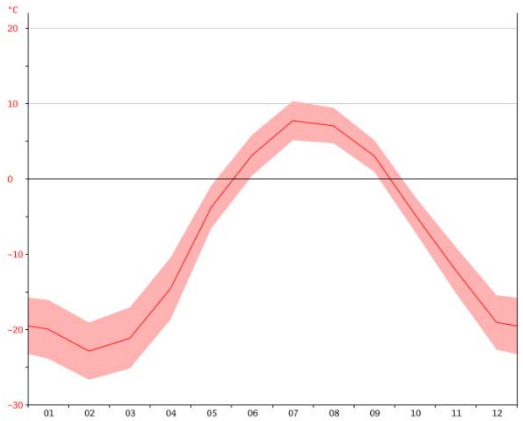

Fig.10. Diagram of annual change of air temperatur in Point Hope, Alaska, USA [18]

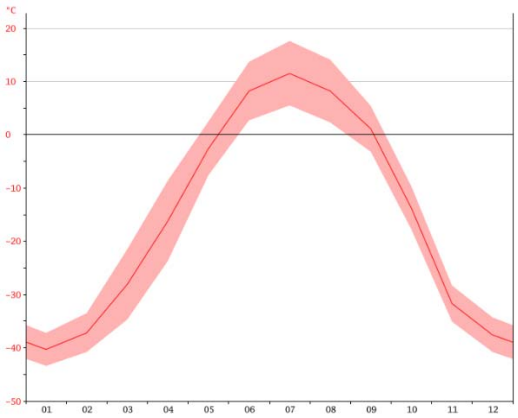

Fig.11. Diagram f annual change of air temperature in Tiksi, Russian Federation [18]

Calculation of the integral efficiency of thermoelectric and compression air-conditioners for different climatic zones

Calculation procedure

The selected calculation procedure lies in determination of the integral efficiency factor of air-conditioner for transport κ which is equal to the ratio between heat flow Q transferred by the air-conditioner and energy costs for its functioning W (1).

$$\kappa = \frac{Q}{W} \tag{1}$$

In so doing, in cooling mode, when the ambient temperature exceeds +20 °C (the temperature difference between the air outside and inside the vehicle $\Delta T > 0$ K), heat flow Q is refrigerating capacity of air conditioner, and, accordingly, factor κ is coefficient of performance ε (2). In the case when $\Delta T < 0$ K (ambient temperature is lower than +20 °C), coefficient μ is heating coefficient of air-conditioner (2).

$$\begin{aligned} \Delta T > 0 \text{ K} \quad &\rightarrow \quad \kappa = \varepsilon, \\ \Delta T < 0 \text{ K} \quad &\rightarrow \quad \kappa = \mu. \end{aligned} \tag{2}$$

Further, the average values of the coefficient κ were determined at certain time intervals, which are a function of the temperature difference ΔT and the ambient temperature value. The 4 hours interval was selected. Thus, during the day 6 values of κ were determined.

It should be noted that, in accordance with the sanitary requirements for air-conditioned rooms [25], the temperature difference between the ambient air and the cooled air-conditioner should not exceed 17 K. However, depending on the value of the ambient air temperature, this difference is different [25]. These requirements were also used in the calculations.

Then, the obtained data on energy conversion coefficients κ averaged over a time interval were summed up and their average value $\hat{\kappa}$ was determined over a whole year (3).

$$\hat{\kappa} = \frac{\sum_{i=0}^{n} \kappa_i}{n}, \tag{3}$$

where n is the number of intervals in which the average value κ was determined ($n = 365 \cdot 6 = 2190$).

The following is a calculation procedure of κ and $\hat{\kappa}$ for compression and thermoelectric air-conditioners.

Compression air-conditioners

The data on the properties of compression air-conditioners in cooling and heating modes [2 - 24] were used to determine in the form of polynomials the dependences of energy efficiencies of compression air-conditioners on ambient air temperature and temperature difference between the air inside a car (20 ^{0}C) and the ambient air.

It is significant that energy conversion coefficient of compression air-conditioners in heating mode is lower than in cooling mode. Morover, as is shown in [15, 16], their effcieincy decreases with decreasing power and and a rise in the ambient temperature. A compression air-conditioner was selected as a prototype for calculations; its maximum cooling power 4kW corresponds to typical values for air-conditioners of vehicles.

Based on the obtained data arrays, calculations were made of the averaged energy conversion coefficients of compression air-conditioners to determine time intervals in the course of a year and their integration was performed to obtain the values of the integral efficiency factor.

Table 1 shows the results of calculations in the form of integral efficiency factor values for different climatic zones (climate types) – 1. equatorial climate; 2. tropical monsoon climate; 3. tropical dry climate; 4. subtropical dry climate; 5. Mediterranean climate; 6. moderate maritime climate; 7. moderate continental climate; 8.moderate monsoon climate; 9. subarctic climate; 10. arctic climate.

As is seen from Table 1, with a change in climatic zones from equator to poles, the integral efficiency factor of compression air-conditioners decreases from 3.18 to 1.2.

Table 1

Dependence of integral efficiency factor of compression air-conditioners on different climatic zones

Climatic zones	1	2	3	4	5	6	7	8	9	10
Integral efficiency factor	3.18	3.17	2.98	3.02	2.76	2.66	2.25	2.06	1.5	1.2

Thermoelectric air-conditioers

As is shown in [15, 16], the real coefficient of performance and heating coefficient of thermoelectric air-conditioner are found from the relationships (4, 5):

coefficient of performance

$$\varepsilon_r = \frac{Q_c}{W_{TE} + W_1 + W_2} = \frac{\alpha I(T_c + Q_c N_1) - 0.5I^2 R - \lambda(T_h - T_c - (Q_h N_2 + Q_c N_1))}{W_{TE} + W_1 + W_2}, \quad (4)$$

where χ_i are thermal resistances of heat-exchangers, Q_c is refrigerating capacity, Q_h is thermal productivity, W_{TE} is electric power of thermoelectric converter, α is the Seebeck coefficient, I is electrical current, R is electrical resistance, λ is heat transfer coefficient of heat exchangers, T_h, T_c are the hot and cold side temperatures of thermoelectric converter, W_i is additional power supply of heat exchange system,

$N_1 = \frac{(\chi_1 + \chi_2)}{\chi_1 \chi_2}$, $N_2 = \frac{(\chi_3 + \chi_4)}{\chi_3 \chi_4}$.

Heating coefficient in this case will be given by:

$$\mu_r = \frac{Q_h}{W_{TE} + W_1 + W_2} = \frac{\alpha I(T_h + Q_h N_2) + 0.5I^2 R - \lambda(T_h - T_c - (Q_h N_2 + Q_c N_1))}{W_{TE} + W_1 + W_2}. \quad (5)$$

The coefficient of performance and heating coefficient of thermoelectric air-conditioner are related as:

$$\mu_r = \varepsilon_r + 1. \quad (6)$$

Relationship (6) indicates that the use of thermoelectric air-conditioner in heating mode has the advantage over a similar mode of compression air-conditioner.

It is also noteworthy that unlike compression air-conditioners, the efficiency of thermoelectric air-conditioners increases with decreasing power and a rise in air temperature [15, 16], which creates additional advantages for them.

Fig.12 shows a typical dependence of the coefficient of performance of thermoelectric air-conditioner on supply current for different values of temperature difference between its hot and cold sides. The data is given for the ambient temperature of 30 ^{0}C. Similar dependences were obtained for all considered temperature ranges and were written in the form of polynomials.

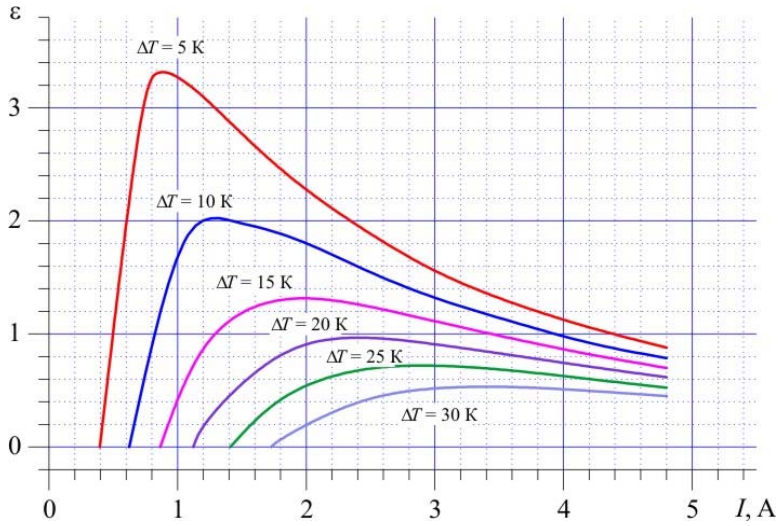

Fig. 12 Typical dependence of the coefficient of performance of t hermoelectric air-conditioner on supply current for different values of t emperature difference between its hot and cold sides.

Based on the obtained data arrays, the averaged energy conversion coefficients of thermoelectric air-conditioners were calculated for the selected time intervals in the couse of a year and their integration was performed to obtain the values of the integral efficiency factor.

Table 2 shows the results of calculations in the form of the values of the integral efficiency factor of thermoelectric air-conditioners for different climatic zones.

As is seen from Table 2, with a change in climatic zones from equator to poles, the integral efficiency factor of thermoelectric air-conditioners changes from 1.5 for a dry tropical climate to 3.06 for a moderate maritime climate.

Table 2

Dependence of integral efficiency factor of compression air-conditioners on geographic latitude

Climatic zones	1	2	3	4	5	6	7	8	9	10
Integral efficiency factor	1.99	2.09	1.5	2.14	2.62	3.06	2.38	2.21	1.75	1.55

Comparison of compression and thermoelectric air-conditioners

Thus, comparison of the values of averaged efficiency of thermoelectric and compression air-conditioners from Tables 1 and 2 testifies to the advantage of compression air-conditioners under hot climatic conditions of equator, tropics and subtropics (Fig.13). However, starting from moderate climatic conditions, thermoelectric air-conditioners offer the advantage in efficiency up to 20 %.

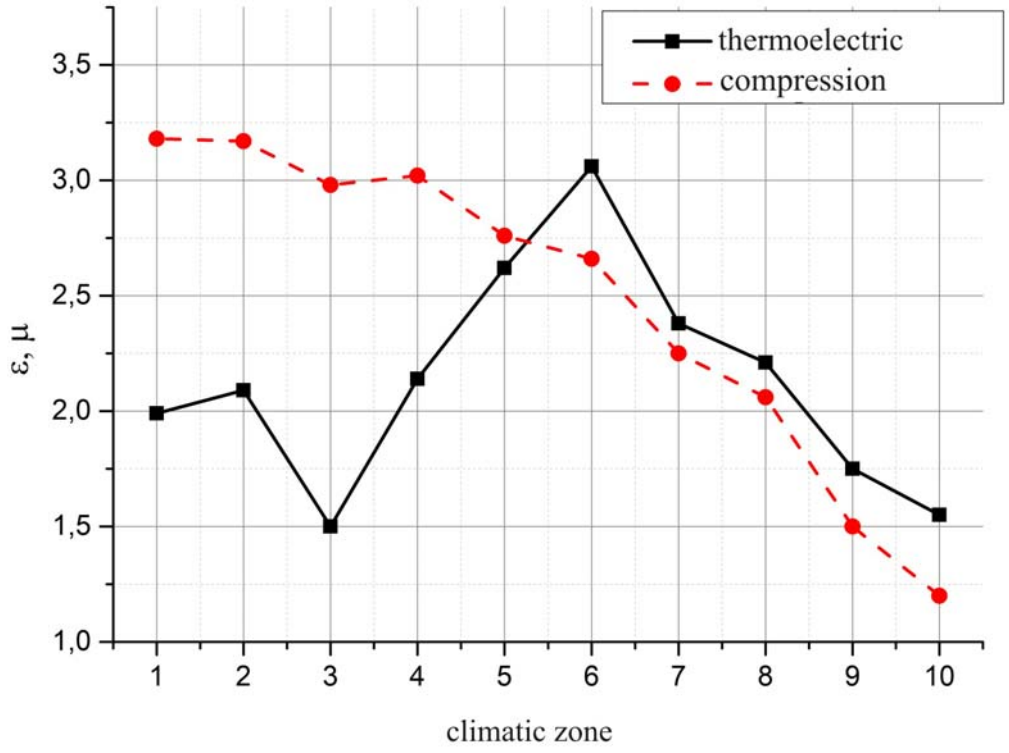

Fig. 13. Comparison of the integral efficiency factor (ε, μ) of compression and thermoelectric air-conditioners in different climatic zones.

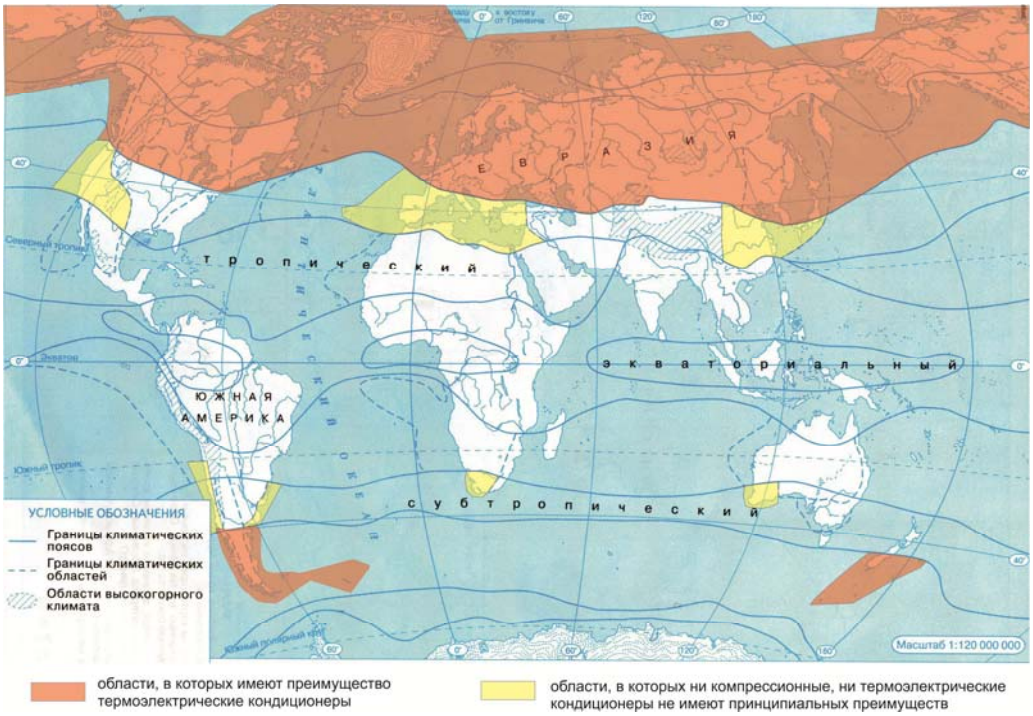

Fig. 14. Areas on the planet where the use of thermoelectric air-conditioners is rational.

To illustrate Fig.13, on the map of the Earth (Fig.14) areas have been plotted where the use of thermoelectric air-conditioners has evident advantages in efficiency (marked in red), and the areas where the use of thermoelectric and compression air-conditioners is approximately equal in efficiency (marked in yellow).

As is seen from Fig.14, the rational areas of using thermoelectric air-conditioning includes almost all Europe, China, Russia, Canada, part of the USA and the Mediterranean countries, which alongside with other advantages thereof (ecological compatibility, lower mass-dimensional indicators), makes this variant of air-conditioning attractive for use in automobile transport, especially in electric vehicles.

Conclusions

1. Calculations were made of the averaged efficiency factor of compression air-conditioners with their constant use in the course of a year in different climatic zones. It was established that with a change in climatic zones from equator to poles, the integral efficiency factor of compression air-conditioners is reduced from 3.18 to 1.2.
2. Calculations were made of the integral efficiency factor of thermoelectric air-conditioners with their constant use in the course of a year in different climatic zones. It was established that with a change in climatic zones from equator to poles, the integral efficiency factor of thermoelectric air-conditioners is changed from 1.5 for a dry tropical climate to 3.06 for a moderate maritime climate.
3. Comparison of the integral efficiency values of thermoelectric and compression air-conditioners testifies to the advantage of compression air-conditioners in the hot climatic conditions of equator, tropics and subtropics. However, starting from the moderate climatic conditions, thermoelectric air-conditioners offer the advantage in efficiency up to 20 %, which, alongside with other advantages thereof (ecological compatibility, lower mass-dimensional indicators, reliability), makes this variant of air-conditioning attractive for use in automobile transport, especilaly in electric vehicles.

References

1. https://www.zr.ru/content/news/350201-kolichestvo_avtomobilej_v_mire_perevalilo_za_milliard/.
2. Lee M.Y. Lee, D.Y. (2013). Review on conventional air conditioning, alternative refrigerants and CO2 heat pumps for vehicles. *Adv. Mech. Eng*., 5, 713924
3. Lee H.S. Lee, M.-Y. (2013). Cooling performance characteristics on mobile air-conditioning system for hybrid electric vehicles. *Adv. Mech. Eng*., 5, 282313.
4. Ma G.Y. (1998). Study on thermoelectric air conditioning for electric vehicles. *Refrig. Air Cond.*, 14, 5–10.
5. Lee, D. (2015). Experimental study on the heat pump system using R134a refrigerant for zero-emission vehicles. *Int. J. Automot. Technol*., 16, 923–928.
6. Qi Z.G. (2014). Advances on air conditioning and heat pump system in electric vehicles – A review. *Renew. Sustain. Energy Rev*., 38, 754–764.
7. Qinghong Peng and Qungui Du. (2016). Progress in heat pump air conditioning systems for electric vehicles – A Review. *Open Access Energies* , 9(4), 240; doi: 10.3390/en9040240.
8. Rozver Yu.Yu. (2003). Thermoelectric air conditioner for vehicles. *J.Thermoelectricity*, 2, 52 – 56.
9. Mei V.C., Chen F.C., Mathiprakasam B., Heenan P.(1993). Study of solar-assisted thermoelectric technology for automobile air conditioning. *J. Sol. Energy*, 115, 200–205.
10. Cao Z.Y. (2008). Solution to air conditioning on EVs. *Auto Electric. Parts*, 47, 1–4.
11. Zhang J.Z. (2006). Structural features of fully electric air conditioning system. *Automob. Maint*., 12, 4–5.
12. Guyonvarch G., Aloup C., Petitjean C. Savasse ADMD. 42V Electric air conditioning systems (E-A/CS) for low emissions, architecture, comfort and safety of next generation vehicles; *SAE Technical Paper No. 2001-01-2500; SAE International: Warrendale, PA, USA, 2001.*
13. Randall B. (2006). Blowing hot and cold. Available online: *https://www.teslamotors.com/blog/blowing-hot-and-cold (accessed on 20 December 2006).*
14. Torregrosa B, Payá J., Corberán J.M. (2011). Modeling of mobile air conditioning systems for electric vehicles. *Proc. of the 4th European Workshop – Mobile Air Conditioning and Vehicle Thermal Systems* (Torino, Italy, 1–2 December 2011).
15. Anatychuk L.I., Prybyla A.V. (2016). Comparative analysis of thermoelectric and compression heat pumps for individual air conditioners. *J.Thermoelectricity*, 2, 33 – 42.
16. Anatychuk L.I., Prybyla A.V., Korop M.M. (2016). Comparative analysis of thermoelectric and compression heat pumps for individual air-conditioners at elevated ambient temperatures. *J.Thermoelectricity*, 5, 95 – 98.
17. https://uk.wikipedia.org/wiki/%D0%9A%D0%BB%D1%96%D0%BC%D0%B0%D1%82%D0%B8%D1%87%D0%BD%D0%B8%D0%B9_%D0%BF%D0%BE%D1%8F%D1%81
18. https://climate-data.org/.
19. http://www.holodilshchik.ru/index_holodilshchik_issue_4_2005_Compressors_hermetic_Atlant.html
20. http://www.aholod.ru/upload/docs/tabl-compr.pdf.
21. http://www.eurobi.ru/zapchasti/kompressory/rotary/tecumseh.html.
22. http://www.rembittex.ru/holod/remholod.pdf.
23. http://holodprom.com.ua/sites/default/files/Catalog.pdf.
24. http://www.garantzelremont.ru/images/remont-holodilnikov.pdf.
25. http://zakon.rada.gov.ua/laws/show/v1182400-74.

Submitted 06.03.2019

Анатичук Л.І., *акад. НАН Украини*[1,2]
Прибила А.В., *канд. физ.– мат. наук*[1,2]

[1]Інститут термоелектрики НАН і МОН України,
вул. Науки, 1, Чернівці, 58029, Україна;
e–mail: anatych@gmail.com;
[2]Чернівецький національний університет
ім. Юрія Федьковича, вул. Коцюбинського 2,
Чернівці, 58012, Україна

ПРО ЕФЕКТИВНІСТЬ ТЕРМОЕЛЕКТРИЧНИХ КОНДИЦІОНЕРІВ ДЛЯ ТРАНСПОРТНИХ ЗАСОБІВ

У роботі наводяться результати розрахунків та порівняльного аналізу інтегральної ефективності термоелектричних та компресійних кондиціонерів при умові їх використання для кондиціонування повітря у транспортних засобах протягом цілого року в різних кліматичних умовах. Бібл. 25, Табл. 2, Рис. 14 .
Ключові слова: термоелектричний кондиціонер, компресійний кондиціонер, ефективність.

Анатычук Л.И., *акад. НАН Украини*[1,2]
Прибыла А.В., *канд. физ.– мат. наук*[1,2]

[1]Институт термоэлектричества НАН и МОН Украины,
ул. Науки, 1, Черновцы, 58029, Украина,
e–mail: anatych@gmail.com;
[2]Черновицкий национальный университет
им. Юрия Федьковича, ул. Коцюбинского, 2,
Черновцы, 58012, Украина

ОБ ЭФФЕКТИВНОСТИ ТЕРМОЭЛЕКТРИЧЕСКИХ КОНДИЦИОНЕРЫ ДЛЯ ТРАНСПОРТНЫХ СРЕДСТВ

В работе приводятся результаты расчетов и сравнительного анализа интегральной эффективности термоэлектрических и компрессионных кондиционеров при условии их использования для кондиционирования воздуха в транспортных средствах в течение целого года в различных климатических условиях. Библ. 25, Табл. 2, Рис. 14 .
Ключевые слова: термоэлектрический кондиционер, компрессионный кондиционер, эффективность.

References

1. https://www.zr.ru/content/news/350201-kolichestvo_avtomobilej_v_mire_perevalilo_za_milliard/.
2. Lee M.Y. Lee, D.Y. (2013). Review on conventional air conditioning, alternative refrigerants and CO2 heat pumps for vehicles. *Adv. Mech. Eng*., 5, 713924
3. Lee H.S. Lee, M.-Y. (2013). Cooling performance characteristics on mobile air-conditioning system for hybrid electric vehicles. *Adv. Mech. Eng*., 5, 282313.
4. Ma G.Y. (1998). Study on thermoelectric air conditioning for electric vehicles. *Refrig. Air Cond.*, 14, 5–10.
5. Lee, D. (2015). Experimental study on the heat pump system using R134a refrigerant for zero-emission vehicles. *Int. J. Automot. Technol*., 16, 923–928.
6. Qi Z.G. (2014). Advances on air conditioning and heat pump system in electric vehicles – A review. *Renew. Sustain. Energy Rev*., 38, 754–764.
7. Qinghong Peng and Qungui Du. (2016). Progress in heat pump air conditioning systems for electric vehicles – A Review. *Open Access Energies* , 9(4), 240; doi: 10.3390/en9040240.
8. Rozver Yu.Yu. (2003). Thermoelectric air conditioner for vehicles. *J.Thermoelectricity*, 2, 52 – 56.
9. Mei V.C., Chen F.C., Mathiprakasam B., Heenan P.(1993). Study of solar-assisted thermoelectric technology for automobile air conditioning. *J. Sol. Energy*, 115, 200–205.
10. Cao Z.Y. (2008). Solution to air conditioning on EVs. *Auto Electric. Parts*, 47, 1–4.
11. Zhang J.Z. (2006). Structural features of fully electric air conditioning system. *Automob. Maint*., 12, 4–5.
12. Guyonvarch G., Aloup C., Petitjean C. Savasse ADMD. 42V Electric air conditioning systems (E-A/CS) for low emissions, architecture, comfort and safety of next generation vehicles; *SAE Technical Paper No. 2001-01-2500; SAE International: Warrendale, PA, USA, 2001.*
13. Randall B. (2006). Blowing hot and cold. Available online: *https://www.teslamotors.com/blog/blowing-hot-and-cold (accessed on 20 December 2006).*
14. Torregrosa B, Payá J., Corberán J.M. (2011). Modeling of mobile air conditioning systems for electric vehicles. *Proc. of the 4th European Workshop – Mobile Air Conditioning and Vehicle Thermal Systems* (Torino, Italy, 1–2 December 2011).
15. Anatychuk L.I., Prybyla A.V. (2016). Comparative analysis of thermoelectric and compression heat pumps for individual air conditioners. *J.Thermoelectricity*, 2, 33 – 42.
16. Anatychuk L.I., Prybyla A.V., Korop M.M. (2016). Comparative analysis of thermoelectric and compression heat pumps for individual air-conditioners at elevated ambient temperatures. *J.Thermoelectricity*, 5, 95 – 98.
17. https://uk.wikipedia.org/wiki/%D0%9A%D0%BB%D1%96%D0%BC%D0%B0%D1%82%D0%B8%D1%87%D0%BD%D0%B8%D0%B9_%D0%BF%D0%BE%D1%8F%D1%81
18. https://climate-data.org/.
19. http://www.holodilshchik.ru/index_holodilshchik_issue_4_2005_Compressors_hermetic_Atlant.html
20. http://www.aholod.ru/upload/docs/tabl-compr.pdf.
21. http://www.eurobi.ru/zapchasti/kompressory/rotary/tecumseh.html.
22. http://www.rembittex.ru/holod/remholod.pdf.
23. http://holodprom.com.ua/sites/default/files/Catalog.pdf.
24. http://www.garantzelremont.ru/images/remont-holodilnikov.pdf.
25. http://zakon.rada.gov.ua/laws/show/v1182400-74.

Submitted 06.03.2019

ARTICLE SUBMISSION GUIDELINES

For publication in a specialized journal, scientific works are accepted that have never been printed before. The article should be written on an actual topic, contain the results of an in-depth scientific study, the novelty and justification of scientific conclusions for the purpose of the article (the task in view).

The materials published in the journal are subject to internal and external review which is carried out by members of the editorial board and international editorial board of the journal or experts of the relevant field. Reviewing is done on the basis of confidentiality. In the event of a negative review or substantial remarks, the article may be rejected or returned to the author(s) for revision. In the case when the author(s) disagrees with the opinion of the reviewer, an additional independent review may be done by the editorial board. After the author makes changes in accordance with the comments of the reviewer, the article is signed to print.

The editorial board has the right to refuse to publish manuscripts containing previously published data, as well as materials that do not fit the profile of the journal or materials of research pursued in violation of ethical norms (for instance, conflicts between authors or between authors and organization, plagiarism, etc.). The editorial board of the journal reserves the right to edit and reduce the manuscripts without violating the author's content. Rejected manuscripts are not returned to the authors.

Submission of manuscript to the journal

The manuscript is submitted to the editorial office of the journal in paper form in duplicate and in electronic form on an electronic medium (disc, memory stick). The electronic version of the article shall fully correspond to the paper version. The manuscript must be signed by all co-authors or a responsible representative.

In some cases it is allowed to send an article by e-mail instead of an electronic medium (disc, memory stick).

English-speaking authors submit their manuscripts in English. Russian-speaking and Ukrainian-speaking authors submit their manuscripts in English and in Russian or Ukrainian, respectively. Page format is A4. The number of pages shall not exceed 15 (together with References and extended abstracts). By agreement with the editorial board, the number of pages can be increased.

To the manuscript is added:

1. Official recommendation letter, signed by the head of the institution where the work was carried out.

2. License agreement on the transfer of copyright (the form of the agreement can be obtained from the editorial office of the journal or downloaded from the journal website – Dohovir.pdf). The license agreement comes into force after the acceptance of the article for publication. Signing of the license agreement by the author(s) means that they are acquainted and agree with the terms of the agreement.

3. Information about each of the authors – full name, position, place of work, academic title, academic degree, contact information (phone number, e-mail address), ORCID code (if available). Information about the authors is submitted as follows:

authors from Ukraine - in three languages, namely Ukrainian, Russian and English;

authors from the CIS countries - in two languages, namely Russian and English;

authors from foreign countries – in English.

4. Medium with the text of the article, figures, tables, information about the authors in electronic

form.

5. Colored photo of the author(s). Black-and-white photos are not accepted by the editorial staff. With the number of authors more than two, their photos are not shown.

Requirements for article design

The article should be structured according to the following sections:

- *Introduction*. Contains the problem statement, relevance of the chosen topic, analysis of recent research and publications, purpose and objectives.
- *Presentation of the main research material* and the results obtained.
- *Conclusions* summing up the work and the prospects for further research in this direction.
- *References*.

The first page of the article contains information:

1) in the upper left corner – UDC identifier (for authors from Ukraine and the CIS countries);

2) surname(s) and initials, academic degree and scientific title of the author(s);

3) the name of the institution where the author(s) work, the postal address, telephone number, e-mail address of the author(s);

4) article title;

5) abstract to the article – not more than 1 800 characters. The abstract should reflect the consistent logic of describing the results and describe the main objectives of the study, summarize the most significant results;

6) key words – not more than 8 words.

The text of the article is printed in Times New Roman, font size 11 pt, line spacing 1.2 on A4 size paper, justified alignment. There should be no hyphenation in the article.

Page setup: "mirror margins" – top margin – 2.5 cm, bottom margin – 2.0 cm, inside – 2.0 cm, outside – 3.0 cm, from the edge to page header and page footer – 1.27 cm.

Graphic materials, pictures shall be submitted in color or, as an exception, black and white, in .opj or .cdr formats, .jpg or .tif formats being also permissible. According to author's choice, the tables and partially the text can be also in color.

Figures are printed on separate pages. The text in the figures must be in the font size 10 pt. On the charts, the units of measure are separated by commas. Figures are numbered in the order of their arrangement in the text, parts of the figures are numbered with letters – a, b, .. On the back of the figure, the title of the article, the author (authors) and the figure number are written in pencil. Scanned images and graphs are not allowed to be inserted.

Tables are provided on separate pages and must be executed using the MSWord table editor. Using pseudo-graph characters to design tables is inadmissible.

Formulae shall be typed in Equation or MatType formula editors. Articles with formulae written by hand are not accepted for printing. It is necessary to give definitions of quantities that are first used in the text, and then use the appropriate term.

Captions to figures and tables are printed in the manuscript after the references.

Reference list shall appear at the end of the article. References are numbered consecutively in the order in which they are quoted in the text of the article. References to unpublished and unfinished works are inadmissible.

Attention! In connection with the inclusion of the journal in the international bibliographic abstract database, the reference list should consist of two blocks: CITED LITERATURE and REFERENCES (this requirement also applies to English articles):

CITED LITERATURE – sources in the original language, executed in accordance with the Ukrainian standard of bibliographic description DSTU 8302:2015. With the aid of VAK.in.ua

(http://vak.in.ua) you can automatically, quickly and easily execute your "Cited literature" list in conformity with the requirements of State Certification Commission of Ukraine and prepare references to scientific sources in Ukraine in understandable and unified manner. This portal facilitates the processing of scientific sources when writing your publications, dissertations and other scientific papers.

REFERENCES – the same cited literature list transliterated in Roman alphabet (recommendations according to international bibliographic standard APA-2010, guidelines for drawing up a transliterated reference list "References" are on the site http//www.dse.org.ua, section for authors).

To speed up the publication of the article, please adhere to the following rules:

- in the upper left corner of the first page of the article – the UDC identifier;
- family name and initials of the author(s);
- academic degree, scientific title;

begin a new line, Times New Roman font, size 12 pt, line spacing 1.2, center alignment;

- name of organization, address (street, city, zip code, country), e-mail of the author(s);

begin a new line 1 cm below the name and initials of the author(s), Times New Roman font, size 11 pt, line spacing 1.2, center alignment;

- the title of the article is arranged 1 cm below the name of organization, in capital letters, semi-bold, font Times New Roman, size 12 pt, line spacing 1.2, center alignment. The title of the article shall be concrete and possibly concise;
- the abstract is arranged 1 cm below the title of the article, font Times New Roman, size 10 pt, in italics, line spacing 1.2, justified alignment in Ukrainian or Russian (for Ukrainian-speaking and Russian-speaking authors, respectively);
- key words are arranged below the abstract, font Times New Roman, size 10 pt, line spacing 1.2, justified alignment. The language of the key words corresponds to that of the abstract. Heading "Key words" - font Times New Roman, size 10 pt, semi-bold;
- the main text of the article is arranged 1 cm below the abstract, indent 1 cm, font Times New Roman, size 11 pt, line space spacing 1.2, justified alignment;
- formulae are typed in formula editor, fonts Symbol, Times New Roman. Font size is "normal" – 12 pt, "large index" – 7 pt, "small index" – 5 pt, "large symbol" – 18 pt, "small symbol" – 12 pt. The formula is arranged in the text, center aligned and shall not occupy more than 5/6 of the line width, formulae are numbered in parentheses on the right;
- dimensions of all quantities used in the article are represented in the International System of Units (SI) with the explication of the symbols employed;
- figures are arranged in the text. The figures and pictures shall be clear and contrast; the plot axes – parallel to sheet edges, thus eliminating possible displacement of angles in scaling; figures are submitted in color, black-and-white figures are not accepted by the editorial staff of the journal;
- tables are arranged in the text. The width of the table shall be 1 cm less than the line width. Above the table its ordinary number is indicated, right alignment. Continuous table numbering throughout the text. The title of the table is arranged below its number, center alignment;
- references should appear at the end of the article. References within the text should be

enclosed in square brackets behind the text. References should be numbered in order of first appearance in the text. Examples of various reference types are given below.

Examples of LITERATURE CITED

Journal articles

Anatychuk L.I., Mykhailovsky V.Ya., Maksymuk M.V., Andrusiak I.S. Experimental research on thermoelectric automobile starting pre-heater operated with diesel fuel. *J.Thermoelectricity*. 2016. №4. P.84–94.

Books

Anatychuk L.I. *Thermoelements and thermoelectric devices. Handbook.* Kyiv, Naukova dumka, 1979. 768 p.

Patents

Patent of Ukraine № 85293. Anatychuk L.I., Luste O.J., Nitsovych O.V. Thermoelement.

Conference proceedings

Lysko V.V. *State of the art and expected progress in metrology of thermoelectric materials.* Proceedings of the XVII International Forum on Thermoelectricity (May 14-18, 2017, Belfast). Chernivtsi, 2017. 64 p.

Authors' abstracts

Kobylianskyi R.R. *Thermoelectric devices for treatment of skin diseases*: extended abstract of candidate's thesis. Chernivtsi, 2011. 20 p.

Examples of REFERENCES

Journal articles

Gorskiy P.V. (2015). Ob usloviakh vysokoi dobrotnosti i metodikakh poiska perspektivnykh sverhreshetochnykh termoelektricheskikh materialov [On the conditions of high figure of merit and methods of search for promising superlattice thermoelectric materials]. *Termoelektrichestvo - J.Thermoelectricity,* 3, 5 – 14 [in Russian].

Books

Anatychuk L.I. (2003). *Thermoelectricity. Vol.2. Thermoelectric power converters*. Kyiv, Chernivtsi: Institute of Thermoelectricity.

Patents

Patent of Ukraine № 85293. Anatychuk L. I., Luste O.Ya., Nitsovych O.V. Thermoelements [In Ukrainian].

Conference proceedings

Rifert V.G. Intensification of heat exchange at condensation and evaporation of liquid in 5 flowing-down films. In: *Proc. of the 9th International Conference Heat Transfer.* May 20-25, 1990, Israel.

Authors'abstracts

Mashukov A.O. *Efficiency hospital state of rehabilitation of patients with color carcer.* PhD (Med.) Odesa, 2011 [In Ukrainian].